Investigation of the Impact of Material Models on Reliability Assessment of Electronic Packages

By

Abel Misrak

Presented to the Faculty of the Graduate School of

The University of Texas at Arlington

in Partial Fulfillment of the Requirements

for the Degree of

DOCTOR OF PHILOSOPHY

THE UNIVERSITY OF TEXAS AT ARLINGTON

August 2020

Acknowledgements

I would like to thank Prof. Dereje Agonafer for serving as chair of my dissertation committee and for his guidance and mentorship during my graduate career. I would also like to thank my dissertation committee members: Prof. A. Haji-Sheikh, Prof. Zeynep Çelik-Butler, Dr. Miguel Amaya, and Dr. Fahad Mirza for their time and valuable inputs. Some of the work presented in this dissertation was completed as part of Semiconductor Research Corporation (SRC) funded project with Texas Instruments and a collaboration with TDK InvenSense. I would like to acknowledge the support of Dr. Luu Nugyen, Steven Kummerl, Dr. Alok Lohia from Texas Instruments, and Dr. Fahad Mirza and Dr. Ben Gholami from TDK InvenSense. I would also like to acknowledge the masters and PhD students at EMNSPC I had the chance to work with through the years. Special thanks go to: Rabin Bhandari, Tushar Chauhan, Akshay Lakshminaraya, Unique Rahangdale, Pavan Rajmane, and Raufur Chowdhury. I would also like to thank the staff in MAE department for their help and support through the years. Last but not least, I would like to acknowledge my mother, Misrak T. Taddese and my father, Misrak T. Limneih, whose unwavering support and encouragement made it all possible.

August 2020

Abstract

Investigation of the Impact of Material Models on Reliability Assessment of Electronic Packages

Abel Misrak, PhD

The University of Texas at Arlington, 2020

Supervising Professor: Dereje Agonafer

Drop testing, thermal cycling, power cycling, etc. are some of the tests used to assess the reliability of new electronic products. However, performing experimental study of every new design is costly and time consuming. Computational tools are often employed to perform the required reliability analysis in a shorter time period and save valuable resources. Extensive set of material characterization work needs to be done before an accurate material model can be developed and used in computational analysis. Structural components such as printed circuit boards (PCBs) are critical in the thermomechanical reliability assessment of electronic packages. The bulk material properties of PCBs are commonly characterized using equipment such as tensile testers and used in computational studies. However, if a detailed layer by layer model is required for the study, it is often difficult to obtain location dependent mechanical properties for a given woven glass/epoxy substrate. In this work, nanoindentation technique is used to measure the modulus and creep behavior for a specific layer in the PCB stack-up. Using measurements at room temperature, the effects of surface roughness, hold time, and maximum load on measurement values are examined. Moreover, frequency domain master curve results from dynamic mechanical analysis are used to obtain Prony series terms and perform finite element analysis on the impact of adding viscoelastic properties of PCBs when performing reliability analysis under thermal cycling and under drop

testing for wafer level chip scale packages. Another important component of electronic packaging that are presented here are thermal interface materials (TIMs). Most of the study in the literature focuses on studying the changes in thermal properties, and there is a lack of understanding when it comes to studying the mechanical behavior of TIMs. Degradation of mechanical properties is the cause for the loss in thermal performance and is critical during TIM selection process. Moreover, mechanical properties such as modulus and thermal expansion coefficient (CTE) are critical to assess performance of TIMs using finite element analysis (FEA) and potentially save time and money in the evaluation and selection process. In this work, commercially available TIMs are studied using TMA, DMA, and FTIR to evaluate the changes in mechanical properties due to thermal aging. In the last chapter of this work, the effect of parameters such as temperature curing profile, application of pressure during curing, and sample preparation technique on temperature dependent thermo-mechanical properties of die attach elastomers is investigated. The mechanical properties, including elastic modulus (E), coefficient of thermal expansion (CTE), and the glass transition temperature (Tg) of the die attach material, are measured using a suite of techniques such as dynamic mechanical analysis (DMA) and thermomechanical analysis (TMA). The analysis is performed for a wide temperature range corresponding to typical MEMS sensor applications. It is shown that sample preparation and characterization techniques have a considerable impact on the measurements which results in different MEMS sensor performance predictions through computational modeling.

Contents

Acknowledgements iii

Abstract iv

List of Figures ix

List of Tables xiii

Chapter 1 Introduction 1

Dynamic Mechanical Analyzer (DMA) 3

Thermomechanical Analyzer (TMA) 4

Fourier-Transform Infrared Spectroscopy (FTIR) 5

References 6

Chapter 2 Characterization of Mechanical Properties and Creep Behavior of Woven Glass/Epoxy Substrates by Nanoindentation 8

2.1 Abstract 8

2.2 Introduction 9

2.3 Methods 13

2.3.1 Sample Preparation 13

2.3.2 Experiment 14

2.3.3 Data Analysis 15

2.4 Results 16

2.5 Discussion 21

2.6 Summary 23

2.7 Nomenclature 23

2.8 References 24

Chapter 3 Impact of Aging on Mechanical Properties of Thermally Conductive Gap Fillers 26

3.1 Abstract 26

3.2 Introduction 27

3.2.1 Background 27

3.2 Materials and Methods 31

3.2.1 Sample Preparation 31

3.2.2 Experimental Procedure 34

3.3 Results 37

3.4 Discussion 44

3.4 Conclusions 47

3.5 References 48

Chapter 4 Viscoelastic Influence on the Board Level Reliability Assessment of Wafer Level Packages Under Drop Impact and Under Thermal Cycling 54

4.1 Abstract 54

4.2 Introduction 55

4.3 Materials and Methods 62

4.4 Computational Study 69

4.5 Results 76

4.6 Discussion 81

4.7 Conclusions 83

4.8 Nomenclature 83

4.9 References 85

Chapter 5 Impact of Die Attach Sample Preparation on its Measured Mechanical Properties for MEMS Sensor Applications 91

5.1 Abstract 91

5.2 Introduction 92

5.3 Materials and Methods 95

5.3.1 Sample Preparation 95

5.3.2 Experimental Procedure 100

5.4 Results 101

5.5 Discussion 104

5.6 Conclusions 107

5.7 References 108

Chapter 6 Summary and Conclusions 111

Appendix I 114

Appendix II 116

List of Figures

Figure 1-1: Major components of Dynamic Mechanical Analyzer (DMA). [5] 3

Figure 1-2: Major components of Thermomechanical Analyzer (TMA). [8] 4

Figure 1-3: Schematic of the Michelson Interferometer used in the FTIR study. 5

Figure 2-1: Loading and unloading curve from a Nanoindentation experiment. 10

Figure 2-2: Standard linear solid model with two elastic and one viscous element. 12

Figure 2-3: Sample prepared for cross-section imaging. 13

Figure 2-4: Exposed substrate layers (right) and cross section image under optical microscope (left). 14

Figure 2-5: Polished sample mounted on a metal the disk before test. 14

Figure 2-6: An optical image of the exposed substrate layer of PCB. 16

Figure 2-7: Enhanced contrast NC-AFM images of different regions on the exposed substrate layer. 17

Figure 2-8: A representative load vs. indentation depth curve..... 18

Figure 2-9: A representative indentation depth vs. time for 60 s holding time. 18

Figure 2-10: A representative creep data set and curve fit for the standard linear model with 15 s hold time. 20

Figure 2-11: Creep time constant (s) vs. hold times (s) for three sample measurements. 21

Figure 3-1: Thermal interface with an ideal TIM [5]..... 28

Figure 3-2: TIM 1 and TIM 2 used in electronic packaging. TIM 1 is used between die and lid, while TIM 2 is used between lid and heat sink..... 29

Figure 3-3: TIM placed on stage for TMA testing. 34

Figure 3-4: TIM attached for DMA testing. 36

Figure 3-5: Sample placed in FTIR for measurement..... 37

Figure 3-6: Pre-aging DMA measurements. Comparison between TIM A and B shown for storage modulus (top), loss modulus (bottom). 38

Figure 3-17: Post-aging DMA measurements. Comparison between TIM A and B shown for storage modulus (top), loss modulus (bottom). 39

Figure 3-8: Complex modulus comparison between pre aging and post aging samples for TIM A (top), TIM B (bottom). 40

Figure 3-9: FTIR result showing major peaks. All the TIMs studied as part of this work exhibited the same peaks. A representative result for TIM A is shown above. 41

Figure 3-10: FTIR comparison between pre aged and post aged samples for TIM B. 42

Figure 3-11: TMA result comparison between TIM A and TIM B before high temperature aging. 42

Figure 3-12: TMA comparison for before and after aging cases for TIM B (top) and TIM A (bottom). 43

Figure 4-1: Bathtub curve showing failure rate as a function of time. 56

Figure 4-2: General Maxwell model used to represent viscoelastic materials. 59

Figure 4-3: Major components of DMA [22]. 60

Figure 4-4: DMA7100 used for testing (left). Samples used for measurement (right). 62

Figure 4-5: Samples attached using DMA bending mode. 63

Figure 4-6: DMA result showing temperature dependent modulus, loss modulus, and loss tangent. 64

Figure 4-7: Three approaches to measure glass transition temperature (Tg). Onset of E', peak of E'', or peak of $Tan\ \delta$ may be considered as Tg. 65

Figure 4-8: Master curve showing storage modulus, loss modulus, and $Tan\ \delta$ as a function of frequency. The terms for the WLF shift function are also given in the figure. 66

Figure 4-9: Computed vs measured storage, loss, and complex modulus for 160 °C. Comparisons for 170 °C and 180 °C given in Appendix II. 68

Figure 4-10: Schematic of WCSP model used to perform computational study. 70

Figure 4-11: Boundary conditions used for the computational study. 70

Figure 4-12: Temperature cycling profiles used for the study: condition G (solid line) and H (dotted line) of JEDEC standard JESD22-A014D are shown. 73

Figure 4-13: Quarter symmetry of the JEDEC board used for the computational study. 74

Figure 4-14: Plot comparing the number of cycles to failure between the two cases where PCB were modeled elastic and viscoelastic. 76

Fig. 4-15: Equivalent stress on corner solder for the elastic case for thermal cycling for -40 °C to 165 °C. 77

Figure 4-16: Total deformation of the quarter model at 135 °C for the case PCB is modeled as viscoelastic. 77

Figure 4-17: Comparison of average total deformation between models that represented the PCB elastic and viscoelastic. Results shown for different temperatures. 78

Figure 4-18: Comparison of average total acceleration between models that represent the PCB as elastic and viscoelastic. Results shown for different temperatures. 79

Figure 4-19: Comparison of strain between models that represent the PCB elastic and viscoelastic. Results shown for different temperatures. 80

Figure 5-1:Schematic diagram showing components of a MEMS package. 93

Figure 5-2: Temperature profile used for curing the samples. 96

Figure 5-3: Sample preparation without the top plate (left) and cured sample (right). 97

Figure 5-4: Sample dispensed on the Teflon sheet attached to the steel plate (left), assembly ready to cure on (right). 97

Figure 5-5: Sample preparation setup with torque control. 98

Figure 5-6: Sample prepared using a hot press machine. 98

Figure 5-7: Log of geometric factor vs expected modulus for different sample sizes. The expected modulus shown here corresponds to temperatures above room temperature. The measurable ranges for DMA shown in black. 99

Figure 5-8: Sample preparation of DAF samples: thicker samples prepared without a roller (top), with a roller (bottom). 100

Figure 5-9: Die attach material mounted for DMA measurement (left) and TMA measurement (right). 100

Figure 5-10: Normalized complex modulus as a function of temperature for different sample preparation methods for curable die attach samples. 102

Figure 5-11: Comparison of DMA results for different sample preparation of DAF samples. .. 102

Figure 5-12: Change of relative length with temperature for different sample preparation methods for curable die attach samples. 103

Figure 5-13: Normalized modulus of curable die attach materials after the samples were exposed to reflow temperature profile commonly used for SAC solder alloys. 103

List of Tables

Table 2-1: Parameters used for surface roughness measurements. 15

Table 2-2: Roughness measured using NC-AFM at five randomly selected regions of the substrate. 17

Table 2-3: Modulus and hardness measurements for 2 s hold time. Each indentation was made at different location on the substrate surface. 19

Table 2-4: Modulus and hardness measurements for 60 s hold time. Each indentation was made at different location on the substrate surface. 19

Table 2-5: Modulus and hardness measurements with same load but different hold times. Each indentation was made at different location on the substrate surface. 20

Table 3-1: Settings used for DMA testing in tensile mode. 36

Table 3-2: Major Peaks identified from FTIR results [28] [29]. 41

Table 4-1: Geometric dimensions of samples and test parameters used for DMA testing 63

Table 4-2: Prony series terms for 160 °C and 170 °C. Terms for 140 °C, 150 °C, 180 °C, and 190°C given in Appendix I. 69

Table 4-3: Mechanical properties of the different components used in the computational study[7] [36] [26] [37] 71

Table 4-4: Values for the Anand constants used to model solders. Properties for SAC 387 given below [18] 72

Table 4-5: Average plastic work (Pa) for the different thermal cycling conditions 76

Table 5-1: Settings used for testing die attach samples on TMA. 101

Table 5-2: Settings used for testing die attach samples on DMA. 101

Table 5-3: Settings used for testing DAF samples on TMA. 101

Table 5-4: Settings used for testing DAF samples on DMA. 101

Chapter 1
Introduction

In 1965, when Gordon Moore published an article titled *Cramming more Components onto Integrated Circuits* and forecasted the increase in circuit density for the following decade, there were roughly 32 transistors on a single chip. Since then, following Moore's predictions, the number of transistors on a single chip has increased exponentially to billions of transistors per chip [1]. The shrinking transistor features along with improvements in interconnect technology have enabled increased integration levels and made possible improvements in digital, memory, analog, and other electronic applications [1]. This has revolutionized the electronics industry and led to the proliferation of handheld devices such as phones and personal computers.

During the design cycle of such electronic products, significant amount of time and resources are spent in optimizing the thermal and mechanical designs. Thermal designs are made to ensure that the temperature of the devices will not exceed limits and degrade performance, while mechanical designs are optimized in order to ensure the devices are reliable under loading conditions such as drop testing and thermal cycling. During this design process, computational tools, such as finite element analysis (FEA) or computational fluid dynamic (CFD) tools, are heavily used and are integral parts of the process.

There are numerous factors that affect the accuracy of computational studies: representation of the boundary conditions, mesh of the model, and accuracy of the material models used. Often, getting detailed accurate material property data is time consuming and expensive. As a compromise between computational time and accuracy, bulk material properties are often used for computational studies. When we look at the thermomechanical analysis of electronic packages, equipment such as tensile testers, thermo-mechanical analyzers (TMAs), Dynamic Mechanical Analyzers (DMAs), etc. have often been used to obtain bulk material properties. However, it has

been shown that detailed material property characterizations can improve the accuracy of computational studies for optimizing designs and predicting residual stresses due to manufacturing processes [2] [3]. Moreover, roadmaps outlined by organizations such as The International Technology Roadmap for Semiconductors (ITRS) have proposed heterogenous integration as the future means of attaining enhanced functionality and improved operating characteristics [4]. When using heterogeneous integration, components with different functions are manufactured separately and heterogeneously integrated on a common platform resulting in higher functional density and higher performance. When designing such systems, thermomechanical reliability assessment is critical and obtaining accurate material properties is of paramount importance.

There is a need to understand the scale dependence of material characterizations, impact of environmental conditions on mechanical properties, and impact of material model on computational reliability assessments. In the work presented in the following chapters, the following have been addressed: use of nanoindentation technique to obtain location dependent material properties and creep behavior of PCB substrates, study of the thermomechanical properties of thermal interface materials and their change due to thermal aging, and an alternative approach of characterizing the viscoelastic properties of materials using frequency domain master curve data obtained from dynamic mechanical analysis. As an example, Prony series terms representing the viscoelastic material properties of PCBs are obtained from dynamic mechanical analysis. The obtained Prony series terms are used to study the reliability assessment of Wafer Level Chip Scale Packages (WCSPs) under thermal cycling and under drop testing loading conditions. In the last chapter, the impact of material models on analysis results is further investigated by studying the impact of material characterization techniques on the measurement

results for die attach elastomers. The major equipment used for the work presented in chapters 2 – 5 are given in the following sections.

Dynamic Mechanical Analyzer (DMA)

DMA uses a technique that measures kinetic properties of samples by measuring stress or strain generated by oscillating strain or stress applied to samples [5]. Using different attachments (bending or tensile), loss modulus (E''), storage modulus (E'), and loss tangent ($Tan\ \delta$) can be measured [6]. The major components of DMA are shown Figure 1-1. Output of DMA consists of temperature dependent loss and storage moduli of materials at different frequencies. Relationship between these properties and complex modulus (E^*), whose magnitude is comparable to Young's modulus, is given by Equations (1-1) and (1-2). Relation of modulus values to Loss tangent is given by Equation (1-3). Using the "time-temperature superposition", the DMA results can be expanded to a wider frequency range and a master curve can be obtained.

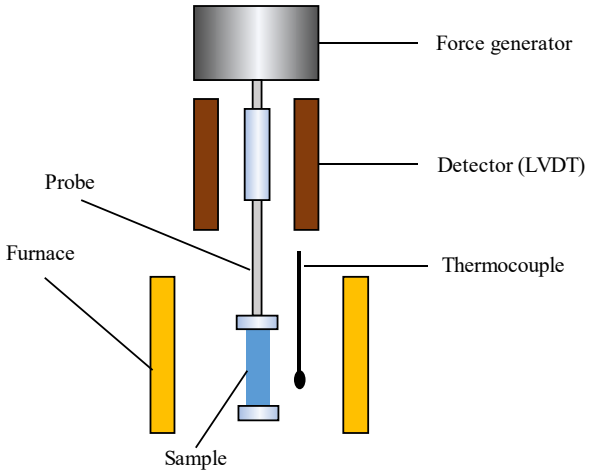

Figure 1-1: Major components of Dynamic Mechanical Analyzer (DMA). [5]

$$E^* = E' + iE'' \qquad (1\text{-}1)$$

$$|E^*| = \sqrt{E'^2 + E''^2} \qquad (1\text{-}2)$$

$$Tan\ \delta = \frac{E''}{E'} \qquad (1\text{-}3)$$

Thermomechanical Analyzer (TMA)

TMA is often used to characterize the thermomechanical properties of materials such as thermal expansion coefficient (CTE) and glass transition temperature (Tg). TMA measures the deformation of samples under non-oscillating stress. A small furnace is used to heat or cool samples. The deformation of samples is measured by using linear variable differential transformer (LVDT) [7]. The measurement results are used to compute the CTE and Tg of materials. Depending on the sample dimensions and expected measurement results, a compression probe or tensile attachment may be used. For both attachments, a negligible amount of load is applied on samples to ensure there is proper contact between the samples and probe. For very thin and soft samples, the TMA machine may also be used to measure the modulus of materials. However, in this work, the TMA is used only for measuring the CTE of die attach materials. A schematic diagram of a TMA is shown in Figure 1-2.

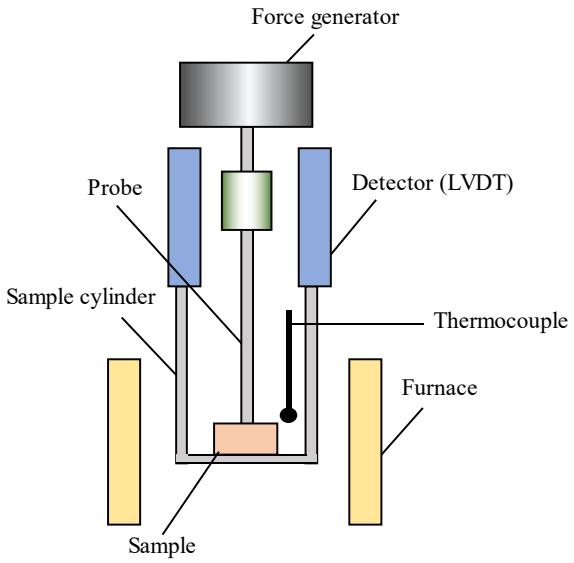

Figure 1-2: Major components of Thermomechanical Analyzer (TMA). [8]

Fourier-Transform Infrared Spectroscopy (FTIR)

The vibration spectroscopy is used to analyze molecular structures by examining the interaction between infrared light and nuclear vibrations in molecules. Fourier Transform Infrared Spectroscopy (FTIR) detects the molecular vibrations by measuring the absorption of infrared light. This approach can be used to study organic and inorganic materials. However, metallic materials cannot be studied using FTIR because of their strong reflective property.

The infrared source in FTIR produces light at different wavelengths. One of the mirrors is fixed while the other is moved to measure an interferogram using a Michelson interferometer. The FTIR receives the interferogram signals which are transmitted to or reflected from a sample. The interferogram measured while scanning is Fourier transformed to yield a spectrum. Schematic of the setup used for FTIR study is given in Figure 1-3 below.

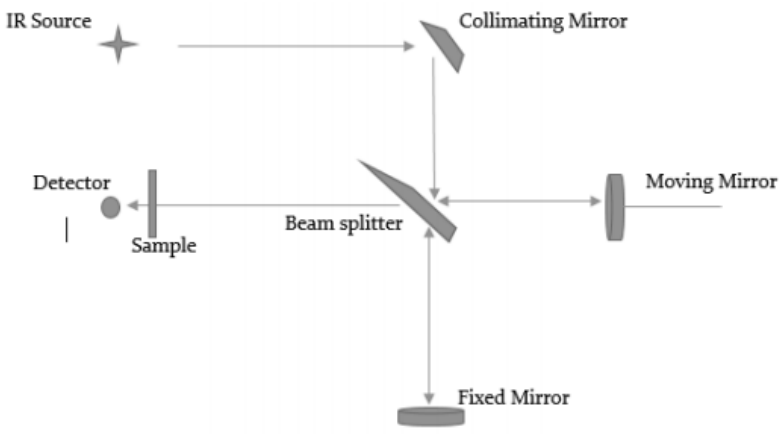

Figure 1-3: Schematic of the Michelson Interferometer used in the FTIR study.

References

[1] "Chapter 2," The scaling of MOSFETs, Moore's law, and ITRS.[Online]. Available: http://userweb.eng.gla.ac.uk/fikru.adamu-lema/Chapter_02.pdf.[Accessed 2020 July 21].

[2] Y. Wang, K. Low, H. Pang, K. H. Hoon , F. X. Che and Y. S. Yong, "Modeling and simulation for a drop-impact analysis of multi-layered printed circuit boards," *Microelectronics Reliability,* vol. 46, no. 2-4, pp. 558-573, 2006.

[3] P. Shrotriya and N. Sottos, "Creep and relaxation behavior of woven glass/epoxy substrates for multilayer circuit board applications," *Polymer Composites ,* vol. 19, no. 5, pp. 567-578, 1998.

[4] B. Bayraktaroglu, *Heterogeneous Integration Technology,* AFRL/RYDD. APRS-RY-17-0383., May 19 2017.

[5] H. H.-T. Corporation, "Principle of Dynamic Mechanical Analysis (DMA).," 2018. [Online]. Available: https://www.hitachi-hightech.com/global/products/science/tech/ana/thermal/descriptions/dma.html. [Accessed 01 07 2019].

[6] TA Instruments, [Online]. Available: https://www.tainstruments.com/products/rheology/dynamic-mechanical-analyzers/. [Accessed 10 November 2019].

[7] A. Misrak, T. Chauhan, P. Rajmane, R. Bhandari and D. Agonafer, "Impact of Aging On Mechanical Properties of Thermally Conductive GAP Fillers," *Journal of Electronic Packaging,* vol. 142, no. 1, 2020.

[8] H. H.-T. Corporation, "Principle of Thermomechanical Analysis (TMA)," 2018. [Online]. Available: https://www.hitachi-hightech.com/global/products/science/tech/ana/thermal/descriptions/tma.html. [Accessed 01 07 2019].

[9] "Principle of Dynamic Mechanical Analysis (DMA)," Hitachi High-Tech Corporation, [Online]. Available: https://www.hitachi-hightech.com/global/products/science/tech/ana/thermal/descriptions/dma.html. [Accessed 02 April 2020].

[10] "Principle of Thermomechanical Analysis (TMA)," Hitachi High-Tech Corporation, [Online]. Available: https://www.hitachi-hightech.com/global/products/science/tech/ana/thermal/descriptions/tma.html. [Accessed 02 April 2020].

Chapter 2

Characterization of Mechanical Properties and Creep Behavior of Woven Glass/Epoxy Substrates by Nanoindentation[1]

2.1 Abstract

Reliability is of a concern when designing new products. Extensive set of reliability tests are performed before a product is ready to be shipped for use. Drop testing, thermal cycling, power cycling, etc. are some of the tests used to assess the reliability of new electronic products. However, performing experimental study of every new design is costly and time consuming. Computational tools (such as finite element analysis software) are often employed to perform the required reliability analysis in a shorter time period and save valuable resources. One of the challenges of performing computational analysis is obtaining accurate material property data to be used for building accurate models. Extensive set of material characterization work needs to be done before an accurate model can be developed. For example, for a new printed circuit board (PCB), the bulk properties are often characterized by equipment such as thermomechanical analyzer (TMA) and tensile testing machines to obtain the bulk properties that can be used for the computational study. However, if a detailed layer by layer model is required for the study, it is often difficult to obtain location dependent mechanical properties for a given woven glass/epoxy substrate. In this paper, the use of nanoindentation technique to measure the modulus and creep behavior for a specific layer in the PCB stack-up is investigated. Using measurements at room temperature, the effect of surface roughness, hold time, and maximum load on measurement values is examined.

[1] *The work presented in this chapter has been published in the Journal of Microelectronic and Electronic Packaging. Included here with written permission from IMAPS. Citation of the publication is given below:*
Abel Misrak, Luu Nguyen, Steven Kummerl, and Dereje Agonafer (2018) Characterization of Mechanical Properties and Creep Behavior of Woven Glass/Epoxy Substrates by Nanoindentation. Journal of Microelectronics and Electronic Packaging: April 2018, Vol. 15, No. 2, pp. 95-100. https://doi.org/10.4071/imaps.654387

2.2 Introduction

Electronic products are designed to perform in a wide range of environmental conditions: hot, cold, humid, dry, etc… In addition to the vast range of environmental conditions, the products are designed to withstand accidental loads such as drops and vibrations during their life time. Different standards, such as JEDEC, are devised to ensure the reliability of the electronic devices under such conditions. Reliability tests, such as thermal cycling and thermal shock, are very time consuming. In order to save time and money, commercially available computational tools are used to test for reliability and accelerate the product development cycle. Moreover, computational tools have been used to perform design optimization and improve the reliability of products [1]. One of the challenges of using computational tools is obtaining accurate material properties and developing accurate models. Components such as the solder ball and the PCB are highly non-linear and different approaches are employed to accurately represent their material properties. Lumped modeling approach, explicit approach, and electronic computer aided design (ECAD) approach are the three widely used approaches for creating models for Printed Circuit Boards (PCBs).

Lumped approach models the PCB as a block and uses bulk properties obtained from tests such as tensile testing, and dynamic mechanical analysis (DMA)/thermomechanical analysis (TMA) tests. For explicit approach, individual layers of the PCB are modeled and properties are assigned accordingly. The ECAD approach uses the files in the PCB design process to build a very accurate model. Though the explicit and ECAD approaches are very accurate, they are computationally expensive. Hence, the lumped approach is widely implemented. Though computationally expensive, the use of layer by layer model of PCBs is an appealing approach. In the layer by layer approach, orthotropic properties are assigned to PCB layers**.** Wang et al. have shown that a multi-layered PCB model gives more accurate results when compared to simplified isotropic and

orthotropic models [2]. Including location dependent material properties of a PCB layer will improve the model and help to capture location dependent properties. In this paper, the use of nanoindentation to measure location dependent material properties is investigated.

Nanoindentation is a technique often employed to characterize mechanical behavior of materials at small scales. The technique is often implemented to characterize the properties of films micrometers thick and biological samples such as bone tissues [3][4]. One of the main advantages of nanoindentation is that the hardness and modulus values of samples can be measured from the indentation load and displacement data without having the need to image the hardness impressions [2]. A typical data obtained from nanoindentation experiment shows the loading and unloading curves from the measurement process as shown in Figure 2-1. The accuracy of the measurement depends on how well the maximum load, maximum indentation, and contact stiffness (slope of the initial phase of the unloading process) can be measured [4]. Advances in understanding of the mechanics of elastic-plastic contact and use of improved testing equipment have shown improvement in the accuracy of measurements since the techniques started being widely used in the 90s [5].

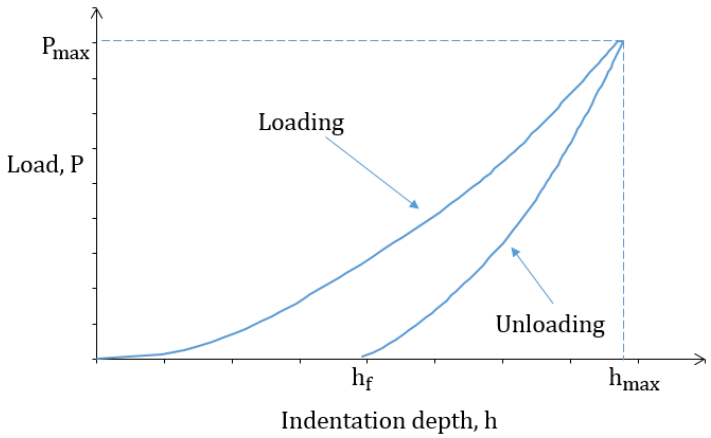

Figure 2-1: Loading and unloading curve from a Nanoindentation experiment.

Nano-indentation has been widely implemented in various fields ranging from biology to material science. Oyen et al. have used nanoindentation to study biological materials and biomimetic hydrogels [6]. While Ender et al. have demonstrated that nanoindentation can be used to study compliant and highly structured biological composite materials [7]. Nanoindentation has also been widely used to study electronic materials. Liu et al. have used a Nanoindenter to study the hardness, reduced modulus, and creep rate sensitivity and perform comparative study on different solder alloys [8]. Nanoindentation has also been used to study the elastic-plastic properties of intermetallic (IMC) layers [9][10].

In addition to hardness and modulus values, the nanoindentation technique has also been implemented to characterize the viscoelastic properties of materials [3]. Wu et al. have investigated the viscoelastic behavior of biological samples by keeping a constant load and measuring the indentation depth [3]. Viscoelastic materials are materials that exhibit both viscous and elastic behavior. Different rheological models are used to model viscoelastic materials by using a combination of linear elastic springs and dashpots. Experimentally, the viscoelastic behavior is characterized through stress relaxation and creep-recovery tests. Nanoindentation has been previously used to characterize viscoelastic property through the creep test [3]. One of the rheological models used to study the viscoelastic behavior of materials is the standard linear solid model shown in Figure **2-2**. In this model, the creep behavior for a step load is given by equation 2-1 below [3].

$$h^2(t) = \frac{\pi}{2} P_o \cot\alpha \, (1 - \nu^2) \left[\frac{1}{E_1} + \frac{1}{E_2} (1 - e^{-t/\tau}) \right] \tag{2-1}$$

h(t) is indentation depth, P_o is peak force, α is equivalent cone semi-angle (70.3° for Berkovich indenter), v is Poisson's ratio, E_1 and E_2 are moduli for the elastic elements in the standard linear solid model, η is long-term creep viscosity, and τ is the creep time constant given by E_2/η.

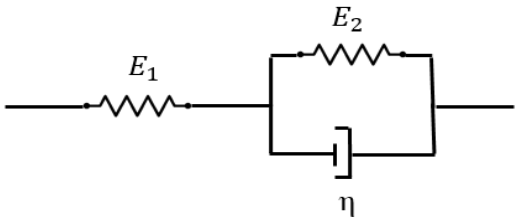

Figure 2-2: Standard linear solid model with two elastic and one viscous element.

For actual experimental conditions, a step load is hard to produce. As shown in Figure 2-1, a ramp load is often used in nanoindentation tests. Oyen has shown that the initial loading rate does not affect the time constant during the constant loading period, and the time constants can be accurately determined even for tests with ramp load conditions [3] [11]. For data analysis purposes, equation 2-1 can be simplified as follows:

$$h^2(t) = A_0 + A_1(1 - e^{-t/\tau}) \tag{2-2}$$

Where A_0 and A_1 represent the constants:

$$A_0 = \frac{\pi}{2} P_o \cot\alpha \, (1 - v^2) \frac{1}{E_1} \tag{2-3}$$

$$A_1 = \frac{\pi}{2} P_o \cot\alpha \, (1 - v^2) \frac{1}{E_2} \tag{2-4}$$

At different stages of the manufacturing process, residual stresses and strain are formed. Accurately characterizing the thermo-mechanical properties of the substrate is important to predict the residual stresses and strain and design dimensionally stable boards [12]. Shrotriya et al. have

extensively studied the creep and relaxation behavior of woven glass and epoxy substrates using dynamic mechanical analysis [12].

In this paper, the nanoindentation technique is used to measure the modulus and creep behavior of woven glass/epoxy composite substrate. By applying a constant load and measuring the indentation depth as a function of time, the viscoelastic properties of the substrate are characterized using standard linear solid model. The effect of hold time on the results from the creep test are also investigated.

2.3 Methods

2.3.1 Sample Preparation

A 134 mil board used for quad-flat no lead (QFN) packages was used for this experiment. After studying the cross section of the board under optical microscope, the required FR4 layer was exposed using a computer numerical control (CNC) machining tool. The exposed surface was polished using 1μm alumina suspension. The roughness of the surface was first measured using non-contact atomic force microscopy (NC-AFM) before the nanoindentation tests. For all tests, the sample was mounted on a metal disk as shown in Figure 2-5. Figure 2-3 and Figure 2-4 show the intermediate steps in the preparation of the sample.

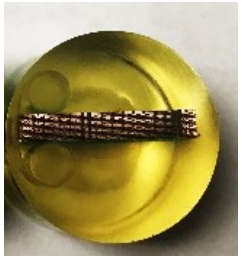

Figure 2-3: Sample prepared for cross-section imaging.

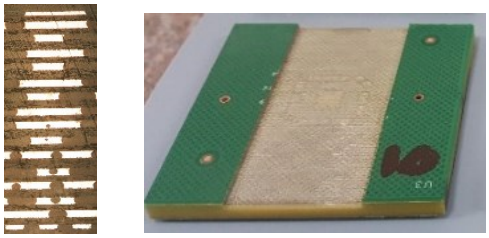

Figure 2-4: Exposed substrate layers (right) and cross section image under optical microscope (left).

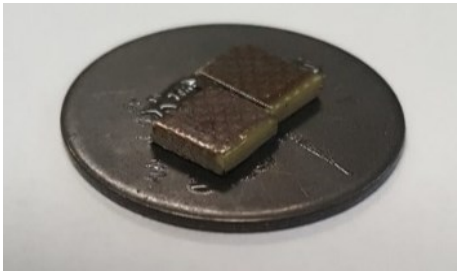

Figure 2-5: Polished sample mounted on a metal the disk before test.

2.3.2 Experiment

Surface Roughness Measurement

To measure the roughness of the surface, a non-contact tip was used on Park XE 70 AFM. The cantilever on which the tip is suspended vibrates near the surface of the sample where the near-field forces is attractive. The resonance frequency and amplitude of the vibration changes due to the tip-sample interaction. Using the oscillation amplitude as the feedback loop input, the topography of the sample is mapped. Using the parameters given in Table 2-1, the surface roughness was measured at five different locations on the exposed substrate, and the results were averaged to obtain the average roughness of the surface.

Table 2-1: Parameters used for surface roughness measurements.

Scan Rate	0.7 Hz
Z Servo Gain	6.16
Set Frequency	348.14 KHz
Amplitude	0.24 µm
X Scan Size	5µm
Y Scan Size	5µm

Nanoindentation

After the roughness of the surface was determined, a Hysitron Ubi1 Nanoindenter was used to make indents on the sample using a 100 nm diameter Berkovich tip. Two sets of experiments were carried out. For the first set of experiments, the indenter was advanced at a rate of 2.0 mN/s, held at a constant load and unloaded at 2.0 mN/s. Different loads were applied, and the modulus and hardness values were studied. For the second set of experiments, the load wad held constant for 60s at 9 mN, and the subsets of the data were analyzed to determine the effects of hold times on the viscoelastic characterization of the material. The indenter was measured to have exhibited a thermal drift of 0.21 nm/s. That was taken into consideration when studying the effect of hold time.

2.3.3 Data Analysis

The standard linear solid model was used to study the effect of hold time on characterizing the viscoelastic property the sample. The hold time is the duration for which the load was kept constant once the maximum load was reached. A maximum load of 9 mN was held for 60 s at three locations on the surface of the substrate. Using the indentation depth vs. hold time, a curve fit was performed

to obtain the corresponding creep time constant. A Mathematica code, CurveFit [13], was used to perform the fit. The parameter A_0 was taken to be 0 since the indentation depth at t = 0 due to creep is 0. To minimize the effect of thermal drift, only the indentation depth vs. time data for the first 30 s was used. A subset of the data, for hold times of 5 s, 10 s, 15 s, 20 s, 25 s, and 30 s were used to study the effect of hold time in determining the characteristics time.

2.4 Results

Roughness measurements were done using NC-AFM at five different locations of the exposed substrate layer of PCB. A zoom out image of the surface from an optical microscope is given in Figure 2-6, while a contrast NC-AFM images of different regions of the surface are given in Figure 2-7.

Figure 2-8 to Figure 2-10 show representative plots from measurement and analysis.

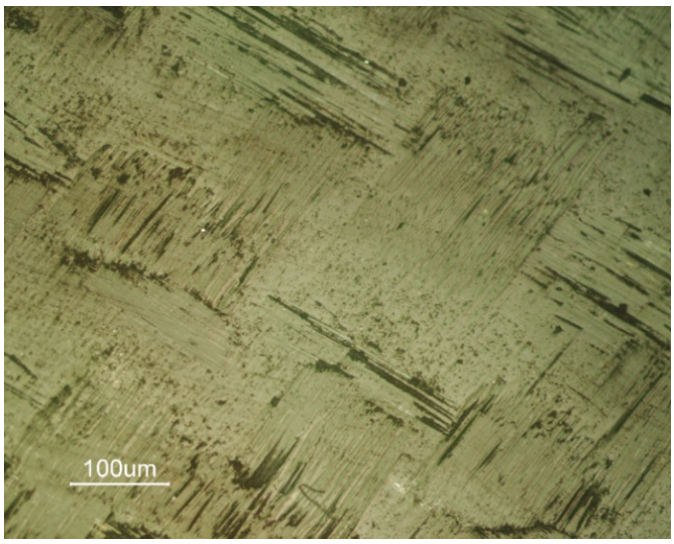

Figure 2-6: An optical image of the exposed substrate layer of PCB.

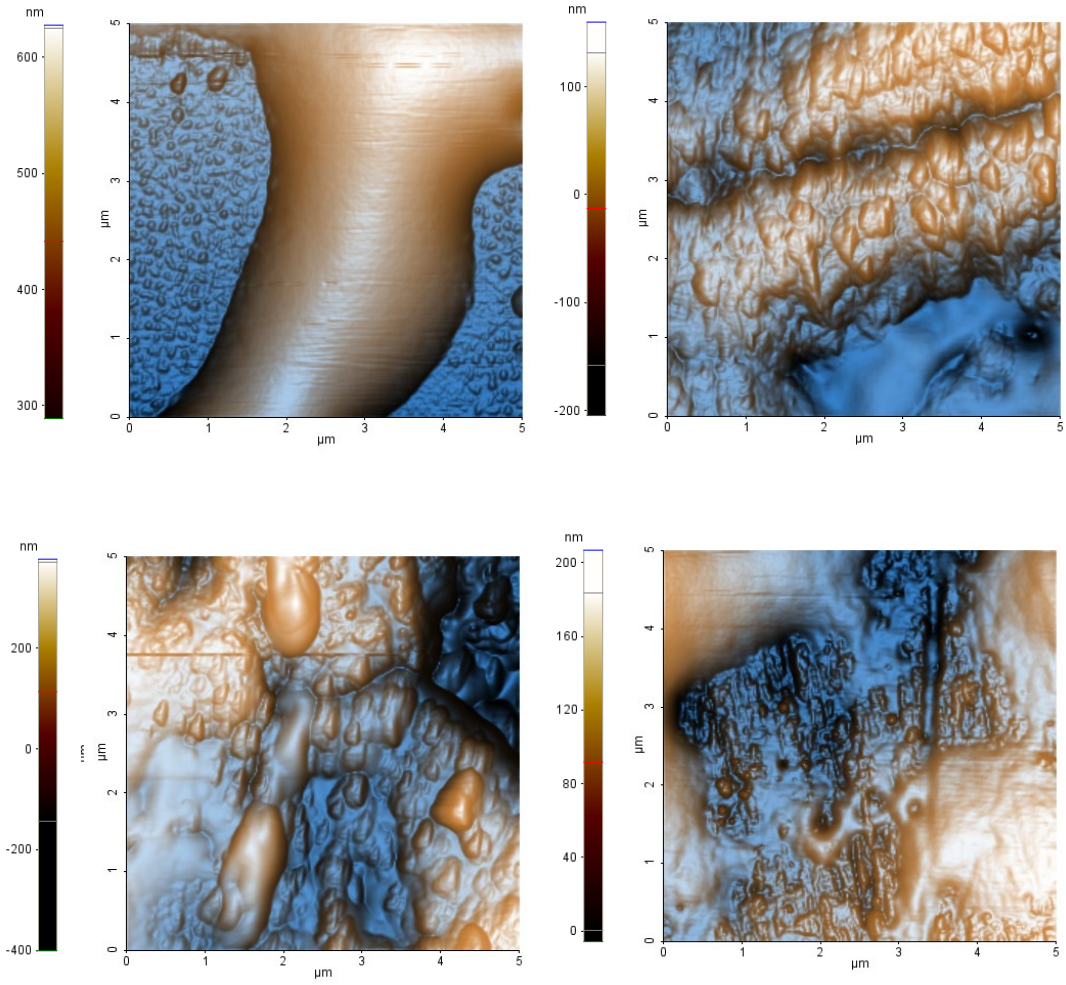

Figure 2-7: Enhanced contrast NC-AFM images of different regions on the exposed substrate layer.

Table 2-2: Roughness measured using NC-AFM at five randomly selected regions of the substrate.

Region	**1**	**2**	**3**	**4**	**5**	**Average**
Ra(nm)	79.380	61.031	95.905	37.718	36.653	62.137

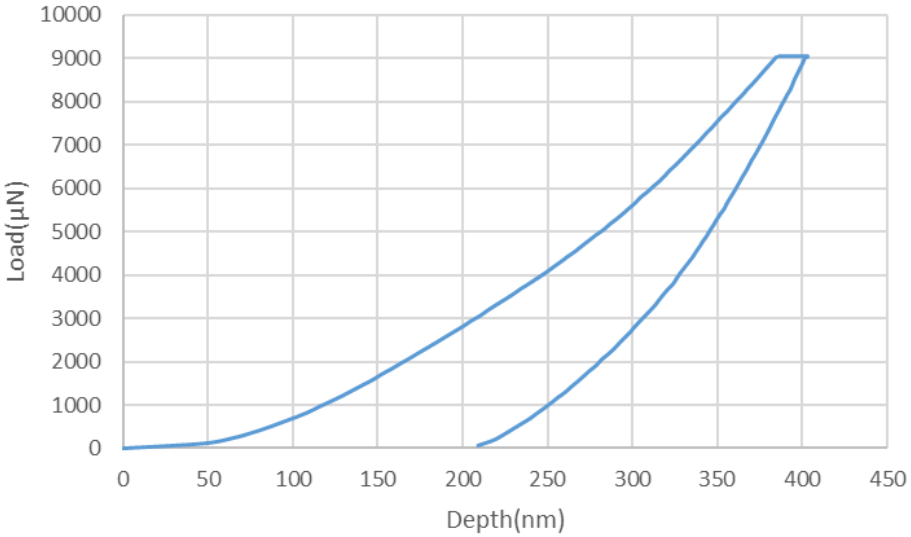

Figure 2-8: A representative load vs. indentation depth curve.

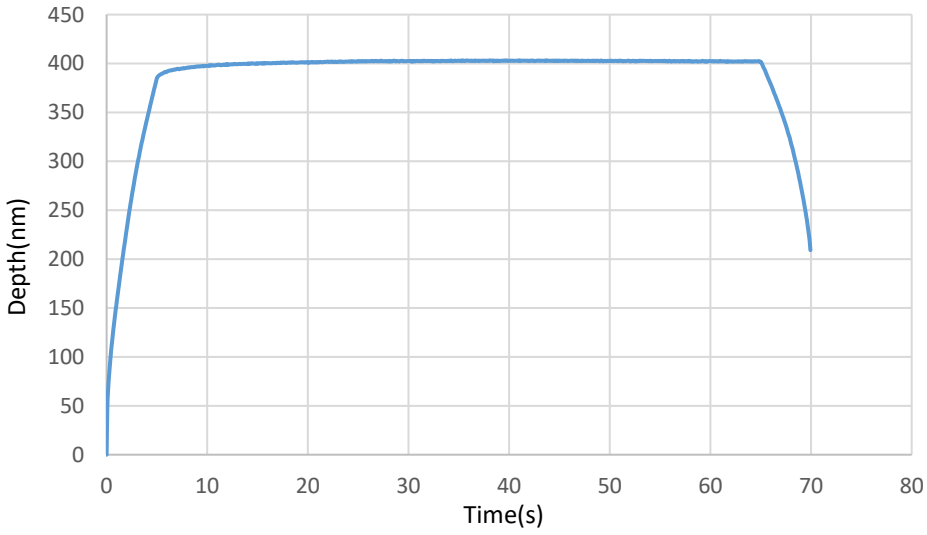

Figure 2-9: A representative indentation depth vs. time for 60 s holding time.

Table 2-3: Modulus and hardness measurements for 2 s hold time. Each indentation was made at different location on the substrate surface.

Max Load (μN)	Indentation Depth (nm)	Modulus (GPa)	Hardness (GPa)
2000.00	124.75	32.78	3.26
2000.00	92.13	49.31	5.50
4000.00	173.73	26.15	3.68
4000.00	180.35	25.70	4.32

Table 2-4: Modulus and hardness measurements for 60 s hold time. Each indentation was made at different location on the substrate surface.

Max Load (μN)	Indentation Depth (nm)	Modulus (Gpa)	Hardness (GPa)
9000.00	319.29	40.00	2.83
9000.00	360.48	38.64	2.27
9000.00	249.51	45.87	4.39

Table 2-5: Modulus and hardness measurements with same load but different hold times. Each indentation was made at different location on the substrate surface.

Maximum Load (μN)	Indentation Depth (nm)	Modulus (Gpa)	Hardness (GPa)	Hold Time (s)
3000.00	218.94	31.39	1.83	2.0
3000.00	133.40	37.30	4.36	30.0
4000.00	180.35	25.70	4.32	2.0
4000.00	173.73	26.15	3.68	2.0
4000.00	268.91	26.67	1.69	10.0

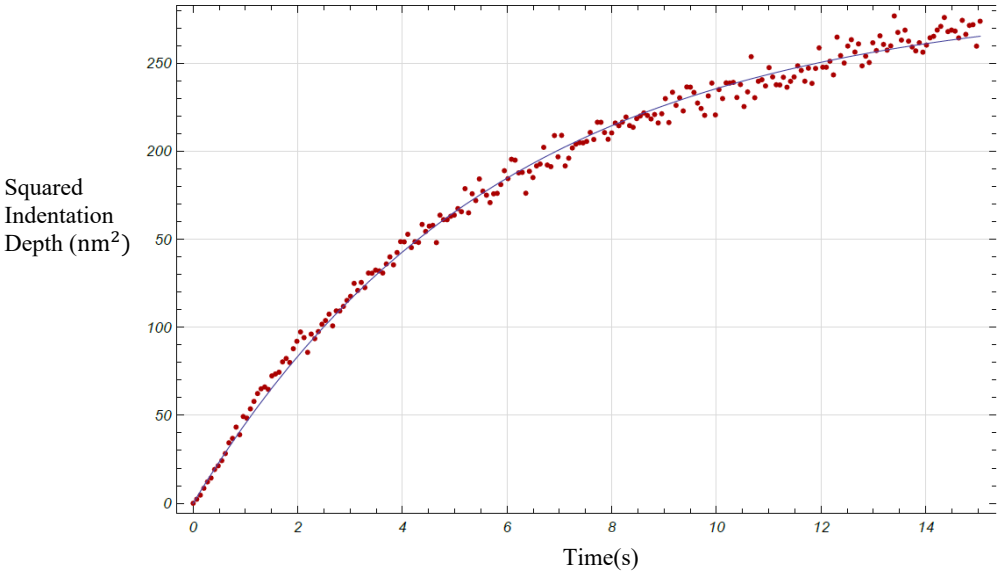

Figure 2-10: A representative creep data set and curve fit for the standard linear model with 15 s hold time.

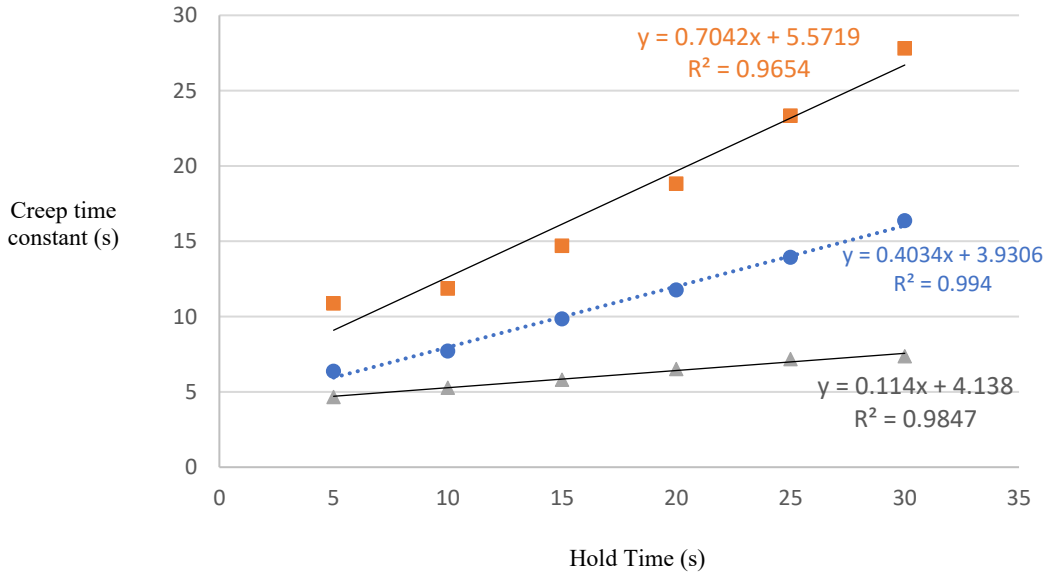

Figure 2-11: Creep time constant (s) vs. hold times (s) for three sample measurements.

2.5 Discussion

Each of the indentations was performed at different locations on the substrate. In addition, the maximum load and hold time for the measurements were varied to obtain the results presented in Table 2-3, Table 2-4, and Table 2-5. From Table 2-4, it can be seen that for the same load (9mN) and hold time (60s), the indentation depth varied by 44.5%, modulus value by 18.7%, and hardness value by 93.4%. This shows that the mechanical properties of the substrate are location dependent, and nanoindentation measurement captured the location to location variation of the mechanical properties of the substrate. In Table 2-5, nanoindentation measurements were performed at different locations with same load (3 mN and 4 mN) and different hold times. With a longer hold time, we expect larger indentation depth due to creep behavior. However, for the two measurements with 3 mN load, the indentation depth is smaller for the test with longer hold time. This is contrary to what one expects and shows that the location-to-location variation of the measurements is very strong.

After measuring 5 random locations on the surface of the substrate, the average roughness was determined to be 62.127 nm as shown in Table 2-2. Donnelly et. al. have shown that reducing the surface roughness of a sample studied using nanoindentation minimizes the variability in the measured material properties [14]. Specifically, they have shown that as the ratio of the indentation depth to surface roughness is below 3:1, the variability in the measurements is increased significantly [3]. From our measurements presented in Table 2-3, it is shown that a large load value is required to have indentation depths greater than 3x the average surface roughness. Hence, a load value of 9 mN was used for subsequent measurements.

To study creep behavior, three locations were selected on the surface of the substrate, and nanoindentation tests were performed with a load of 9 mN and a hold time of 60 s. As mentioned in the method section above, the nanoindentation measurements performed at room temperature exhibited a thermal drift of 0.21 nm/s. In order to minimize the effect of thermal drift, the subset of the data with up to 30 s of hold time was used. To obtain the time constants, the simplified equation for the standard linear model (equation 2-2) was used. The fit results were independent of the initial values used for the fit. As shown in Figure 2-11 the creep time constant is linearly proportional with the hold time. This is in agreement to what was previously reported in literature. Wu et al. has shown that the creep time constant is linear proportional to the hold time for indentation measurements done with bone samples [1]. The location dependence of the creep behavior is also evident from the three curves given in Figure 2-11.

2.6 Summary

In summary, the nanoindentation technique was successfully implemented to characterize the mechanical property of a substrate of a PCB. It was shown that a maximum load of more than 4 mN is required to have indentation depth more than 3x the average surface roughness of the sample. The surface roughness, maximum load, hold time, and location on the substrate surface were shown to be the main factors affecting the measurement values. Using the standard linear solid model, it was also shown that the characteristic time is linear dependent to the hold time.

2.7 Nomenclature

$h(t)$: Indentation depth at time t

P_0 : Peak force

E : Modulus (Pa)

η : Long-term creep viscosity (GPa s)

τ : Creep time constant (s)

v : Poisson's ratio

A_0 : Parameter used for curve fitting

A_1 : Parameter used for curve fitting

P_{max} : Maximum load

h_f : Final indentation depth

h_{max} : Maximum indentation depth

α : Equivalent cone semi-angle

2.8 References

[1] S. G. Jagarkal, M. M. Hossain, D. Agonafer, M. Lulu and S. Reh, "Design optimization and reliability of PWB level electronic package," *The Ninth Intersociety Conference on Thermal and Thermomechanical Phenomena In Electronic Systems (IEEE Cat. No.04CH37543)*, 2004, pp. 368-376 Vol.2.

[2] Wang, Yuqi, et al. "Modeling and simulation for a drop-impact analysis of multi-layered printed circuit boards." Microelectronics Reliability 46.2-4 (2006): 558-573.

[3] Wu, Ziheng, et al. "The effect of holding time on nanoindentation measurements of creep in bone." Journal of biomechanics 44.6 (2011): 1066-1072.

[4] Oliver, Warren C., and Georges M. Pharr. "Measurement of hardness and elastic modulus by instrumented indentation: Advances in understanding and refinements to methodology." Journal of materials research 19.1 (2004): 3-20.

[5] Oliver, W., & Pharr, G. (2004). Measurement of hardness and elastic modulus by instrumented indentation: Advances in understanding and refinements to methodology. Journal of Materials Research, 19(1), 3-20.

[6] Oyen, M. L. "Nanoindentation of biological and biomimetic materials." Experimental Techniques 37.1 (2013): 73-87.

[7] Enders, S., et al. "Exploring biological surfaces by nanoindentation." Journal of materials research 19.3 (2004): 880-887.

[8] Liu, C. Z., and J. Chen. "Nanoindentation of lead-free solders in microelectronic packaging." Materials Science and Engineering: A 448.1-2 (2007): 340-344.

[9] Xu, L., & Pang, J. H. L. (2006). Nanoindentation on SnAgCu lead-free solder joints and analysis. Journal of Electronic Materials, 35(12), 2107-2115.

[10] Choudhury, Soud Farhan, and Leila Ladani. "Grain growth orientation and anisotropy in Cu6Sn5 intermetallic: nanoindentation and electron backscatter diffraction analysis." Journal of electronic materials 43.4 (2014): 996-1004.

[11] Oyen, Michelle L. "Spherical indentation creep following ramp loading." Journal of Materials Research 20.8 (2005): 2094-2100.

[12] Shrotriya, P., and N. R. Sottos. "Creep and relaxation behavior of woven glass/epoxy substrates for multilayer circuit board applications." Polymer composites 19.5 (1998): 567-578.

[13] Caltech Ph 6. http://www.sophphx.caltech.edu/Physics_6/CurveFit/ . 26 November 2017.

[14] Donnelly, Eve, et al. "Effects of surface roughness and maximum load on the mechanical properties of cancellous bone measured by nanoindentation." Journal of Biomedical Materials Research Part A77.2 (2006): 426-435.

Chapter 3
Impact of Aging on Mechanical Properties of Thermally Conductive Gap Fillers[2]

3.1 Abstract

Thermal interface materials (TIMs) are an important component in electronic packaging, and there is a concerted effort to understand their reliability when used under various environmental load conditions. Previous researchers have investigated gap fillers and other types of TIMs to understand their performance degradation under loading conditions such as thermal cycling and thermal aging. Most of the study in the literature focuses on studying the changes in thermal properties, and there is a lack of understanding when it comes to studying the mechanical behavior of TIMs. Degradation of mechanical properties is the cause for the loss in thermal performance and is critical during TIM selection process. Moreover, mechanical properties such as modulus and thermal expansion coefficient (CTE) are critical to assess performance of TIMs using finite element analysis (FEA) and potentially save time and money in the evaluation and selection process. Due to the very soft nature of TIMs, sample preparation is a challenging part of material characterization. In this paper, commercially available TIMs are studied using testing methods such as TMA, DMA, and FTIR. These methods are used to characterize the material properties and study the changes in properties due to aging. In this work, the followings are presented: impact of filler content on the mechanical properties, sample preparation method for curable TIM materials with specified thicknesses, and impact of thermal aging on mechanical properties.

[2] *The work presented in this chapter has been published in ASME Journal of Electronic Packaging. Included here with written permission from ASME. Citation of the publication is given below:*
Misrak, A., Chauhan, T., Rajmane, P., Bhandari, R., and Agonafer, D. (November 8, 2019). "Impact of Aging on Mechanical Properties of Thermally Conductive Gap Fillers." ASME. J. Electron. Packag. *March 2020; 142(1): 011011.* https://doi.org/10.1115/1.4045157

3.2 Introduction

3.2.1 Background

Thermal Interface Materials (TIMs) are an important component of electronic packages that are used to minimize contact resistance between mating parts. With the utilization of more efficient thermal cooling options (e.g. liquid cooling solutions), a significant portion of the temperature drop from the die to the ambient occurs across TIMs. Due to this, TIMs are the bottle necks in the thermal design process and a wide range of research is currently being undertaken to develop next generation TIMs. Chow et. al. have investigated electroplated copper nanowires as Thermal Interface Materials [1]; Sun et. al. have proposed a novel nanocomposite thermal interface material [2] ; while, Tong et. al. have investigated the use of carbon nanotube (CNT) arrays as thermal interface materials [3]. More recently, cubic boron arsenide and boron phosphide crystals have been used to develop high thermal conductivity thermal interface materials [4] [5]. Li et. al. used chemical vapor transport technique to develop high thermal conductivity cubic boron arsenide crystals that have thermal conductivity values closer to 1000 W/mK [4]. Zheng et. al. studied cubic boron phosphide crystals and showed that thermal conductivity of close to 500 W/mK can be attained at room temperature [5]. Yuan et. al. studied vertically aligned carbon nanotube arrays (VACNTs) used to make light weighted TIMs with improved mechanical properties [6]. Novel concepts such as metal nano-springs [7] and graphene aerogel [8] have also been investigated by other researchers. These are exciting frontiers but are years away from being widely used in the industry.

Without the use of TIMs, the actual contact area between two mating surfaces is reduced by up to two orders of magnitude due to the microscopic surface roughness [9]. Air has a very low thermal conductivity and will significantly increase the contact resistance between the mating surfaces if no thermal interface material is used. According to Gwinn et. al., an ideal TIM would

have the following characteristics: very high thermal conductivity, low thickness, deformable in order to conform to rough surfaces (Figure 3-1), maintain performance indefinitely, manufacturable, stay in place, and not toxic [10]. Unfortunately, an ideal TIM that satisfied all these criteria has not been developed yet.

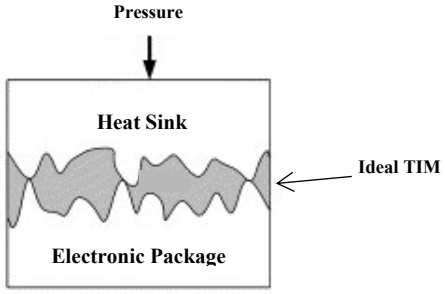

Figure 3-1: Thermal interface with an ideal TIM [5]

Commercially available TIMs, though are not ideal, excel in some of the criteria and are used in different applications. The major types of TIMs currently used in the industry can be categorized to the following groups: greases, phase change materials (PCMs), elastomeric pads, thermal conductive gap fillers, and epoxies [11] [12]. Most of these TIMs are manufactured by adding high thermal conductivity fillers such as metals (e.g. silver) or ceramics (e.g. aluminum nitride or boron nitride) to organic matrix such as silicone grease [13]. The mechanical compliance due to the mechanical properties of the organic matrix and the higher thermal conductivity due to the fillers is the desired property of such TIMs [13].

Thermal greases are one of the most extensively used types of TIMs in the industry [13]. Thermal greases are pastes made up of a silicone or hydrocarbon oil and highly thermal conductive fillers [10]. Thermal greases excel at achieving high thermal conductivity with small contact pressures [14]. The ease of rework also makes them ideal for many applications [13]. However, their susceptibility to pump-out and dry-out put them at a great disadvantage [10]. The pump-out is caused by the coefficients of thermal expansion (CTE) mismatch between the components that

sandwich the thermal grease [15]. Dry-out of thermal greases happen due to the separation of the fillers from the matrix due to thermal cycling [16] or high temperatures [17] [18]. On the other hand, thermally conductive elastomer pads are another group of TIMs that are commonly used in the industry. The elastomer pads are solids and can have very high thermal conductivity. However, they require very high contact pressure in order to fill interstitial voids and reduce the contact resistance [19]. Another group of TIMs, thermally conductive gap fillers, can fill interstices like thermal greases but do not pump out as they cure in-place. Thermally conductive gap fillers are elastomer pastes mixed with fillers that have high thermal conductivity [10]. They are applied in paste form and cure in place conforming to mating surfaces without requiring very high contact pressures. Despite their moderate thermal performance, thermally conductive gap fillers offer a unique solution for cases where thermal greases are not applicable and there is a limitation on the amount of pressure that can be applied on packages. Especially, such gap fillers are used as TIM 2 materials as shown in Figure 3-2 below.

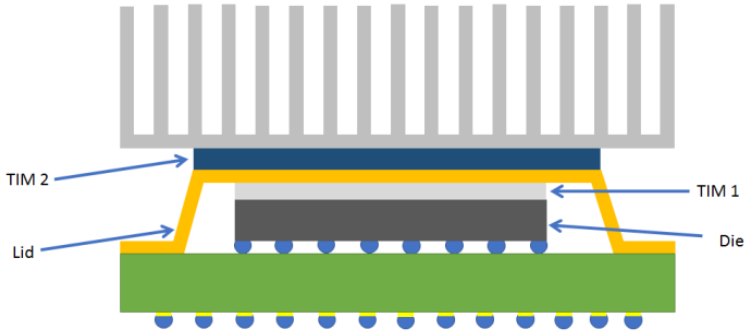

Figure 3-2: TIM 1 and TIM 2 used in electronic packaging. TIM 1 is used between die and lid, while TIM 2 is used between lid and heat sink.

The reliability of TIMs is assessed by comparing the End of Life (EOLife) performance to the Beginning of Life (BOLife) performance [13]. The performance data needed for the assessment is not usually available as the TIM sample is required to have undergone the entirety of its service

life [13]. As Goel et. al. have highlighted, there is a big challenge in studying the degradation of TIMs in use conditions [12]. Standard testing methods such as ASTM D5470 neglect the topography of mating surfaces, loading mechanism, pressure, etc. and are unable to capture thermo-mechanical impact on an application specific use conditions [12]. Hence, accelerated stress tests are used to study the reliability of TIMs and represent the possible environmental load conditions the TIMs may be exposed to [13]. Three of the most common stress test categories are: high temperature storage test, temperature/power cycling tests, and temperature and humidity tests [13]. Previous researchers have studied the reliability of different kinds of TIMs under the various stress conditions. Okereke et. al. numerically studied effect of three-dimensional void morphology on thermal resistance of solder TIMs and showed that the increase in thermal resistance stems from cylindrical and spherical void shapes, distribution and polydispersity [20]. However, as Due et. al. have pointed out, reliability testing of TIMs is not as mature as the reliability study of other components such as solder joints [13]. This lack of literature information on the mechanical properties of TIMs has been the focus of recent publications; for example, Subramanian et. al. has recently published a paper that studied the challenges, such as the soft nature and low thicknesses of samples, in performing mechanical characterization and performing reliability studies of thermal interface materials [21].

High temperature storage test, also known as bake test, is an accelerated stress test that represents the continuous high temperature conditions experienced by TIMs [22]. The thermal resistance of TIMs was observed to have increased after high temperature storage tests [13]. Cracking due to the hardening of the bulk polymer through thermal aging has been attributed as the cause for the increase in thermal resistance for siloxane-based TIMs [23]. For siloxane-based TIMs, thermal degradation of ~15 – 50 % has been reported [23] [24] [25].

Most of the commercially available thermally conductive gap fillers have a siloxane-based matrix mixed with ceramic fillers such as Aluminum Oxide. Unlike siloxane-based thermal greases or gels, these TIMs are in the solid state at BOLife. This presents us with an opportunity to characterize the mechanical properties at BOLife and EOLife, and further understand the causes for increased thermal resistance after thermal aging. In this paper, a repeatable sample preparation method is used to perform material characterization of TIMs using Dynamic Mechanical Analyzer (DMA) and Thermo-mechanical Analyzer (TMA). These methodologies are used to study the impact of filler content and aging on the modulus and CTE values. Fourier Infrared Spectroscopy (FTIR) is also used to study the impact of aging on the samples. The goal of this paper is to study the changes in mechanical properties to understand and assess reliability of thermal interface materials. Understanding the changes in mechanical properties will allow researchers to assess the mechanical behavior of the materials and potentially run computational studies to understand phenomenon such as cracks and delamination. The paper is organized as follows: experimental procedures are discussed in section 2; results are given in section 3, while discussion and conclusions are given in section 4 and 5 respectively.

3.2 Materials and Methods

3.2.1 Sample Preparation

For this study, two commercially available thermally conductive gap fillers were used. They will be referred to as TIM A and TIM B throughout this paper. TIM A has thermal conductivity of ~4 W/m-K, while TIM B has thermal conductivity of ~ 6 W/m-K. Both TIMs are silicone-based materials, and the difference in property is understood to be due to the change in filler content. The assembly shown in Figure 3-3 below was used to prepare samples with uniform thickness.

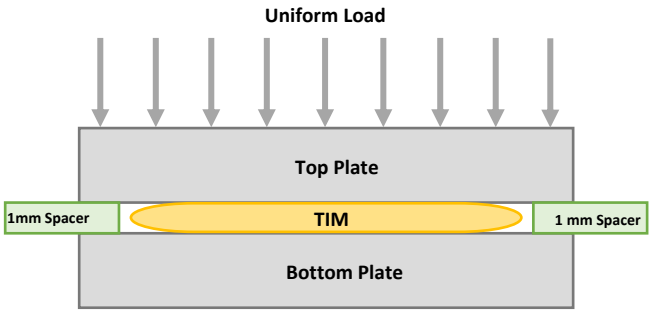

Figure 3-3: Schematic of assembly used to prepare samples.

The TIM was sandwiched between two aluminum plates. 1 mm spacers made of boards were used at the 4 corners of the assembly to maintain uniform thickness. After dispensing the TIMs and applying a uniform load, samples were kept at room temperature (25 °C) for 24 hours to cure. After samples were cured, the load and the top plate were removed. Figure 3-4 shows cured samples for TIM A and TIM B after top plate is removed. Removing the top plate without damaging the samples was a challenging part of the sample preparation.

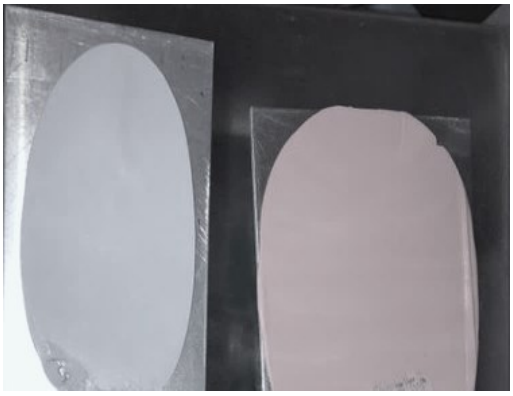

Figure 3-4: Cured samples after removing the top plate.

Authors faced lot of difficulties while separating top plate from the assembly. Figure 3-5 shows wasted samples after removal of top plates. One of the main lessons learnt during the process was that when preparing samples, one need to make sure that the plates used for sample preparation do not have very large surface area. This is because when using larger plates, the

adhesion between the TIMs and plate will be very strong and make it difficult to remove the top plate. The successfully prepared samples were made on rectangular plates which had relatively smaller surface area. Careful inspection is also required to make sure the samples used for testing do not have defects.

Figure 3-5: Wasted samples.

Samples for DMA tests were prepared by cutting the cured samples shown in Figure 3-4. As shown in Figure 3-6, 35 - 40 mm by 10 mm samples were prepared for DMA testing.

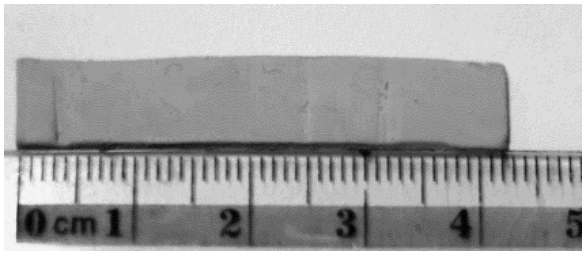

Figure 3-6: Sample used for DMA measurement.

To study the impact of thermal aging on the mechanical properties of TIMs, half of the samples from each set were placed in an environmental chamber for high temperature aging at 125℃ (JESD22-A103, Condition A) for 720 hrs. The remaining samples were tested to obtain pre-aging measurements.

3.2.2 Experimental Procedure

Thermomechanical Analysis

Samples used for TMA testing were rectangular with typical length of 7 mm, width of 7 mm, and 1 mm thickness. The width and length are chosen to maintain minimum of 1 mm margin between sample edge and probe to achieve uniform and even contact between probe and top surface of sample. Visual inspection was performed while selecting the test samples for voids and defects. Stainless steel blade was used to cut the samples.

To make sure TMA probe tip is free of TIM residuals, probe tip was cleaned with ethanol between each experiment. Sanity check was performed by measuring CTE of Aluminum from 25 °C to 180 °C and comparing results with those found in the literature.

For measuring CTE, zero or negligible force is applied on samples to measure expansion/compression with respect to change in temperature. For measuring CTE of aluminum, a load of 100 mN is applied to ensure proper contact between sample and probe. As the TIM samples were significantly softer than Aluminum, set of experiments were carried out to determine the proper loading conditions. Measurements were performed with loads ranging from 1 mN to 100 mN. 100 mN was strong and deformed the sample. 1 mN was too low and proper contact was not maintained between probe tip and sample surface. 10 mN loading proved optimum for maintaining proper contact between TMA probe tip and sample without causing deformation.

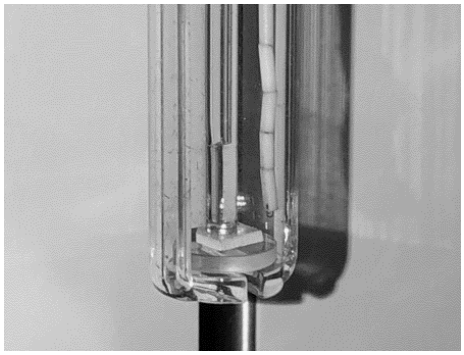

Figure 3-3: TIM placed on stage for TMA testing.

Temperature range of -40 °C to 150 °C was selected for comparing CTE values of the two TIMs. For TMA tests done to study the impact of aging on mechanical properties, a temperature range of 25 °C to 150 °C was selected.

Isothermal hold was applied at the initial temperature to ensure the sample temperature was at the desired value. A stability criterion of having temperature fluctuation within ±2 °C of the initial temperature was used before the start of the test. Isothermal hold also allowed samples to recover the effect of 50 mN load that was applied for 30 – 50 seconds during sample length measurements. Sample dimensions were measured with digital caliper that has an accuracy of 0.02 mm. Thickness of samples was measured by TMA with an accuracy of 0.05 mm. Samples were placed on the sample holder tube as shown in Figure 3-3, and the experiment was performed for the specified temperature range with a ramp rate of 2 °C/min. Due to the small size of samples and good conductivity of the materials, the materials responded well to the temperature changes in the furnace. There was some lag between oven and sample temperatures. This was mitigated by having a lower ramp rate (compared to 10 °C/min used in literature) and by holding at the end temperature for extra minutes.

Dynamic Mechanical Analysis

Samples used for DMA tests had a length of ~35 - 40 mm, width of 7 mm, and 1 mm thickness. Visual inspection was performed to remove samples with voids and defects. Recommended settings (Table 3-1) for soft materials were used for testing the TIMs in the tensile mode. The experiment was performed for 0.5, 1, 2, 5 and 10 Hz. The behavior of viscoelastic materials is temperature and frequency dependent, and the five frequencies selected are those commonly used in the industry. To compare the property of pre-aging and post-aging samples, measurements for 1 Hz were used. Temperature range of -40 °C to 150 °C was used for

the measurements. Sample dimensions were measured using digital caliper which has an accuracy of 0.02 mm. Samples were assumed to have uniform cross section area. Figure 3-4 shows samples mounted for testing.

Table 3-1: Settings used for DMA testing in tensile mode.

Parameters	***Value***
Minimum tension/ compression force	50 mN
Tension/ compression force gain	1.2
Force amplitude	50 mN

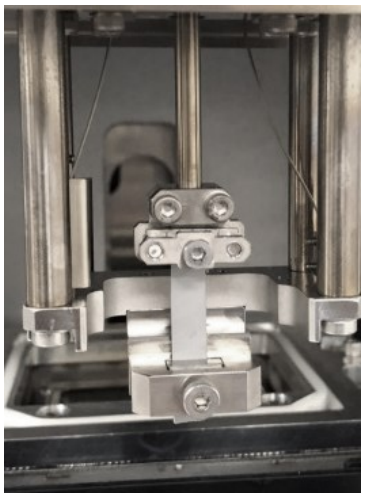

Figure 3-4: TIM attached for DMA testing.

Fourier-Transformed Infrared Spectroscopy (FTIR)

For absorbance measurements, the following parameters were selected: 32 scans, resolution of 4 cm^{-1}, and range of 4000 – 600 cm^{-1}. After collecting the background, a small sample with dimensions of 1 mm by 1 mm was prepared and placed for measurement as shown in Figure 3-5.

Figure 3-5: Sample placed in FTIR for measurement.

3.3 Results

For each TIM, at least four samples were tested, and the averaged DMA results are used for comparison purposes. Figure 3-6 shows a comparison of storage and loss modulus for TIM A and B before thermal aging. Figure 3-17 shows a comparison of storage and loss modulus for TIM A and B after high temperature aging. For both figures, results are normalized to the measured values of TIM B at the start temperature.

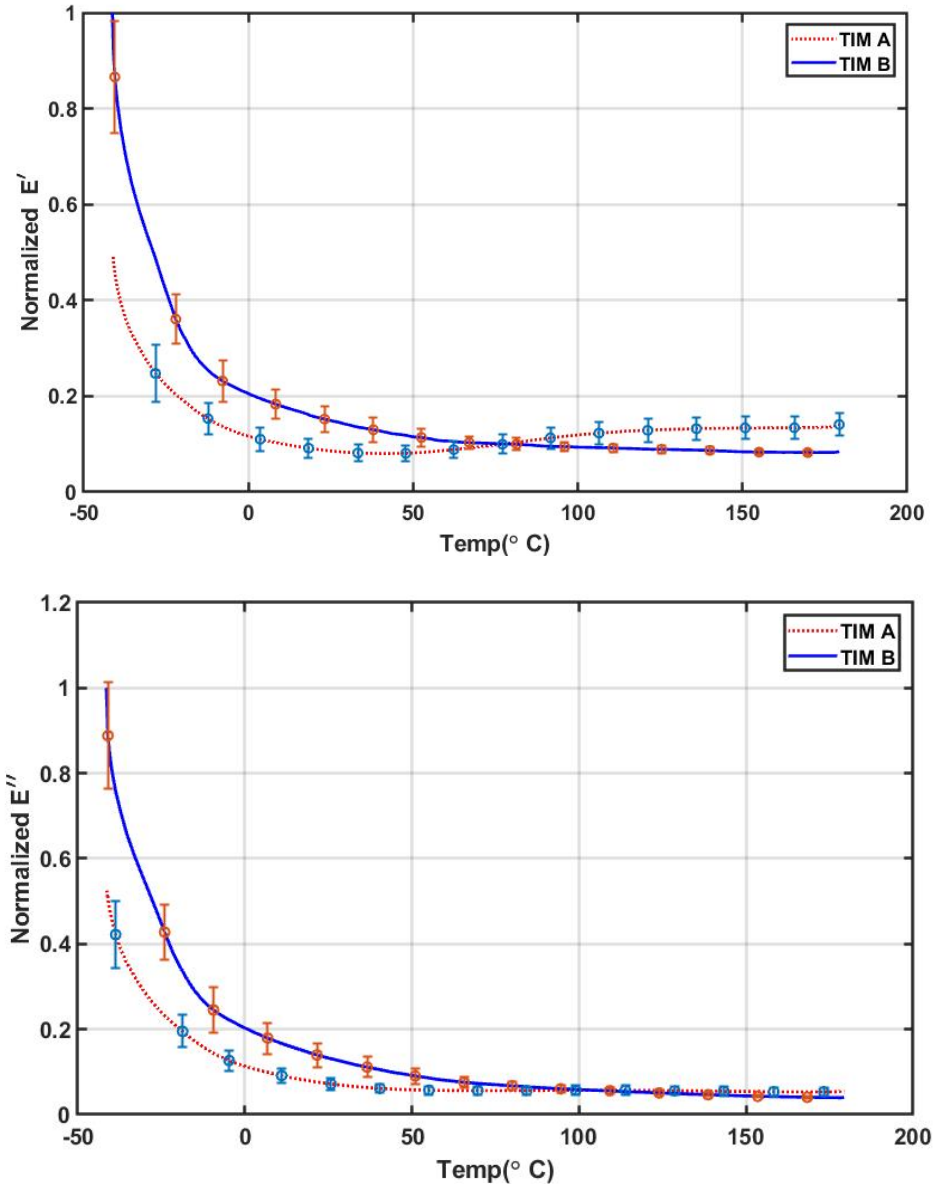

Figure 3-6: Pre-aging DMA measurements. Comparison between TIM A and B shown for storage modulus (top), loss modulus (bottom).

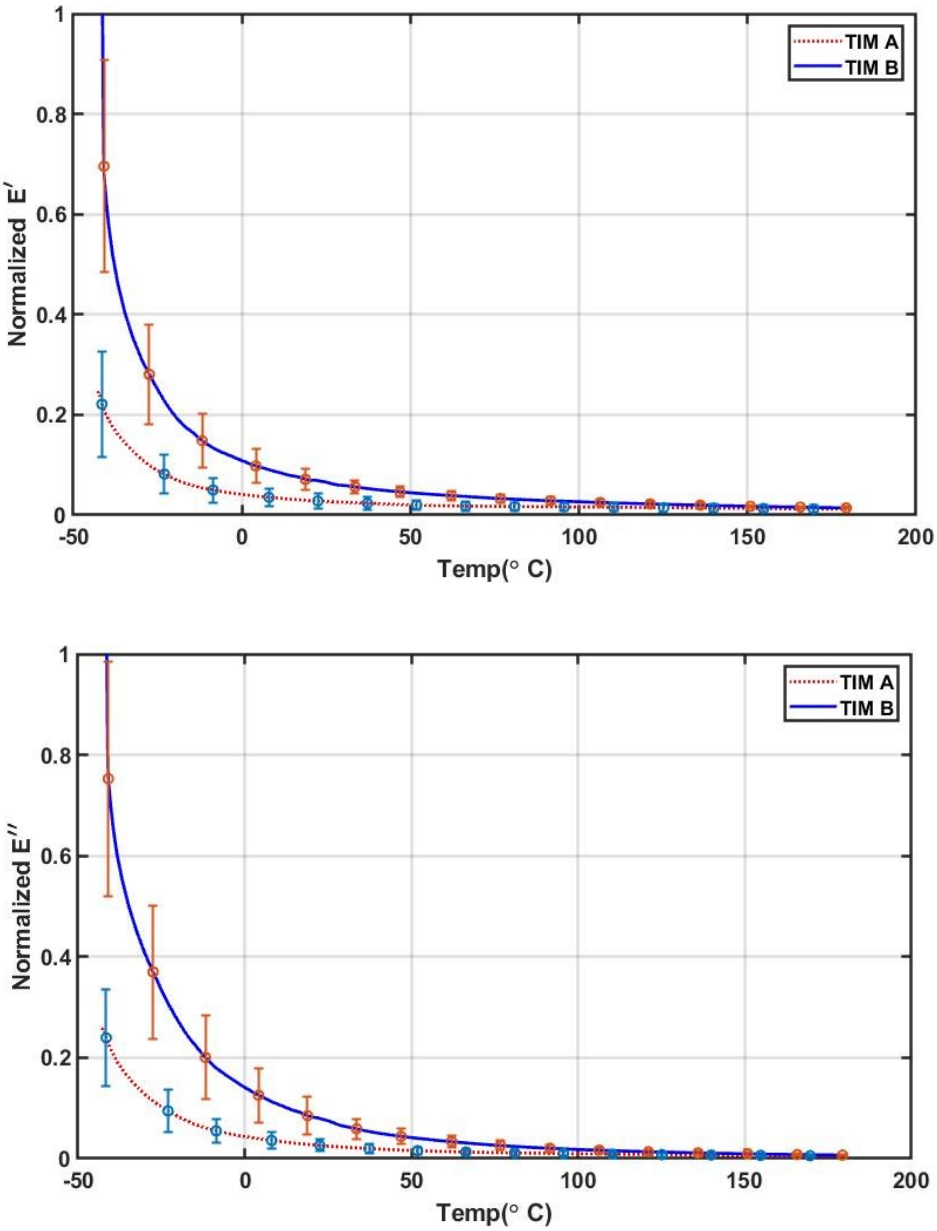

Figure 3-17: Post-aging DMA measurements. Comparison between TIM A and B shown for storage modulus (top), loss modulus (bottom).

Equation (3-2) was used to compute the complex Modulus, and Figure 3-8 shows a comparison between the computed complex Modulus values for pre-aging and post-aging samples. For both figures, results are normalized to the post aging values at the initial temperature.

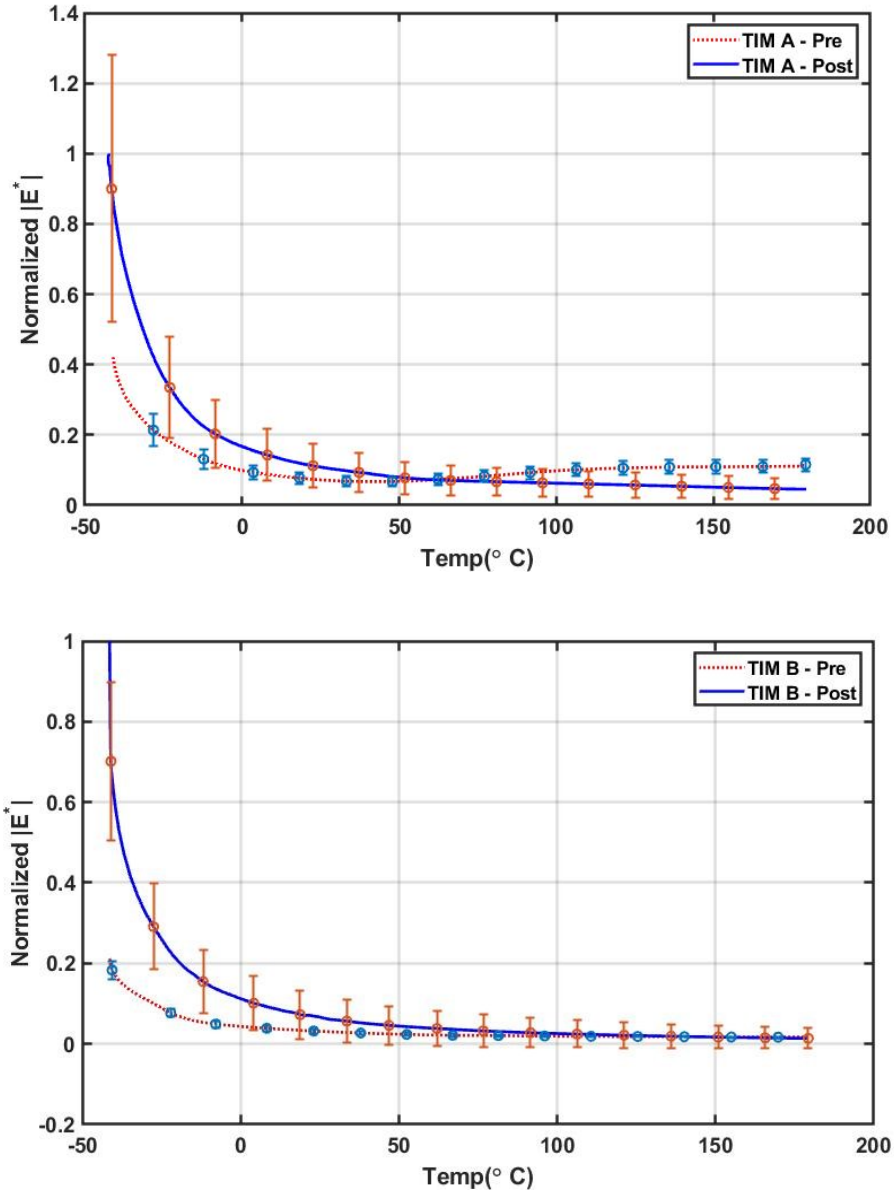

Figure 3-8: Complex modulus comparison between pre aging and post aging samples for TIM A (top), TIM B (bottom).

For the range of wavenumber tested, 4000 – 600 cm^{-1}, a representative FTIR result is given in Figure 3-9. Table 3-2 shows the main peaks identified for the given range. A comparison was also made between measurements taken before and after high temperature aging. Results are given in Figure 3-10.

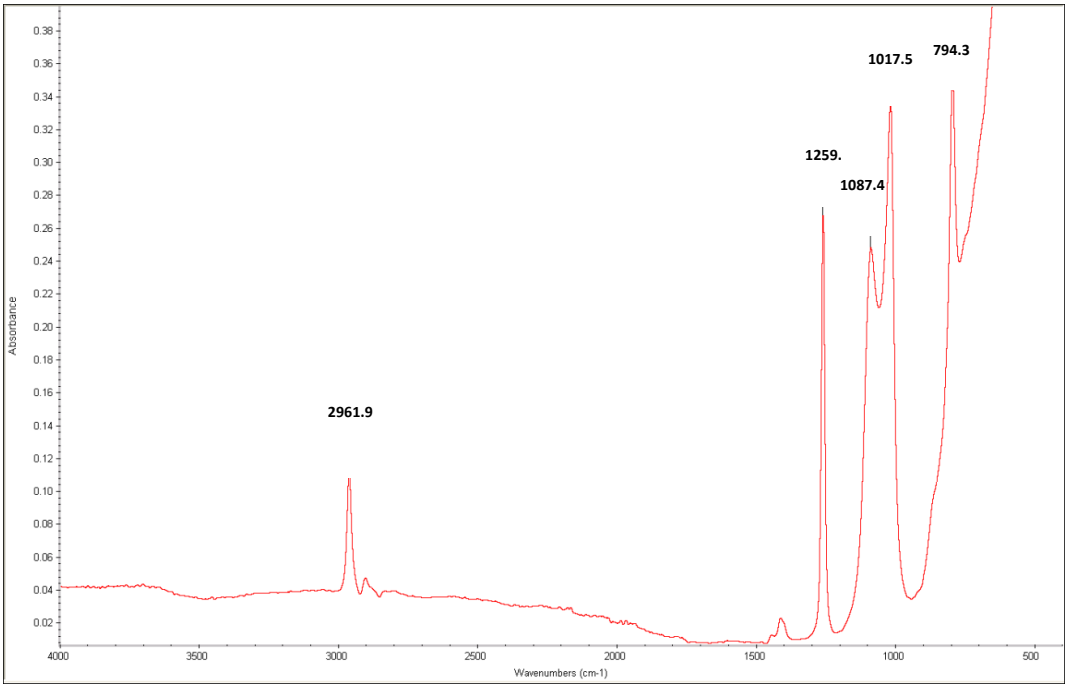

Figure 3-9: FTIR result showing major peaks. All the TIMs studied as part of this work exhibited the same peaks. A representative result for TIM A is shown above.

Table 3-2: Major Peaks identified from FTIR results [28] [29].

Peaks	**Wavenumber (cm^{-1})**	**Possible Group**
1	2961.9	v – (CH_3)
2	1259.5	Si – (CH_3)$_2$
3	1087.4	Si – O
4	1017.5	Si - O
5	794.3	Si - C

Figure 3-11 and Figure 3-12 show results obtained from TMA experiments. Figure 3-11 shows the relative length comparison between TIM A and B samples before high temperature aging. Figure 3-12 shows a relative length comparison between the pre aging and post aging measurements for the two TIMs.

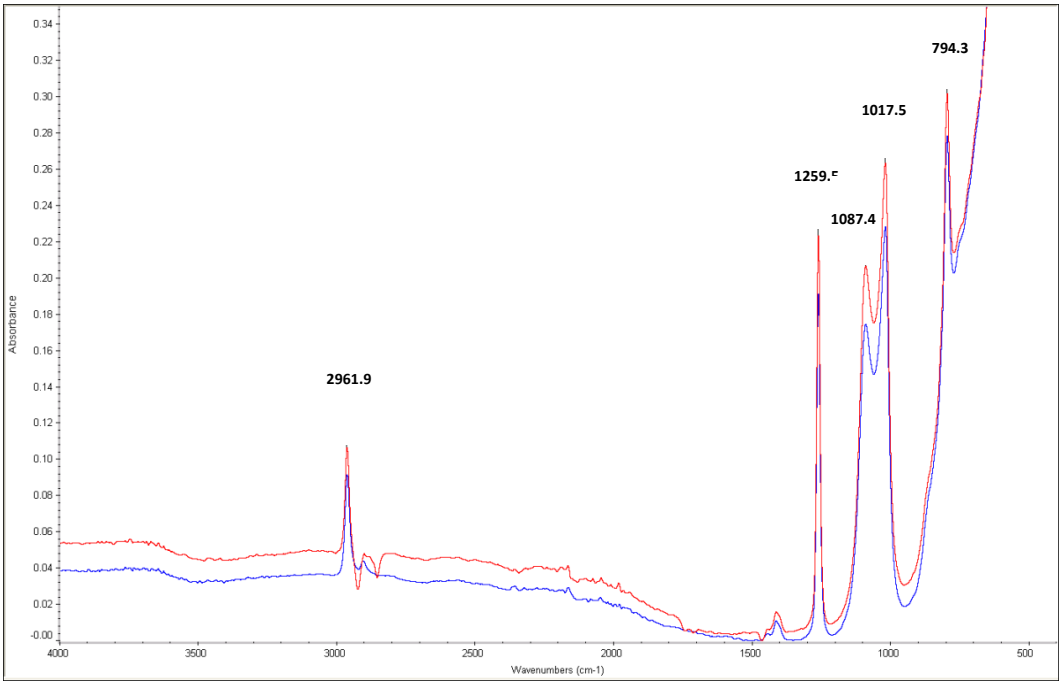

Figure 3-10: FTIR comparison between pre aged and post aged samples for TIM B.

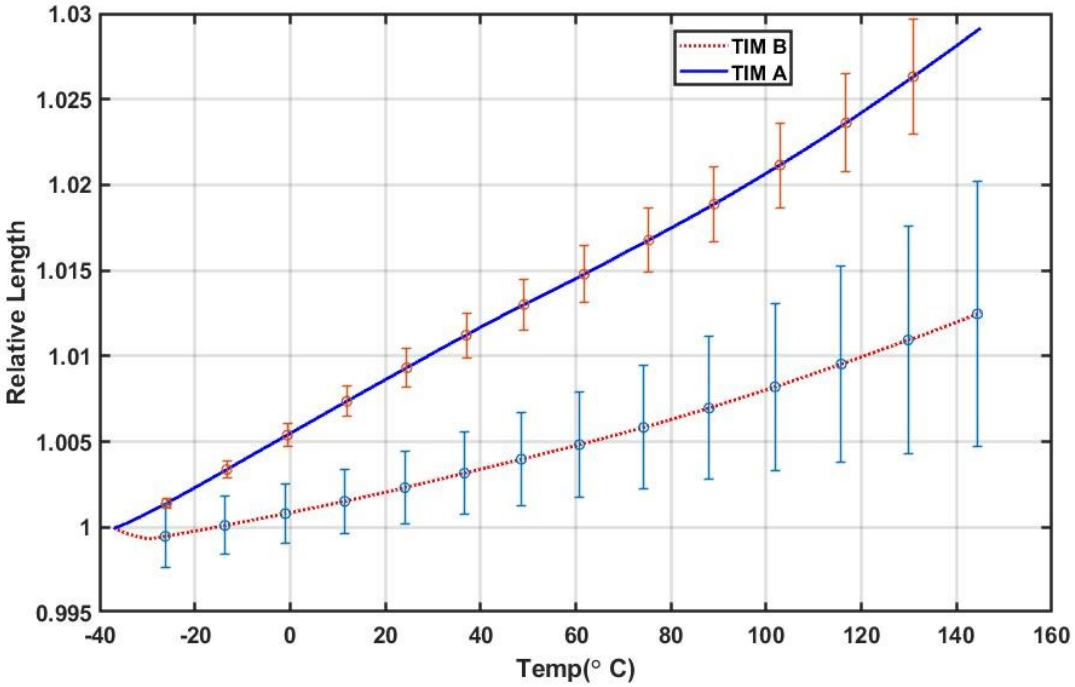

Figure 3-11: TMA result comparison between TIM A and TIM B before high temperature aging.

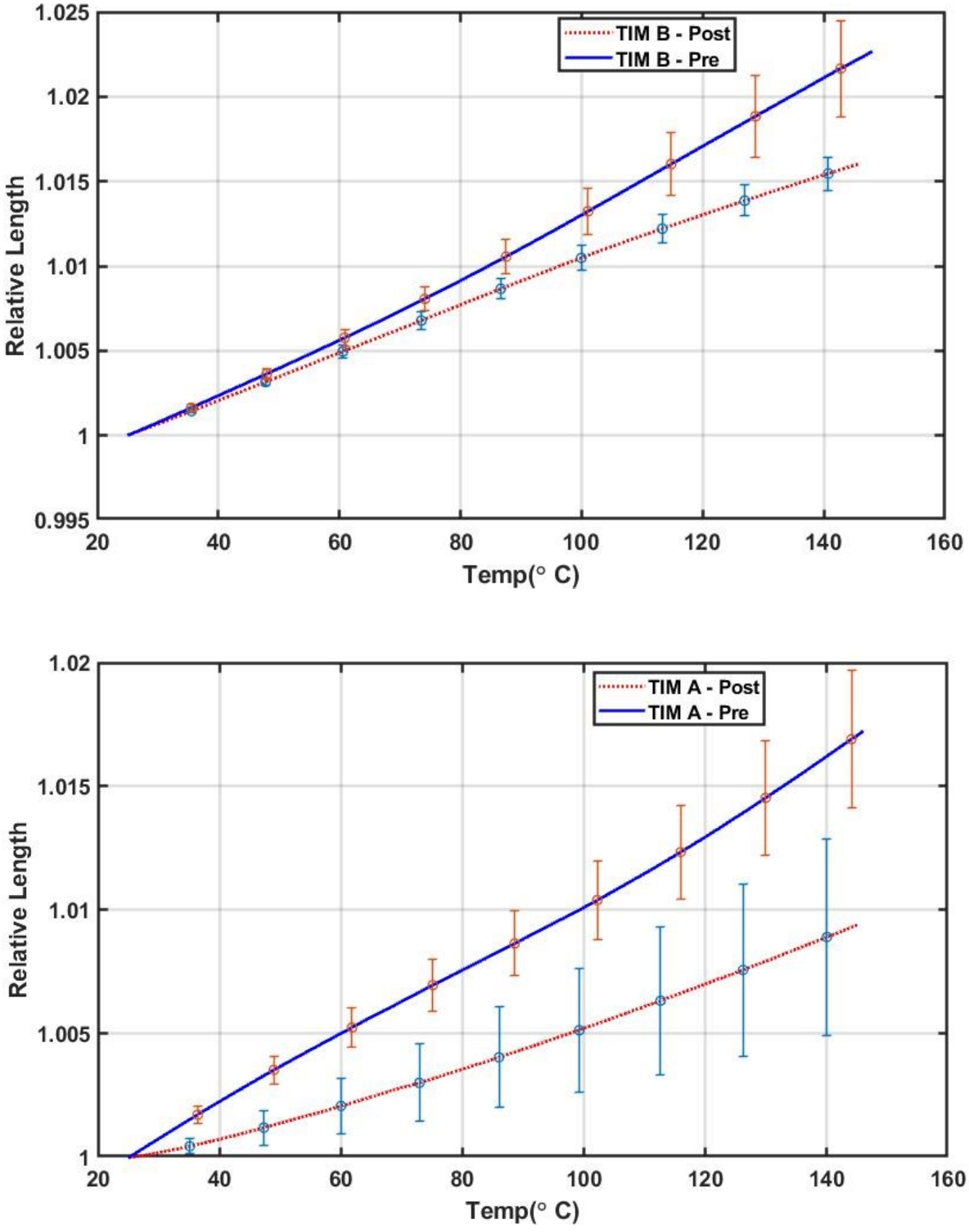

Figure 3-12: TMA comparison for before and after aging cases for TIM B (top) and TIM A (bottom).

3.4 Discussion

In section 3.3, Figure 3-6 to Figure 3-8 show results from DMA measurements for TIM A and TIM B. Each plot is an average of at least four measurements. TIM A results showed an average of 20 % standard deviation, while TIM B showed an average of 13% standard deviation. TIM B which had better thermal performance, i.e. higher filler content, had lower standard deviation because it is stiffer and is easier to mount for measurements. Possible causes for the large deviations for both tests are: sample to sample variation due to void content, slight variation in width of samples, and the difference in clamping force used to attach the samples. Due to the soft nature of both TIM materials, there was a challenge in attaching samples to the tensile attachment shown in Figure 3-4, especially for TIM A. The screws were tightened until there was enough pressure to keep the samples in place during the measurements. However, there were instances where some samples broke due to the force concentration at the clamps. At the start temperature, an isothermal hold was applied until the sample and chamber temperatures reached equilibrium. This significantly increased the test time, and each DMA experiment took about 3 hours to complete. The above presented data shows that the glass transition temperature of the TIM materials lies outside the temperature range used for testing (-40 °C – 150 °C). For all samples tested with DMA, no peak was observed for the loss modulus in the given temperature range. For few DMA measurements performed with starting temperature below -40 °C, it was observed that the samples were significantly stiffer, and the tension/compression force and force amplitude had to be changed from the values shown in Table **3-1**. Hence, we can conclude that the glass transition temperature (T_g) is below -40 °C. From literature, the glass transition temperature for polymer based TIMs is expected be below -80 °C [21].The complex modulus, which is comparable to Young's modulus, value of the two studied TIMs is measured to be orders of magnitudes lower than other components in the stack-up of electronic packages.

As both TIM A and TIM B are silicone based TIMs, the performance enhancement is understood to be due to the higher concentration of high thermal conductivity fillers such as alumina which have higher Modulus when compared to the silicone matrix. The TIMs with higher filler content are generally expected to have higher modulus values. As shown in Figure 3-6 and Figure 3-17, TIM B showed higher modulus values for most cases. The results of TIM A before aging are somewhat unique and are discussed in the following paragraph.

Previous works on siloxane based TIMs have shown that increased thermal resistance was observed after thermal aging [13]. The hardening of the bulk polymer which leads to cracking was discussed as a possible reason for the performance degradation. The results shown in Figure 3-8 validate this argument by showing that the hardening of the polymer after high temperature aging is evident from the increase in the measured modulus values. TIM A showed a significant increase in the complex modulus values after thermal aging, especially at lower temperatures. The normalized average complex modulus for TIM B is shown to have increased after thermal aging for the entire temperature range. On the other hand, aged TIM A samples showed higher average modulus values at lower temperatures and lower modulus values at higher temperatures. This behavior was observed consistently for all samples tested. These aging effects can be explained by the fact that aging leads to increased specific volume and reduced molecular mobility which has significant impact on mechanical properties such as Modulus [30].

A typical FTIR result for the TIMs is shown in Figure 3-9. From the figure, five main peaks were identified in the measurement ranges of 4000 – 600 cm^{-1} and listed in Table 3-2. The five identified peaks are shown to be of silicon functional groups. The measurements also showed identical peaks for the two different TIMs studied. This is because this measurement was done only for a relatively small wavenumber range and the remaining compositions of the TIMs did not

have a signature peak for the given range. Moreover, Figure 3-10 shows that all the peaks have decreased in magnitude after aging. FTIR detects molecular vibrations by measuring the absorption of infrared light, and the reduced molecular mobility due to aging may have contributed to the decrease in peak magnitudes.

Figure 3-11 shows TMA results for the temperature range of -40 °C – 145 °C. For this temperature range, TIM A had a total thermal expansion of ~2.9 % and TIM B had a total thermal expansion of 1.2 %. Both CTE values are significantly higher when compared to other components in the electronic packaging stack up. Moreover, the TIM with higher filler content is shown to have lower CTE value. This agrees with what has been reported in the literature before. Subramanian et. al. have shown that among the three polymer based TIMs (PTIMs) they studied, the lowest CTE value was observed for the PTIM with the highest filler loading [21]. From Figure 3-12, the mean CTE values for both TIM A and TIM B decreased after aging. This is because aging increases the mass density of the polymer materials, and this leads to a decrease in molecular motion resulting in lower CTE [31]. Similar to the observations from DMA results, the softer TIM, TIM B, showed larger standard deviations. Sample to sample variation, ambient noise, accuracy during length measurements, and the force applied during the measurements contributed to the larger standard deviations.

3.4 Conclusions

In conclusion, the thermomechanical properties of two thermally conductive gap fillers were studied using DMA, TMA, and FTIR. After the samples were prepared, half of them were tested for pre-aging measurement values, while the rest were placed in an environmental chamber for 720 hours at 125 °C and were tested afterwards. Multiple samples were tested to obtain average values and standard deviations. The complex modulus of aged samples is shown to have increased when compared to measurements of pre aged samples. Among the two samples studied, the TIM with higher thermal performance (higher filler content) is shown to have higher modulus values. TMA results showed that the samples with lower filler content had higher CTE, and that high temperature aging reduced the CTE of both TIMs studied. The FTIR technique was used to identify the functional groups present in the sample and detect changes after high temperature aging. The sample preparation technique leveraged for this study can be used to prepare samples that match the thicknesses used in various applications. In this paper, it is shown that the changes in mechanical properties can be used to understand and assess reliability of thermal interface materials. There is a lack of work in the literature on the mechanical testing of TIMs, and this work may be used as a guide on the preparation and testing of samples for evaluation of mechanical properties. Moreover, the CTE and modulus values measured using the techniques discussed in this paper may be used to perform FEA and evaluate the reliability of TIMs under different loading conditions.

3.5 References

[1] J. Chow and S. Sitaraman, "Electroplated Copper Nanowires as Thermal Interface Materials," in *Thermal and Thermomechanical Phenomena in Electronic Systems (ITherm)*, 2016.

[2] S. e. a. Sun, "Mechanical and thermal characterization of a novel nanocomposite thermal interface material for electronic packaging," *Microelectronics Reliability,* vol. 56, pp. 129-135, 2016.

[3] T. Tong and e. al., "Dense vertically aligned multiwalled carbon nanotube arrays as thermal interface materials," in *IEEE Transactions on Components and Packaging Technologies*, 2007.

[4] S. Li, Q. Zheng, Y. Lv, X. Liu, X. Wang, P. Y. Huang, D. G. Cahill and B. Lv, "High thermal conductivity in cubic boron arsenide crystals," *Science,* vol. 361, no. 6402, pp. 579-581, 2018.

[5] Q. Zheng, S. Li, C. Li, Y. Lv, X. Liu, P. Y. Huang, D. A. Broido, B. lv and D. G. Cahill, "High thermal conductivity in isotopically enriched cubic boron phosphide," *Advanced Functional Materials,* vol. 28, no. 43, p. 1805116, 2018.

[6] G. Yuan, H. Li, B. Shan and J. Liu, "Thermal Interface Materials Based on Vertically Aligned Carbon Nanotube," *Micro and Nanosystems,* vol. 11, no. 1, pp. 3-9, 2019.

[7] A. Bar-Cohen, K. Matin and S. Narumanchi, "Nanothermal interface materials: Technology review and recent results," *Journal of Electronics Packaging,* vol. 137, no. 4, p. 040803, 2015.

[8] P. Lv, X.-W. Tan, K.-H. Yu, R.-L. Zheng, J.-J. Zheng and W. Wei, "Super-elastic graphene/carbon nanotube aerogel: A novel thermal interface material with highly thermal transport properties," *Carbon,* vol. 99, pp. 222-228, 2016.

[9] R. Prasher, "Thermal interface materials: historical perspective, status, and future directions," in *Proceedings of the IEEE 94.8* , 2006.

[10] J. P. Gwinn and R. L. Webb., "Performance and testing of thermal interface materials," in *Microelectronics Journal 34.3 (2003): 215-222.*, 2003.

[11] J. e. a. Liu, "Recent progress of thermal interface material research-an overview," in *Thermal Inveatigation of ICs and Systems, 14th International Workshop on. IEEE*, 2008.

[12] N. e. a. Goel, "Technical review of characterization methods for thermal interface materials (TIM)," in *Thermal and Thermomechanical Phenomena in Electronic Systems. ITHERM. 11th Intersociety Conference on. IEEE*, 2008.

[13] J. Due and A. J. Robinson, "Reliability of thermal interface materials: A review," in *Applied Thermal Engineering50.1: 455-463*, 2013.

[14] C.-P. Chiu and e. al., "Application of phase-change materials in Pentium (R) III and Pentium (R) III Xeon/sup TM/processor cartridges.," in *Advanced Packaging Materials: Processes, Properties and Interfaces, Proceedings. International Symposium on. IEEE*, 2000.

[15] C.-P. Chiu and e. al., "An accelerated reliability test method to predict thermal grease pump-out in flip-chip applications," in *Proceedings. 51st Electronic Components and Technology Conference (Cat. No. 01CH37220). IEEE*, 2001.

[16] I. M. a. C. F. Nnebe, "Drainage-induced dry-out of thermal greases," in *IEEE Transactions on Advanced Packaging 31.3: 512-518.* , 2008.

[17] A. e. a. Gowda, "Reliability testing of thermal greases.," in *Electronics Cooling 13.4 : 10.* , 2007.

[18] A. e. a. Gowda, "Reliability testing of silicone-based thermal greases [IC cooling applications]," in *Semiconductor Thermal Measurement and Management Symposium, 2005 IEEE Twenty First Annual IEEE. IEEE*, 2005.

[19] M. De Sorgo, "Thermal interface materials.," in *Electronics Cooling 2: 12-17.* , 1996.

[20] M. I. Okereke and Y. Ling, "A computational investigation of the effect of three-dimensional void morphology on the thermal resistance of solder thermal interface materials," *Applied Thermal Engineering,* vol. 142, pp. 346-360, 2018.

[21] V. Subramanian , J. Sanchez, J. Bautista, Y. He, J. Wang, A. Das, G. Schuldes, K. Yazzie, H. Dhavaleswarapu and P. Malatkar, "Mechanical Characterization of Thermal Interface Materials and Its Challenges," *Journal of Electronic Packaging,* vol. 141(1), 2019.

[22] L. Bharatham and e. al., "Qualification of phase change thermal interface material for wave solder heat sink on FCBGA package," in *Electronic Packaging Technology Conference,EPTC. Proceedings of 7th. Vol. 2. IEEE*, 2005.

[23] S. L. B. Dal, "Degradation mechanisms of siloxane-based thermal interface materials under reliability stress conditions.," in *Reliability Physics Symposium Proceedings. 42nd Annual. IEEE International. IEEE,*, 2004.

[24] C. I. Chen and e. al., "PRACTICAL EVALUATION FOR LONG-TERM STABILITY OF THERMAL INTERFACE MATERIAL.," in *Experimental Techniques 33.1: 28-32.*, 2009.

[25] X. Y. X. a. D. D. L. C. Luo, "Thermal stability of thermal interface pastes, evaluated by thermal contact conductance measurement.," in *Journal of Electronic Packaging 123.3 (2001): 309-311.* , 2001.

[26] H. H.-T. Corporation, "Principle of Thermomechanical Analysis (TMA)," 2018. [Online]. Available:https://www.hitachi-hightech.com/global/products/science/tech/ana/thermal/descriptions/tma.html. [Accessed 01 07 2019].

[27] H. H.-T. Corporation, "Principle of Dynamic Mechanical Analysis (DMA).," 2018. [Online]. Available:https://www.hitachi-hightech.com/global/products/science/tech/ana/thermal/descriptions/dma.html. [Accessed 01 07 2019].

[28] N. Pemberger, L. Bittner and C. Huck, "Spectroscopyonline.com," 01 August 2015. [Online]. Available: http://www.spectroscopyonline.com/using-near-infrared-spectroscopy-monitor-curing-reaction-silicone-adhesives?pageID=2. [Accessed 1 May 2019].

[29] A. Shimada, M. Sugimoto, H. Kudoh, K. Tamura and T. Seguchi, "Degradation mechanisms of silicone rubber (SiR) by accelerated ageing for cables of nuclear power plant," in *IEEE Transactions on Dielectric and Electrical Insulation*, 2014.

[30] M. R. Tant , H. L. N. McManus and M. E. Rogers, "High-Temperature Properties and Applications of Polymeric Materials : An Overview," in *High-Temperature Properties and Applications of Polymeric Materials*, Washington, DC, American Chemical Society, 1995, pp. 1-20.

[31] J. C. Adams, "Thermomechanical Analysis (TMA) and its application to polymer systems," Los Alamos National Laboratory, 2016.

[32] N. e. a. Goel, "Technical review of characterization methods for thermal interface materials (TIM)," in *Thermal and Thermomechanical Phenomena in Electronic Systems, ITHERM. 11th Intersociety Conference on. IEEE*.

[33] C. J. e. a. Lasance, "Challenges in thermal interface material testing.," in *Semiconductor Thermal Measurement and Management Symposium, 2006 IEEE Twenty-Second Annual IEEE*.

[34] R. e. a. kuriat, "Degradation of thermal interface materials for high-temperature power electronics applications," *Microelectronics reliability,* no. 53.12, pp. 1933-1942, 2013.

[35] K. C. e. a. Otiaba, "Thermal interface materials for automotive electronic control unit: trends, technology and R&D challenges.," *Microelectronics Reliability ,* vol. 51.12, pp. 2031-2043, 2011.

[36] J. e. a. Hansson, "Novel nanostructured thermal interface materials: a review.," *International Materials Reviews,* vol. 63.1, pp. 22-45, 2018.

[37] D. Jeon, S. H. Kim, W. Choi and C. Byon, "An experimental study on the thermal performance of cellulose-graphene-based thermal interface materials," *International Journal of Heat and Mass Transfer,* vol. 132, pp. 944-951, 2019.

[38] J. Hansson, T. M. J. Nilsson, L. Ye and J. Liu, "Effect of Fiber Concentration on Mechanical and Thermal Properties of a Solder Matrix Fiber Composite Thermal Interface Material," *IEEE TRANSACTIONS ON COMPONENTS, PACKAGING AND MANUFACTURING TECHNOLOGY,* vol. 9, pp. 1045-1053, 2019.

[39] N. Nagabandi, C. Yegin and M. Akbulut, "High Performance Metal-based Nanocomposite Thermal Interface Materials Toward Enhanced Cooling Efficiency in Electronic Applications," *Electronic Components and Technology Conference (ECTC),* vol. 68, pp. 574-579, 2018.

Chapter 4

Viscoelastic Influence on the Board Level Reliability Assessment of Wafer Level Packages Under Drop Impact and Under Thermal Cycling

4.1 Abstract

Obtaining accurate material properties is critical for running successful computational studies. Extensive amount of time and effort is spent in obtaining accurate material properties for individual components or bulk properties depending on the system studied and the level of detail required. Structural components such as printed circuit boards (PCBs) are critical in the thermomechanical reliability assessment of electronic packages. Previous studies have shown that geometric parameters such as thickness and mechanical properties like Modulus of PCBs have direct influence on the reliability of electronic packages. The bulk elastic material properties of PCBs are commonly characterized using equipment such as tensile testers and used in computational studies. However, in certain applications viscoelastic material properties are important. Viscoelastic influence on materials is evident when one exceeds the glass transition temperature of materials. Operating conditions or manufacturing conditions such as lamination and soldering may expose components to temperatures that exceed the glass transition temperatures. Knowing the viscoelastic behavior of the different components of electronic packages is important in order to perform accurate reliability assessment and also design components such as printed circuit boards (PCBs) that will remain dimensionally stable after the manufacturing process. Previous researchers have used creep and stress relaxation test data to obtain the Prony series terms that represent the viscoelastic behavior and perform analysis. Others have used dynamic mechanical analysis in order to obtain time domain master curves that were used to obtain Prony series terms. In this paper, frequency domain master curve results from

dynamic mechanical analysis are used to obtain Prony series terms and perform finite element analysis on the impact of adding viscoelastic properties when performing reliability assessment. The computational study results were used to perform comparative assessment to understand the impact of including viscoelastic behavior in reliability analysis under thermal cycling and under drop testing for wafer level chip scale packages.

4.2 Introduction

Maximizing reliability and the operating life is one of the main goals when designing electronic system [1]. Reliability is defined as "the statistical probability that a device or system will operate without failure for a specified period" [1]. Reliability of electronic systems is impacted by various environmental loads including thermal and mechanical loads. From an earlier study conducted by US navy, the failure rate of electronic equipment was observed to have increased by eight-fold when deliberately exposed to temperature cycling of more than 20 °C [2]. Increasing the operating temperature also have a negative impact on reliability. According to Yeh et. al., a 2°C increase in operating temperature reduces the reliability of silicon chips by 10 % [1]. For these reasons, there is a heavy focus on performing extensive reliability studies before equipment are shipped to customers.

The reliability of products is often described with the use of "bathtub" diagram like the one shown in Figure 4-1. High infant mortalities are observed due to bad product quality. Burn-in and run-in tests are often employed to catch early failures before products are shipped out. Failure rates due to wear out are reduced through improved designs, and guidelines such as IPC-D-279 (Design guidelines for Reliable Surface Mount Technology Printed Board Assemblies) are established to help designers [3]. Depending on the application, electronic components will be exposed to mechanical shock, mechanical vibration, temperature cycling, or high humidity environments. The

reliability of electronic assembly is determined by use conditions, the design life, and acceptable failure probability rates [3]. For example, a failure risk of < 0.1 % may be acceptable for computers, but a failure risk of < 0.001% is needed for commercial aircraft applications [4].

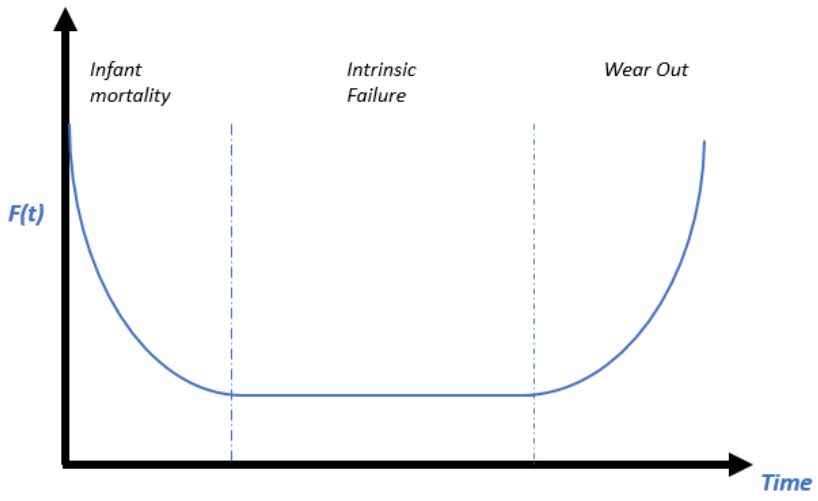

Figure 4-1: Bathtub curve showing failure rate as a function of time.

Thermal cycling and drop testing are two of the most common environmental loading conditions used to assess reliability of electronic equipment. Consumer products such as cell phones and cameras are susceptible to be dropped due to their size and weight [5]. The input acceleration from dropping results in mechanical failure on components such as housing and electrical failures due to cracking of printed circuit boards (PCBs) and solder interconnections [5]. On the other hand, the temperature swing experienced by various electronic products may range from 60 °C for consumer products, to more than 140 °C for electronics in automotive used under the hood of cars [4]. The temperature swings combined with the mismatch of CTE of the different materials used for packaging, subject critical components such as solder joints to stress and strain, eventually leading to failure [6].

In addition to providing electrical connections, solder joints are usually the sole mechanical attachment of electronic components to PCBs [3]. As such, one of the major reliability concerns in microelectronic packaging is the integrity of solder interconnections [7]. Solders are inhomogeneous structures, and their grain structure is inherently unstable [3]. Micro-voids start forming at the grain boundary ~25 % of the fatigue life, eventually coalescing to macro-cracks and leading to total fractures causing electrical failures [3]. Experimental tests and numerical techniques are used to study the thermo-mechanical reliability of solders and other components.

Experimental tests are often expensive and time consuming. To save cost, advanced finite element analysis is often performed during the design and development phases to maximize reliability of products [7]. Finite element analysis is also performed to predict field use limits and analyze field failures [6]. Using numerical techniques requires the use of life prediction methodologies that are based on the different damage mechanisms observed in the field [7]. Numerous solder joint fatigue life prediction models such as Yamada [8], Engelmaier [9], Syed [10], Darveaux [11], can be found in the literature [7]. These different approaches can be grouped into four main categories: strain-based approach, energy-based approach, fracture mechanics-based approach, and evolution-based approach [12]. Darveaux's energy-based fatigue life prediction model has been widely used in the literature to predict the life of Pb-Sn solders [6]. Widely used fatigue life prediction model for lead free solders was proposed by Schubert et. al. and is also used in this paper [13].

Different factors affect the accuracy of numerical studies. Capturing the correct boundary and load conditions, employing the correct numerical models, and obtaining accurate material properties for the components are some of the key challenges in obtaining accurate numerical results. Components such as solder are extremely inhomogeneous, and accurately capturing their

material properties is challenging. The Anand viscoplastic constitutive model, originally proposed to study hot working of metals [14] [15], is widely used to model solders for computational studies [16]. The Anand model uses stress equation, flow equation, and evolution equation, and unifies the creep and rate-independent plastic behaviors of solder [16]. The nine material constants used to define the constitutive equations are experimentally characterized and used in computational studies [17]. Stress-Strain or Creep data measurements have been used in the literature to determine the Anand constants [16]. In this paper, Anand constants for SAC solders obtained from [18] are used for the computational studies.

For structural simulations, most of the components in the electronic packages are modeled as elastic materials. For materials that go close to glass transition temperature (T_g), viscoelastic material properties are often used to accurately capture the material behavior. Viscoelastic materials are materials that exhibit both viscous and elastic behaviors. The Maxwell model, initially proposed in 1867, captures the elastic and viscous properties using Newtonian damper and Hookian spring [19]. However, the simple Maxwell model consisting of a single spring and damper in series had a limitation in modelling creep phenomenon. A generalized Maxwell model with multiple Maxwell branches in parallel as shown in Figure 4-2 overcomes the limitations and is used to model viscoelastic materials. For the generalized model, time dependent shear moduli are represented using Prony series as shown in equations (4-1) below [19]. Taking the Laplace transform of equation 4-1 gives the *complex shear modulus* as shown in equation (4-2). The real part of the complex shear modulus is called *storage shear modulus* while the complex part is called *loss shear modulus* [20]. Storage and loss modulus in terms of Prony series terms are shown in equations (4-3) to (4-4) [21]. The relative moduli (α_i^G) and relaxation time (τ_i^G) terms can be

entered to computational software such as ANSYS to capture the viscoelastic behavior of materials for computational studies.

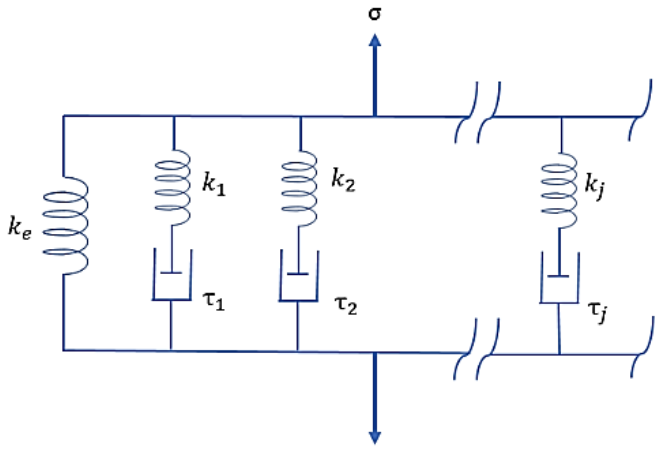

Figure 4-2: General Maxwell model used to represent viscoelastic materials.

$$G(t) = G_0\left[\alpha_\infty^G + \sum_{i=1}^{n_G} \alpha_i^G \, exp\left(-\frac{t}{\tau_i^G}\right)\right] \tag{4-1}$$

$$G^*(j\omega) = G_\infty + \sum_{i=1}^{n_G} \frac{g_i^G \tau_i^G j\omega}{1 + \tau_i^G j\omega} \tag{4-2}$$

$$G'(\omega) = R\{G^*\} = G_\infty + \sum_{i=1}^{n_G} g_i^G \frac{(\tau_i^G \omega)^2}{1 + (\tau_i^G \omega)^2} \tag{4-3}$$

$$G''(\omega) = I\{G^*\} = \sum_{i=1}^{n_G} g_i^G \frac{\tau_i^G \omega}{1 + (\tau_i^G \omega)^2} \tag{4-4}$$

Dynamic Mechanical Analysis

Dynamical mechanical analyzer (DMA) is a technique that applies oscillating strain or stress to samples and uses the result to measure the kinetic properties of samples [22]. The major components of DMA are shown in Figure 4-3. Output of DMA consists of temperature dependent loss and storage moduli of materials at different frequencies. The relations between loss modulus, storage modulus, and complex modulus are given by equations 1-1 to 1-3. Using the "time-temperature superposition", the DMA results are expanded to a wider frequency range and a master curve is obtained. The detail of these procedures is discussed in the materials and methods section.

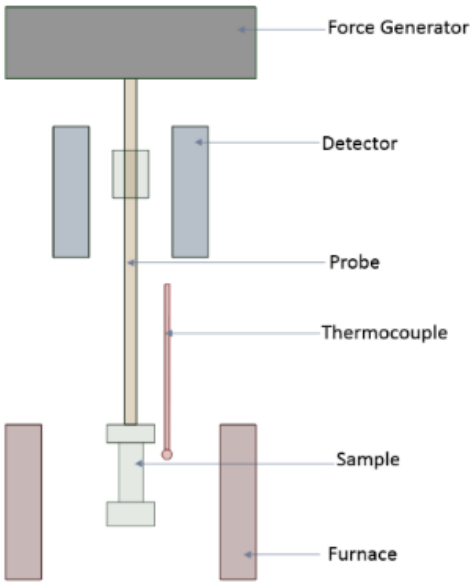

Figure 4-3: Major components of DMA [22].

Shrotriya et. al. used creep data from DMA to develop a micromechanical model that can be used to understand the time-temperature dependent behavior of PCB substrates and understand residual stresses and dimensional changes in the PCBs during processing such as re-lamination and soldering processes [23]. On the other hand, Liu et. al. performed analytical investigation on the viscoelastic influence of PCBs under drop impact [24]. They showed that the viscoelasticity of PCBs has a distinct influence on the system response under board-level impact, and proposed using

PCB substrate with larger viscoelasticity and reduced size in order to improve drop impact reliability [24].

While running FEA simulations for reliability study of electronic packages, PCBs are represented using three different approaches: lumped board modeling approach, explicit geometry approach, and electronic computer aided design (ECAD) approach [25]. Lumped board approach represents PCBs as blocks with effective mechanical properties. Explicit approach uses a layer by layer representation of PCBs, while ECAD approach uses the exact design files used to make PCBs. Explicit geometry and ECAD approach give a more accurate representation of PCBs; however, lumped approach is commonly used as the other approaches require very large mesh sizes and long solution times [25]. In the lump approach, PCBs are characterized using only their orthotropic elastic material properties. However, for computational studies that involve drop impact, or for conditions where temperatures go near and beyond the glass transition temperature (T_g), it is important to include the viscoelastic behavior in computational studies. In this paper, the frequency domain master curve obtained from dynamic mechanical analysis is used to obtain the Prony series terms that are then used to model PCBs as viscoelastic materials. Using the Static and Transient structural packages in ANSYS 2019 R1, the impact of including viscoelastic property of PCBs for board level reliability assessment of Wafer Level Packages (WLPs) is studied. WLP is an advanced packaging technology where packages are fabricated and tested at the wafer level before singulation [26]. WLPs are used for applications such as analog devices, power management devices, image sensors, and integrated passives [26]. In this paper, the reliability of WLPs is assessed under two different loading conditions: thermal cycling and drop impact. The details of the procedure for obtaining the Prony series terms are given in section 4.3, the

computational model is discussed in section 4.4, results are given in section 4.5, discussion and conclusions are given in sections 4.6 and 4.7 respectively.

4.3 Materials and Methods

Dynamic Mechanical Analyzer (DMA) was used to measure the frequency and temperature dependent storage (E') and loss modulus (E'') of the PCBs used for WLP. Measurements were run at frequencies of 0.5, 1, 2, 5, 10 Hz. Figure 4-4 shows the equipment and the sample used for measurement. Figure 4-5 shows sample attached for measurement using the dual cantilever bending attachment. Due to the thickness and the expected Modulus of the sample, the tensile attachment of DMA was found to be not suitable for measurement. The geometric dimensions of the sample along with the test parameters used on DMA are given on Table 4-1. Figure 4-6 shows a DMA result for the temperature and frequency dependent measurement of loss and storage modulus values.

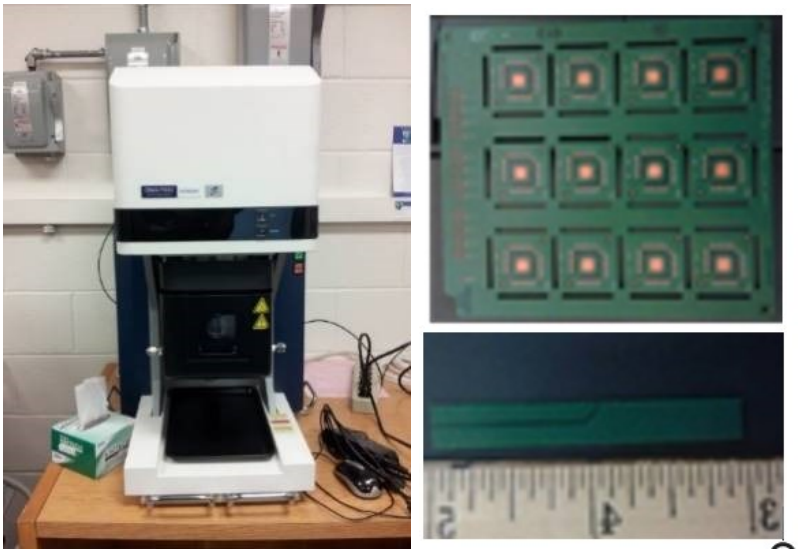

Figure 4-4: DMA7100 used for testing (left). Samples used for measurement (right).

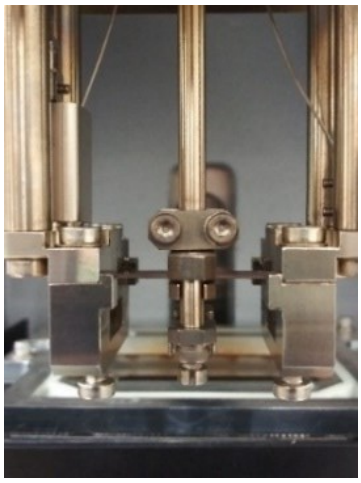

Figure 4-5: Samples attached using DMA bending mode.

Table 4-1: Geometric dimensions of samples and test parameters used for DMA testing

Parameters	***Value***
Minimum tension/ compression force	200 mN
Tension/ compression force gain	1.5
Force amplitude	2000 mN
Temperature Ramp	2 °C/min
Sample Thickness	0.93 mm
Sample Width	7.83 mm
Sample Length	50.00 mm

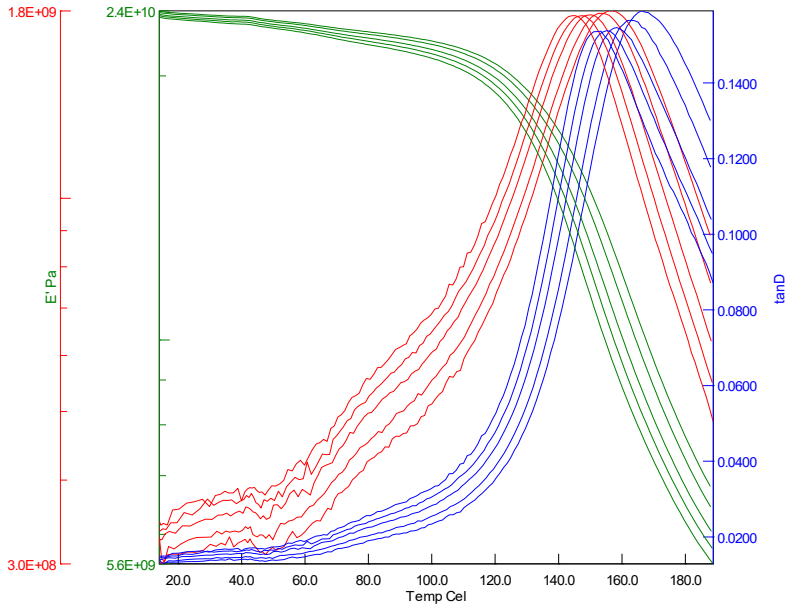

Figure 4-6: DMA result showing temperature dependent modulus, loss modulus, and loss tangent.

After the DMA analysis, the built-in tool for DMA (TA7000) was used to generate the master curve showing the loss and storage modulus for a wider range of frequency values. An important input parameter in obtaining the master curve using shift functions is the glass transition temperature (T_g). Dynamic mechanical analysis is one of the widely used techniques to measure T_g [27]. Results for storage modulus (E'), loss modulus (E''), or $Tan\ \delta$ from DMA measurements may be used to define the glass transition temperature. For results obtained for 1 Hz, the temperature values at the onset of E', peak of E'', or peak of $Tan\ \delta$ may be considered to be the glass transition temperature points [27]. The three approaches are shown in Figure 4-7. The onset of E' is the most conservative of the three approaches and often relates to mechanical failure [27]. In this paper, the onset of E' at 1 Hz is used to measure the T_g as 126.5 °C.

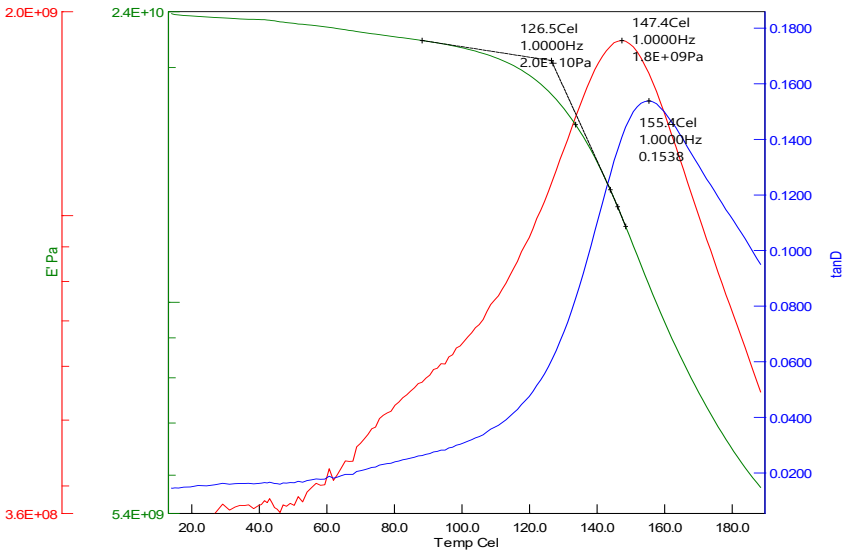

Figure 4-7: Three approaches to measure glass transition temperature (Tg). Onset of E', peak of E'', or peak of $\boldsymbol{Tan\ \delta}$ may be considered as Tg.

The master curve obtained from DMA measurements is one of the available techniques for studying the frequency dependence of viscoelastic properties of materials [28]. The master curve is obtained by using the "time-temperature superposition" that exists in dynamic viscoelastic measurements. Initial measurements are performed at 5 frequency values and a wide temperature range. However, by using the "time-temperature superposition", the viscoelastic properties are predicted for wider frequency ranges for a given temperature value [28]. This "time-temperature superposition" is achieved using the expanded William - Landel - Ferry (WLF) equation given by equation (4-5) [28]. The corresponding master curve obtained showed loss and storage modulus and magnitude of complex modulus as a function of frequency and is shown in Figure 4-8. The WLF equation is best used to obtain the master curve for temperatures equal or greater than the glass transition temperature (T_g) [28]. For temperature values lower than T_g, Arrhenius equation (given in equation 4-6) is preferred to describe the shift factor-temperature relationship and obtain master curves [29].

$$log\ a_T = \frac{C_1(T-T_g)}{C_2+T-T_g} + \frac{C_1(T_r-T_g)}{C_2+T_r-T_g} \quad (4\text{-}5)$$

$$\ln a_T = \frac{E_a}{R}\left(\frac{1}{T} - \frac{1}{T_0}\right) \quad (4\text{-}6)$$

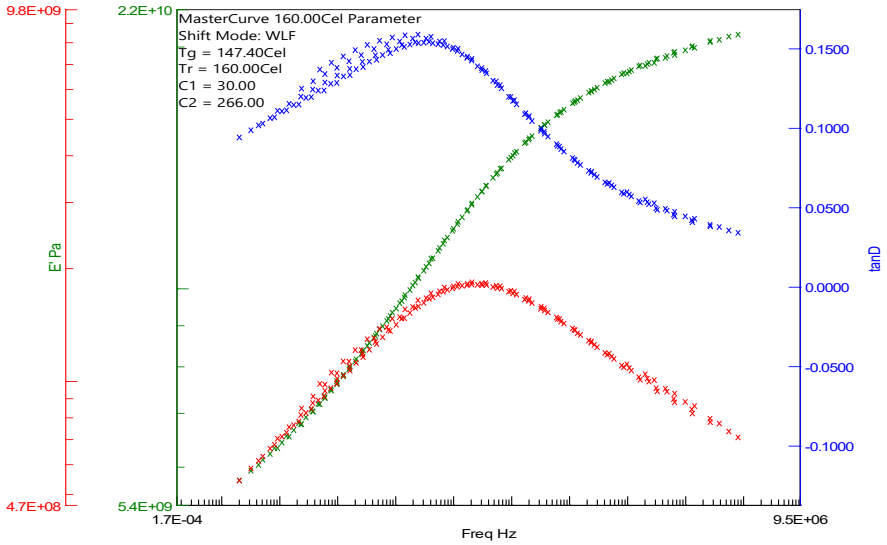

Figure 4-8: Master curve showing storage modulus, loss modulus, and $\boldsymbol{Tan\ \delta}$ as a function of frequency. The terms for the WLF shift function are also given in the figure.

Computational software such as ANSYS require users to input Prony series coefficients to capture viscoelastic properties in simulations. The master curve shown in Figure 4-8 is not in the form that can be included in simulations, and additional post processing is required in order to obtain the Prony series terms that can be included in simulations.

Obtaining the Prony series terms from master curves have been the focus of previous research, and different authors have used different approaches to obtain the time domain master curves and extract Prony series terms. Lakes [30] defined the interrelationship between the moduli as:

$$\frac{2}{\pi}E''(\omega)|_{\omega=1/\tau} \approx -\frac{dE'(\omega)}{d\ln\omega} \approx -\frac{dE(t)}{dln\ t} \qquad (4\text{-}7)$$

With $\tau = 1/t$, equation (4-7) implies that:

$$E'(\omega)|_{\omega=\frac{1}{\tau}} \approx E(t) \qquad (4\text{-}8)$$

Previous studies on the impact of viscoelastic influence on PCBs [31] [32] [33] have made use of the relation given in equation (4-8) to shift the master curve to the time domain and extract the Prony series terms by performing nonlinear curve fitting. Other empirical equations, such as equation (4-9), have also been proposed to shift the frequency domain master curve to time domain [34].

$$E(t) = E'(\omega) + 0.0004E'(0.02\omega) - 0.25E'(5\omega) + 0.35E'(0.2\omega) \qquad (4\text{-}9)$$

In this paper, the Prony series terms are obtained by performing nonlinear fit to the master curve in frequency domain using equations (4-3) and (4-4). Nonlinear parametric fitting tools on OriginPro were used to perform the curve fitting.

From the curve fitting, g_i^G and τ_i^G were obtained. These terms were used in equation (4-1) to obtain G_0. Then the relative moduli terms were obtained using the relation $\alpha_i^G = g_i^G/G_0$. The fit parameters were tested by comparing the computed and measured complex modulus values. Comparison between computed and measured complex modulus values for 160 °C are shown in Figure 4-9. Average difference between measured and fit values < 1%. A representative data for computed Prony series terms for 160 °C and 170 °C are given in Table 4-2.

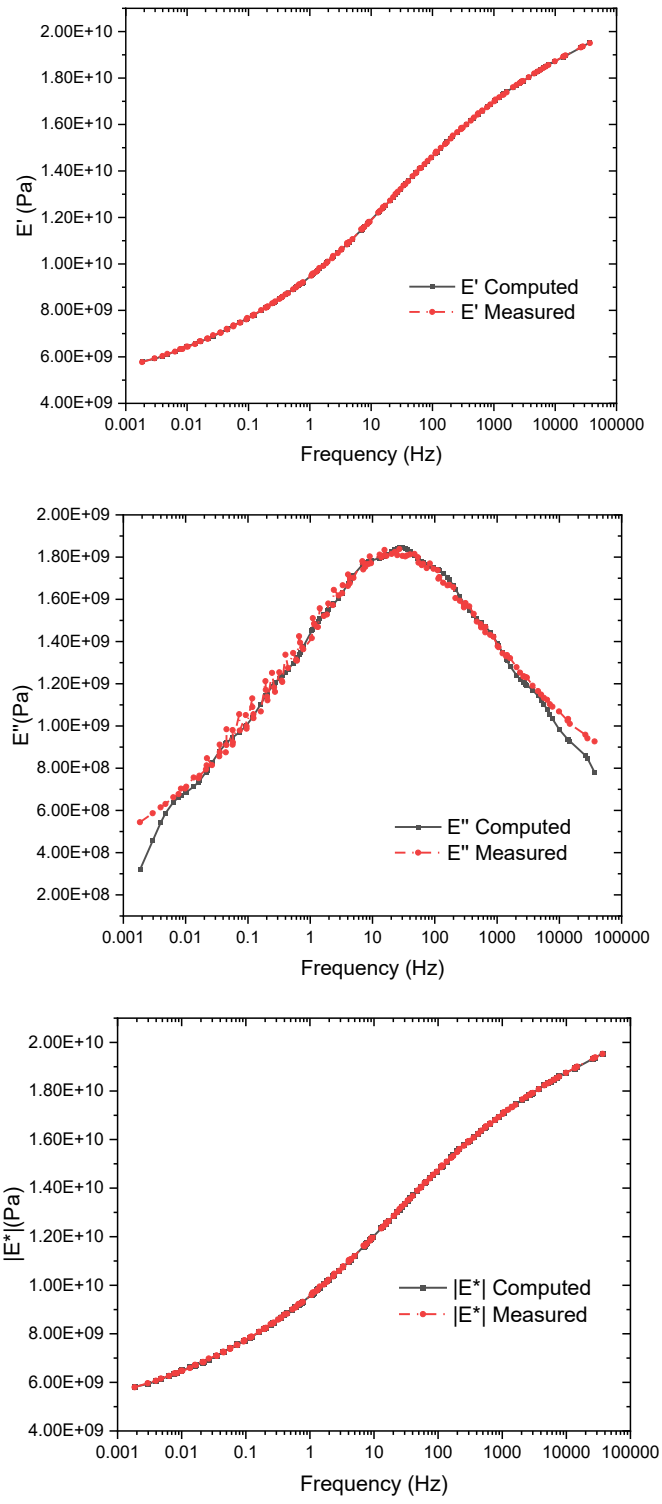

Figure 4-9: Computed vs measured storage, loss, and complex modulus for 160 °C. Comparisons for 170 °C and 180 °C given in Appendix II.

Table 4-2: Prony series terms for 160 °C and 170 °C. Terms for 140 °C, 150 °C, 180 °C, and 190°C given in Appendix I.

i	160 °C		170 °C	
	α_i^G	τ_i^G	α_i^G	τ_i^G
Inf	2.86E-01	N/A	2.86E-01	N/A
1	5.97E-02	3.31E-05	5.97E-02	3.31E-06
2	6.33E-02	2.24E-04	6.33E-02	2.23E-05
3	7.68E-02	1.28E-03	7.68E-02	1.27E-04
4	9.04E-02	6.69E-03	9.04E-02	6.67E-04
5	9.70E-02	0.03268	9.70E-02	0.00326
6	9.15E-02	1.55E-01	9.16E-02	1.55E-02
7	7.70E-02	0.76658	7.70E-02	0.07653
8	6.27E-02	4.0918	6.27E-02	4.09E-01
9	5.15E-02	2.40E+01	5.15E-02	2.40E+00
10	4.45E-02	1.75E+02	4.45E-02	1.75E+01

4.4 Computational Study

Thermal Cycling

Leveraging the symmetry of the models, quarter symmetry models were used for the computational studies. The PCB was extended to avoid edge effects. Hex dominant and body sizing was used to mesh the critical component, solder balls. The schematic of the WCSP model is given in Figure 4-10. Boundary conditions used for the computational study are shown in Figure 4-11. The material property of the different components used the computational study is given in Table 4-3.

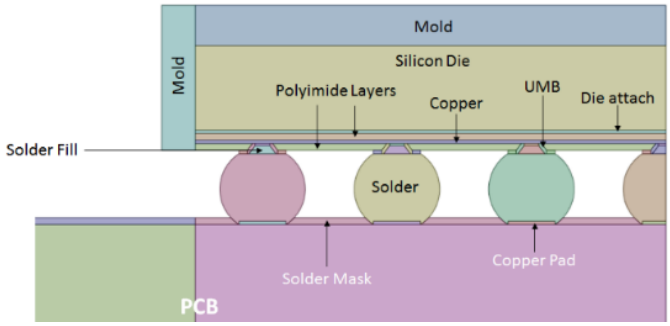

Figure 4-10: Schematic of WCSP model used to perform computational study.

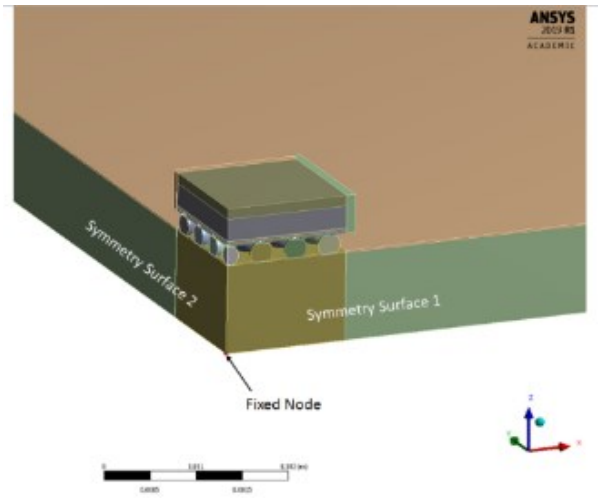

Figure 4-11: Boundary conditions used for the computational study.

Table 4-3: Mechanical properties of the different components used in the computational study[7] [36] [26] [37]

	E (GPa)	**CTE (ppm/°C)**	**ν**
Cu pad	110	17	0.34
Die Attach	10	33	0.3
Mold	24	20	0.3
PCB	24	X, Y 13.2; Z: 50	0.39
Polyimide Layer	1.2	52	0.25
RDL	130	16.8	0.34
Die	131	3	0.28
Solder	55.3 @ -40 °C, 42 @ 25 °C, 33 @ 75 °C, 23 @ 125 °C	20	0.4
UBM	50	16	0.35
Solder Mask	4	30	0.4

Table 4-4: Values for the Anand constants used to model solders. Properties for SAC 387 given below [18]

S. No	Constant	Unit	Value
1	s0	MPa	3.3
2	Q/R	1/K	9883
3	A	sec^{-1}	1.57E+07
4	ξ	Dimensionless	1.06
5	m	Dimensionless	0.3686
6	h0	MPa	1077
7	ŝ	MPa	3.15
8	n	Dimensionless	0.0352
9	a	Dimensionless	1.6832

Regardless of initial stress-free temperature, structure will readjust and reach a 'near-stress-free' at high-dwell temperature after few cycles. Stabilized values of strain or strain energy density per cycle are independent of the initial stress-free setting [26]. For the current study, the high-dwell temperature was selected as the zero thermal strain temperature. Condition G and H of JEDEC standard JESD22-A014D were used [38]. The corresponding temperature profiles are shown in Figure 4-12. Fatigue cracks of solders occur at the package side near the interface of solder bulk/copper or UBM layer [26]. The damage parameters are extracted from 10 um layer of corner solder joint at the package side [26]. The inelastic energy density accumulated per cycle is averaged over the volume of the thin disk (equation 4-10), and the resulting damage metrics is used to predict the number of cycles to failure [26] [39] [40].

$$\triangle W_{ave} = \frac{\sum_i W_i V_i}{\sum_i V_i} \qquad (4\text{-}10)$$

The change in inelastic energy density after the third cycle was determined to be constant. This value was used because of computational resources and the fact that solder joints have reached stability after third cycle [41]. An APDL code from [7] was used to compute the change in inelastic energy density. Then, the model proposed by Schubert et. al. as shown in equation 4-11 below was used to find N_f [13].

$$N_f = \left(\frac{A}{\Delta W}\right)^k \qquad (4\text{-}11)$$

Where A = 8.783 x 10^6 MPa, k = 0.4701 [41] .

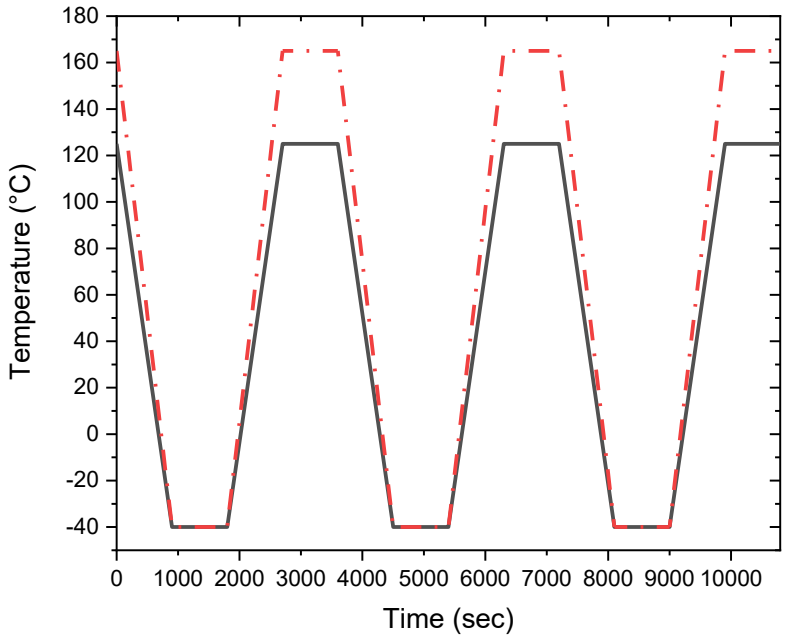

Figure 4-12: Temperature cycling profiles used for the study: condition G (solid line) and H (dotted line) of JEDEC standard JESD22-A014D are shown.

Drop Testing

WLP technology enables smaller, thinner, and faster electronic products, and has been widely used in portable electronic products. To understand the reliability of products under mechanical shock from customer usage or transportation, Joint Electron Device Engineering Council (JEDEC) has developed board designs and test standards that are used in assessing the reliability of handheld electronic products [42]. Due to the symmetry of the JEDEC board, quarter symmetry is used as shown in Figure 4-13 [5].

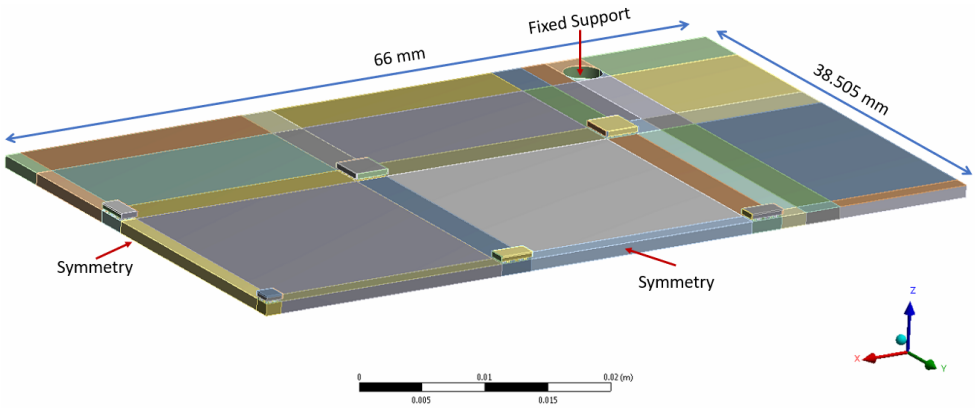

Figure 4-13: Quarter symmetry of the JEDEC board used for the computational study.

For computational analysis of drop testing, different modeling techniques have been developed. Dynamic vs. static analysis type, free-fall vs. Input-G loads, explicit vs. implicit solvers, are some of the approaches that can be used for performing drop testing analysis [42]. For Input-G method, components used in experimental testing (such as drop table, fixture, etc.) are not included in the simulation and their impact is captured by applying an impact impulse to the mounting holes [42]. Simulation results using explicit Input-G method have been shown to correlate well with experimental results [43]. On the other hand, Input-D method applies displacement at the loading points. Solutions for Input-D and Input-G methods include rigid body movement. An alternative method, direct acceleration input (DAI) method removes the rigid body movement and is

commonly used to perform drop study analysis. In the DAI method, acceleration impulse is applied as body force to the problem and the mounting holes are fixed during the dynamic response [42]. Equation 4-12 below shows the impulse conditions applied to the model.

$$\{M\}[\ddot{u}] + \{C\}[\dot{u}] + \{K\}[u] = \begin{Bmatrix} -\{M\}1500g * \sin\frac{\pi t}{t_w}, \text{ where } t < t_w \\ 0, \text{ where } t \geq t_w \end{Bmatrix} \quad (4\text{-}12)$$

t_w = 0.5 ms, Initial Conditions are $[x]|_{t=0} = 0$, $[\dot{x}]|_{t=0} = \sqrt{2gh}$

Boundary Conditions are $[x]|_{\text{at hole}} = 0$

$\{M\}$ is the mass matrix, $\{C\}$ is the damping coefficient, $\{K\}$ is the stiffness coefficient matrix. $[u]$ is displacement vector, $[\dot{u}]$ is the velocity vector, and $[\ddot{u}]$is acceleration vector.

The JEDEC board with multiple components and hundreds of solder balls is a very big model and computationally extensive for FEA analysis. Sub-model technique needs to be applied to be obtain fast solutions while still obtaining accurate results. In the global model, the solder balls are simplified and represented as cubical blocks. For the sub-model, detailed structural components are added and simulated. In this paper, the global model is used to make a comparative study in order to assess the impact of including viscoelastic properties of PCBs when running computational studies for drop testing loading conditions.

4.5 Results

Thermal Cycling Results

The results for the computational study with the thermal cycling boundary conditions are given below. Table 4-5 shows the average inelastic energy density for the different cases investigated. Figure 4-14 shows the comparison of the number of cycles to failure computed using equation 4-11.

Table 4-5: Average plastic work (Pa) for the different thermal cycling conditions

Average Plastic Work for Cycle (Pa)		
Temperature Profile	Elastic	Viscoelastic
-40°C to 125°C	119270	118880
-40°C to 165°C	137490	136630

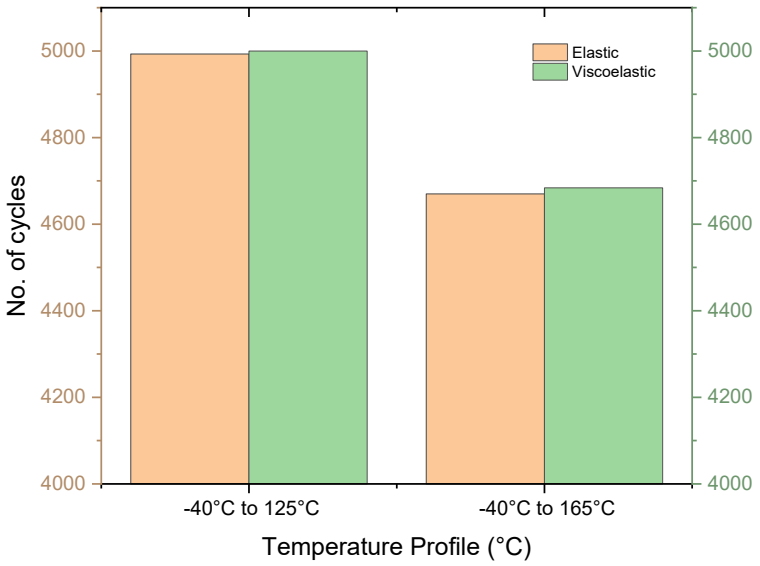

Figure 4-14: Plot comparing the number of cycles to failure between the two cases where PCB were modeled elastic and viscoelastic.

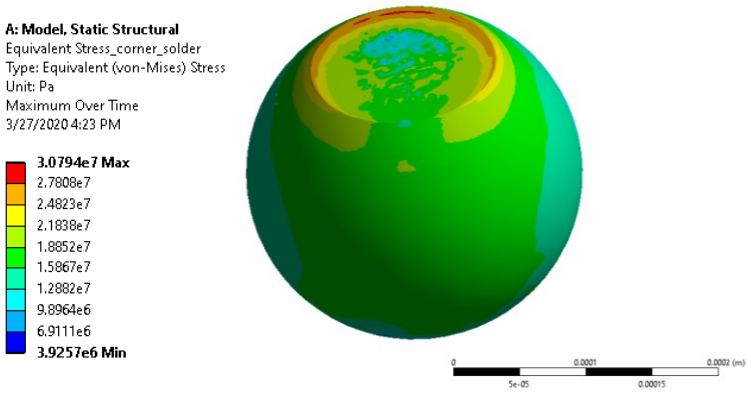

Fig. 4-15: Equivalent stress on corner solder for the elastic case for thermal cycling for -40 °C to 165 °C.

Drop Testing Results

The results for the computational study with the drop testing boundary condition are given below. Figure 4-16 shows the deformation of the quarter model for drop testing at 135°C for the case PCB is modeled as viscoelastic material. Figure 4-17 to Figure 4-19 show the comparison for deformation, strain, and acceleration for the two cases where the PCB was modeled as elastic and viscoelastic.

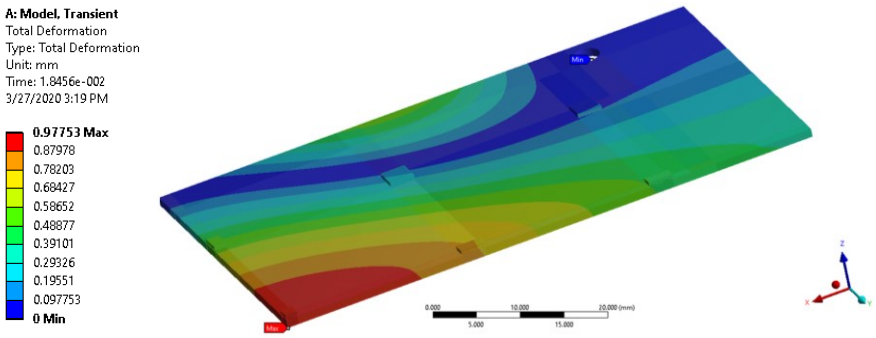

Figure 4-16: Total deformation of the quarter model at 135 °C for the case PCB is modeled as viscoelastic.

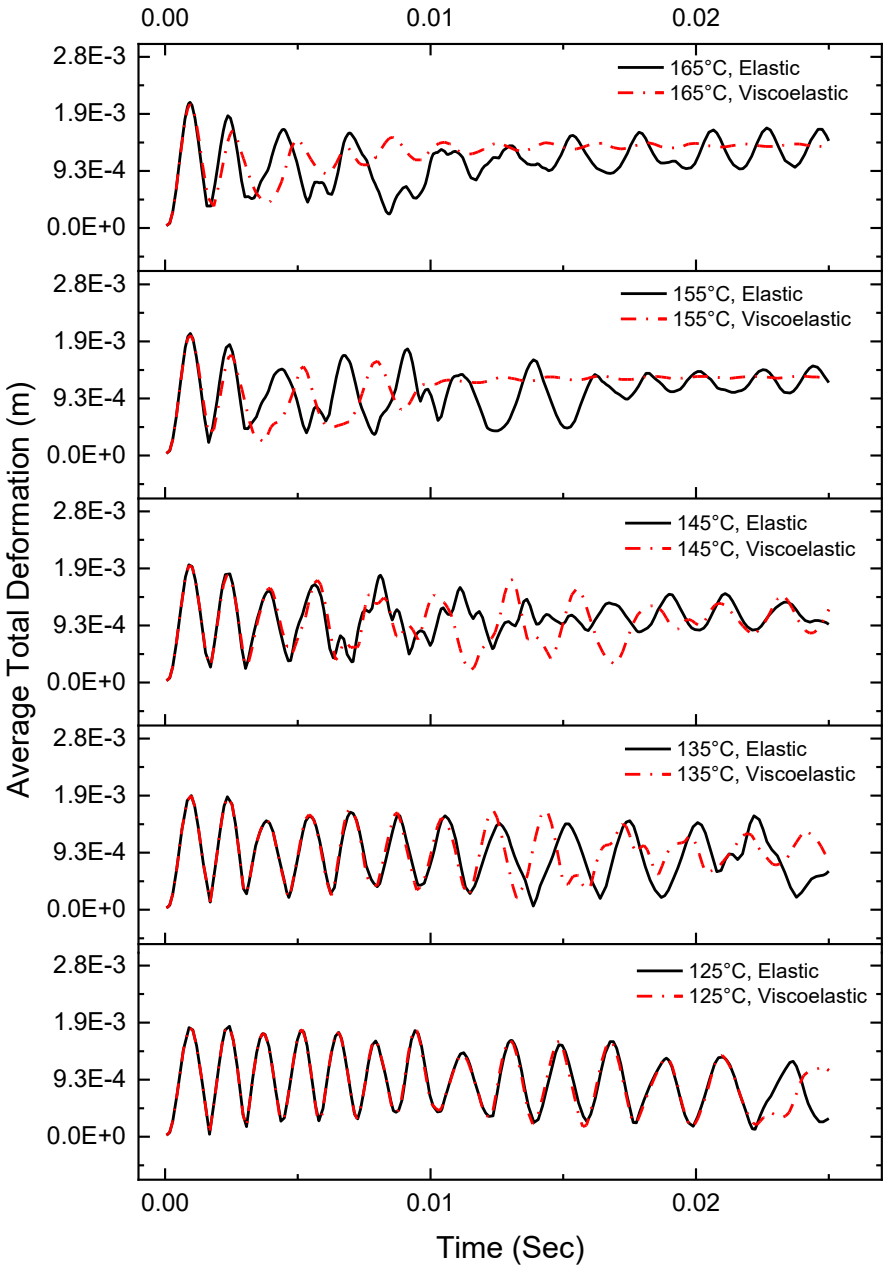

Figure 4-17: Comparison of average total deformation between models that represented the PCB elastic and viscoelastic. Results shown for different temperatures.

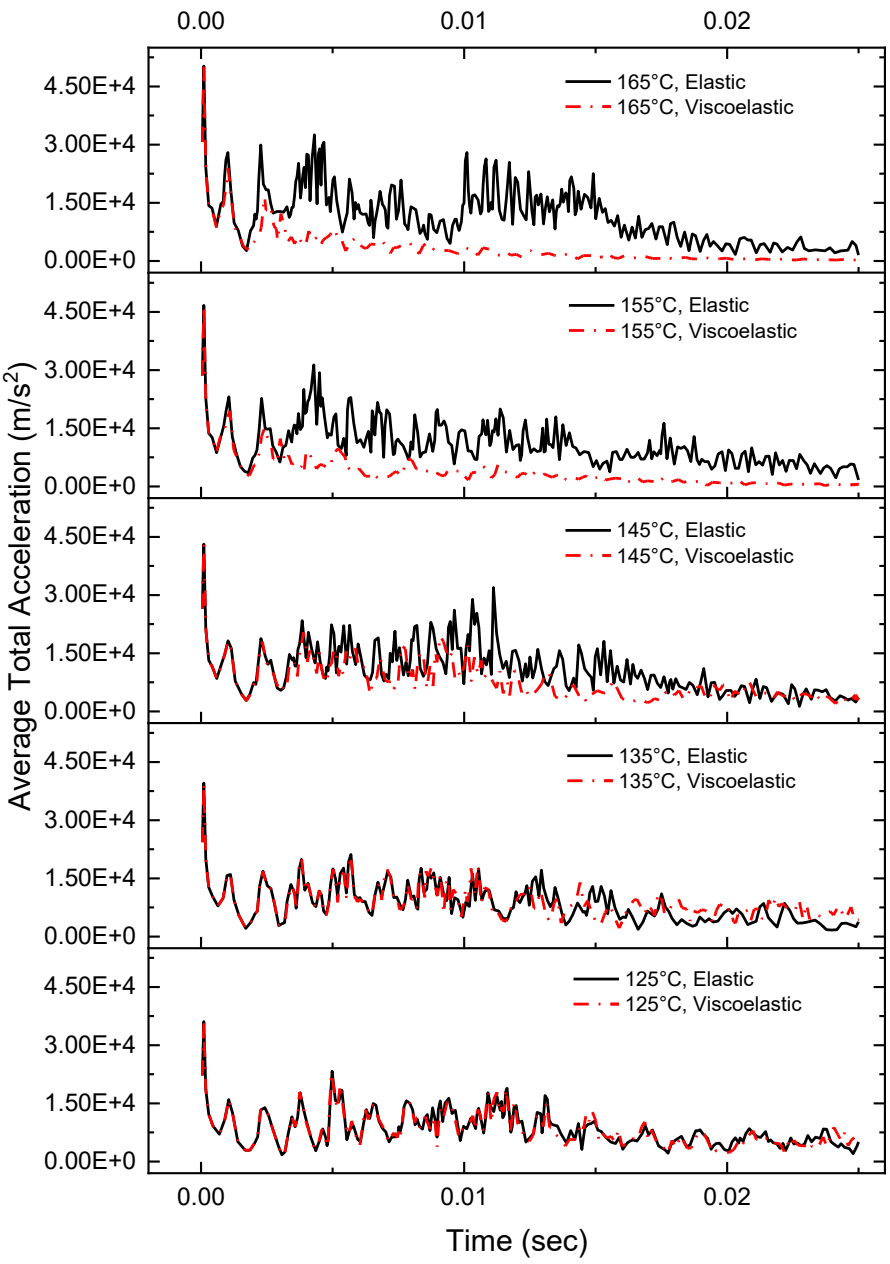

Figure 4-18: Comparison of average total acceleration between models that represent the PCB as elastic and viscoelastic. Results shown for different temperatures.

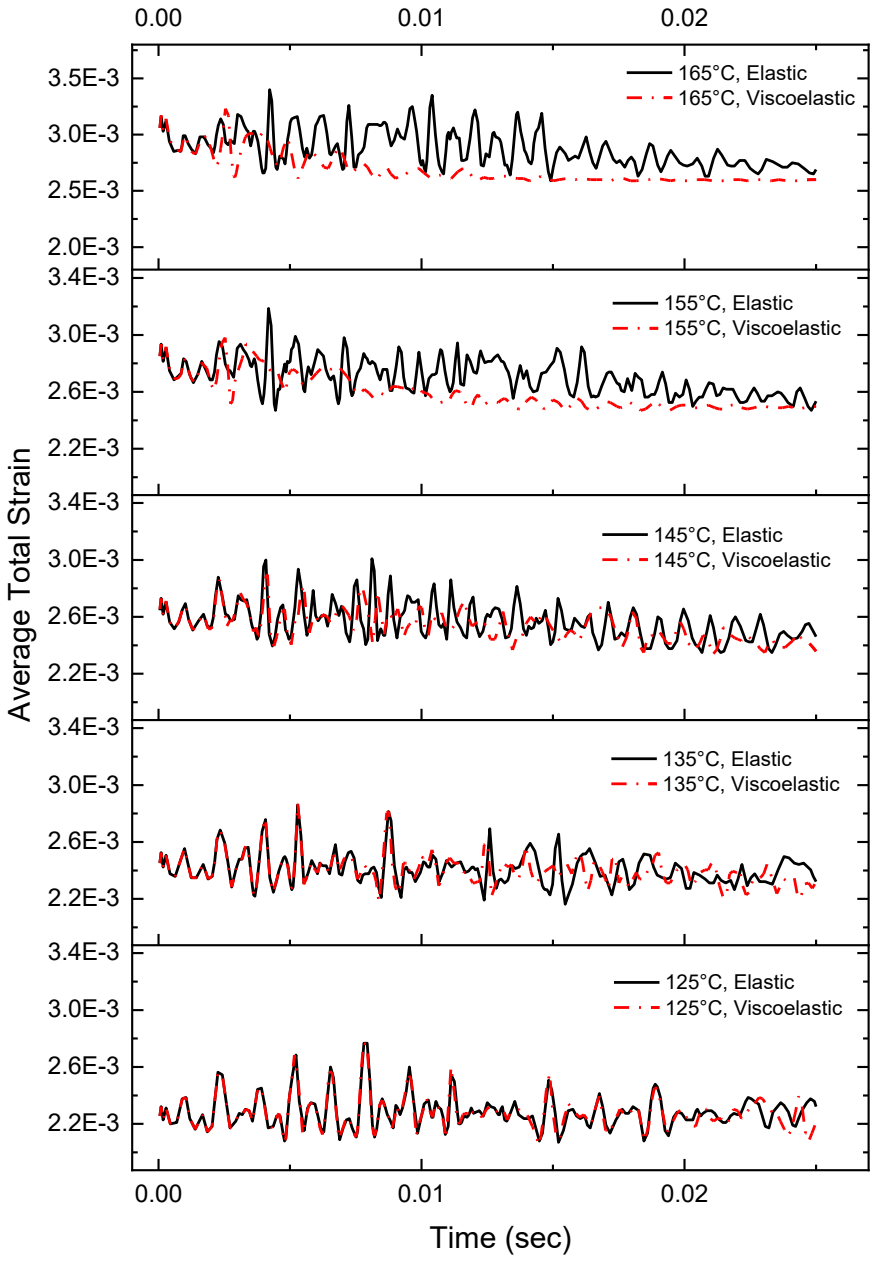

Figure 4-19: Comparison of strain between models that represent the PCB elastic and viscoelastic. Results shown for different temperatures.

4.6 Discussion

Previous studies that investigated the impact of viscoelastic influence of PCBs used different approaches to perform material characterization. Shrotriya et. al. used creep data from DMA to develop a micromechanical model, while others [31] used time domain master curves to develop viscoelastic models. In this paper, frequency domain master curve results were used to obtain the Prony series terms. First, the temperature dependent storage and loss modulus measurements for five different frequencies were obtained as shown in Figure 4-6. Using the WLF shift function, the time domain master curve shown in Figure 4-8 was obtained. The corresponding Prony series terms were obtained from a non-linear fit (values for 160 °C and 170 °C shown in Table 4-2) and included in the subsequent finite element analysis. Figure 4-9 shows a comparison between the computed and experimentally measured frequency dependent storage, loss, and complex modulus values. The difference between the computed and experimentally measured values was found to be on average less than 1%. The difference between the computed and experimentally measured values was found to be slightly higher for low loss modulus values. This is because the non-linear fit was performed for the frequency domain storage modulus data.

The thermal cycling results on the WLP package are shown in section 4.5. Condition G and H of JEDEC JESD22-A014D standard were used to apply the thermal boundary conditions. Simulation was run for three cycles, and the difference in average inelastic energy density between the third and second cycles was computed and tabulated in Table 4-5. Equation (4-14) was then used to compute the number of cycles to failure. Figure 4-14 shows the computed number of cycles to failure for the different cases investigated. It is shown that for both condition G and H thermal cycling conditions, the difference between the models with the PCB modeled elastic and viscoelastic is negligible. This is in agreement to what has previously been reported in literature

[31] [32]. Solder joint failures due to thermal cycling are caused by the mismatch in CTE of the different packaging materials. The inclusion of the viscoelastic property of PCBs is shown to not have an impact for the computational analysis using condition G and H thermal cycling conditions.

In section 4.5, results for the board level drop testing simulations are shown. The computational results for strain, deformation, and acceleration are shown in Figure 4-17 to Figure 4-19. The comparisons were done for drops at different temperatures. Temperatures closer to and significantly higher than the Tg were chosen for the comparisons. Figure 4-17 shows that for 135 °C, the deformation response is dampened after 10 ms. At higher temperatures, the dampened response becomes even more evident as shown with the results for 145 °C and 155 °C. This dampened response of the system is not captured for the case where the viscoelastic property of the PCB is not included in the model. Similar results were obtained for acceleration and strain as shown in Figure 4-18 and Figure 4-19. These show that for applications where temperatures go above the glass transition temperature and a drop testing boundary condition is used, it is important to include the viscoelastic property of PCBs in the computational models in order to accurately capture the system behavior. These observations are aligned with analytical studies by Liu et. al. where it was shown that the increase in viscosity of the PCB will dampen the response under drop testing conditions [24]. Moreover, understanding the time-temperature dependent behavior of PCB substrates is important to understand residual stresses and dimensional changes in the PCBs during processing such as re-lamination and soldering processes [23].

4.7 Conclusions

In this paper, frequency domain master curve results from dynamic mechanical analysis were used to characterize the viscoelastic behavior of PCBs and computationally study the impact of PCB modeling on the assessment of thermomechanical reliability of WCSP packages under thermal cycling and under drop testing conditions. For computational studies with both Condition G and H of *JESD22-A014D* standard, it is shown that the inclusion of viscoelastic properties did not impact the computational results. For computational studies with drop testing boundary conditions, it is shown that for temperatures above the glass transition temperature, the inclusion of viscoelastic properties has significant impact on the board level analysis of deformation, strain, and acceleration.

4.8 Nomenclature

k_j	Stiffness of j^{th} spring
τ_j	Damping of j^{th} damper
σ	Applied stress
$G(t)$	Shear modulus as a function of time
G_0	Instantaneous shear modulus at t = 0
α_∞^G	Long term Prony coefficient (shear)
α_i^G	Relative moduli (G_i/G_0)
τ_i^G	Relaxation times
n_G	Relaxation modes
t	Time
G^*	Complex shear modulus
G_∞	Long term shear modulus
g_i^G	i^{th} Prony series term

G'	Storage shear modulus
G''	Loss shear modulus
E^*	Complex modulus
E'	Storage modulus
E''	Loss modulus
$Tan\ \delta$	Loss angle tangent
a_T	Shift factor
T	Temperature
T_r	Reference temperature
T_g	Glass transition temperature
C_1	First coefficient of shift factor
C_2	Second coefficient of shift factor
ω	Frequency
τ	Time constant
s_0	Initial value of deformation resistance
Q/R	Activation energy/Boltzmann's constant
A	Pre-exponential factor
ξ	Stress multiplier
m	Strain rate sensitivity of stress
h0	Hardening/softening constant
ŝ	Coefficient for saturation value of deformation resistance
n	Strain rate sensitivity of the saturation value
a	Strain rate sensitivity of the hardening/softening

4.9 References

[1] L.-T. Yeh and R. C. Chu, Thermal Management of Microelectronic Equipment, New York: ASME Press, 2002.

[2] W. Hilbert and F. Kube, ""Effects on Electronic Equipment Reliability of Temperature Cycling in Equipment," Report No. EC-69-400 (Final Report)," Grumman Aircraft Corp., Bethpage, NY, 1969.

[3] W. Engelmaier, "Solder Joints in Electronics: Design for Reliability," Keynote Address in Design and Reliability of Solder and Solder Interconnectons, 1997, pp. 9-19.

[4] "Guidelines for Accelerated Reliability Testing of Surface Mount Solder Attachments," IPC Guidelines IPC-SM-785. The Institute of Interconnecting and Packaging Electronic Circuits., Lincolnwood, IL, November 1992 .

[5] JESD22-B111, "Board Level Drop Test Method of Components for Handheld Electronic Products," JEDEC SOLID STATE TECHNOLOGY ASSOCIATION, 2003.

[6] M. M. Hossain, S. Jagarkal, D. Agonafer, M. Lulu and S. Reh, "Design Optimization and Reliability of PWB Level Electronic Package," *Journal of Electronic Packaging ,* vol. 129, no. 1, pp. 9-18, 2007.

[7] B. A. Zahn, "Finite Element Based Solder Joint Fatigue Life Predictions for a Same Die Stacked Chip Scale Ball Grid Array Package," 27th Annual IEEE/SEMI International Electronics Manufacturing Technology Symposium. IEEE, 2002.

[8] S. Yamada, "A Fracture Mechanics Approach to Soldered Joint Cracking," *IEEE CHMT,* vol. 12, no. 1, pp. 99-104, 1989.

[9] W. Engelmaier, "Functional Cycling and Surface Mounting Attachment Reliability," *ISHM Technical Monograph Series 6894-002,* pp. 87-114, 1984.

[10] A. Syed, "Creep Crack Growth Prediction of Solder Joints During Temperature Cycling - An Engineering Approach," *Transactions of the ASME,* vol. 117, pp. 116-122, 1995.

[11] R. Darveaux, K. Baneerji, A. Mawer and G. Dody, "Reliability of Plastic Ball Grid Array Assembly," in *Ball Grid Array Technology*, New York, McGraw-Hill Inc. , 1995, pp. 379-442.

[12] S. Liu and Y. Liu, Modeling and Simulation for Microelectronic Packaging Assembly: Manufacturing, Reliability and Testing, Singapore : Chemical Industry Press, 2011.

[13] A. Schubert, R. Dudek, E. Auerswald, A. Golhardt, B. Michel and H. Reichi, "Fatigue Life Models for SnAgCu and SnPb Solder Joints Evaluated by Experiments and Simulation," in *53rd Electronic Components and Technology Conference, 2003. Proceedings.*, New Orleans, Louisiana, 2003.

[14] L. Anand, "Constitutive Equations for the Rate-Dependent Deformation of Metals at Elevated Temperatures," *Journal of Engineering Materials and Technology,* vol. 104, no. 1, pp. 12-17, 1982.

[15] S. Brown, K. Kim and L. Anand, "An Internal Variable Constitutive Model for Hot Working of Metals," *International Journal of Plasticity,* vol. 5, no. 2, pp. 95-130, 1989.

[16] M. Motalab, Z. Cai, J. C. Suhling and P. Lall, "Determination of Anand constants for SAC Solders using Stress-Strain or Creep Data," in *13th IEEE ITHERM Conference*, San Diego, CA, 2012.

[17] T. C. Lui, "Lifetime Prediction of Viscoplastic Lead-free Solder," in *International Workshop on Integrated Power Packaging*, TU Delft, Netherlands, 2017.

[18] D. Bhate, D. Chan, G. Subbarayan, T. Chiu, V. Gupta and D. Edwards, "Constitutive behavior of Sn3.8Ag0.7Cu and Sn1.0Ag0.5Cu alloys at creep and low strain rate regimes," *IEEE Transactions on Components and Packaging Technologies,* vol. 31, no. 3, pp. 622-633, 2008.

[19] M. Mottahedi, A. Dadalau, A. Hafla and A. Verl, "Numerical analysis of relaxation test based on Prony series material model," *Integrated Systems, Design and Technology,* pp. 79-91, 2010.

[20] S. W. Park and Y. R. Kim, "Fitting Prony-series Viscoelastic Models with Power-law Presmoothing," *Journal of materials in Civil Engineering,* vol. 13, no. 1, pp. 26-32, 2001.

[21] M. Fernanda, P. Costa and C. Ribeiro, "Parameter estimation of viscoelastic materials: a test case with different optimization strategies," *AIP Conference Proceedings ,* vol. 1389, no. 1 , pp. 771-774, 2011.

[22] H. H.-T. Corporation, "Principle of Dynamic Mechanical Analysis (DMA). https://www.hitachi-hightech.com/global/products/science/tech/ana/thermal/descriptions/dma.html," 2018.

[23] P. Shrotriya and N. R. Sottos, "Creep and Relaxation Behavior of Woven Glass/Epoxy Substrates for Multilayer Circuit Board Applications," *Polymer Composites,* vol. 19, no. 5, pp. 567-578, 1998.

[24] F. Liu, G. Meng and M. Zhao, "Viscoelastic Influence on Dynamic Properties of PCB Under Drop Impact," *Journal of Electronic Packaging,* vol. 129, pp. 266-272, 2007.

[25] C. E. Miller, V. Gandhi and T. MacDonald, "Improving Reliability of Electronic Packages," in *ANSYS*, 20 April 2017.

[26] X. Fan, B. Varia and Q. Han, "Design and Optimization of thermo-mechanical reliability in wafer level packaging," *Microelectronics Reliability ,* vol. 50, no. 4, pp. 536-546, 2010.

[27] TA Instruments. , *Measurement of the Glass Transition Temperature Using Dynamic Mechanical Analysis.,* Thermal Analysis and Rheology. TA Instruments. .

[28] Hitachi High-Tech Science Corporation, *Instruction Manual: DMA Master Curve Analysis. Thermal Analysis Software TA7000.,* 0503-YB1-003E Ver.1.3., 2016.

[29] R. Li, "Time-temperature superposition method for glass transition temperature of plastic materials," *Materials Science and Engineering: A,* vol. 278, no. 1-2, pp. 36-45, 2000.

[30] R. Lakes, Viscoelastic Solids, Boca Raton, FL. : CRC Press LLC , 1998.

[31] A. Anaskure, "Effect of Viscoelastic Modeling of PCB on the Board Level Reliability of Wafer Chip Scale Package(WCSP) In Comparison to Orthotropic Linear Elastic Modeling," Dissertation. , 2017.

[32] A. Misrak, A. Anaskure, A. Sakib, U. Rahangdale, A. Lohia and D. Agonafer, "Comparison of the effect of elastic and viscoelastic modeling of PCBs on the assessment of board level reliability.," in *2017 16th IEEE Intersociety Conference on Thermal and Thermomechanical Phenomena in Electronic Systems (ITherm). IEEE.* , Orlando, FL. , May 2017.

[33] K. Reddy and N. S. Reddy , "Comparative Study of Viscoelastic Modeling and Linear Modeling for Wafer Level Chip Scale Package Under Drop Impact," Dissertation, 2017.

[34] E. Barbero, M. Julius and Z. Yao, "Time and Frequency Viscoelastic Behavior of Commercial Polymers," Calabria, Italy. CCCC. , 2003.

[35] A. Amirkhizi, J. Isaacs, J. McGee and S. Nemat-Nasser, "An experimentally-based viscoelastic constitutive model for polyurea, including pressure and temperature effects," *Philosophical magazine ,* vol. 86, no. 36, pp. 5847-5866, 2006.

[36] P. Rajmane, H. Khan, A. Doiphode, U. Rahangdale, D. Agonafer, A. Lohia, S. Kummerl and L. Nguyen, "Failure mechanisms of boards in a thin wafer level chip scale package," in *16th IEEE Intersociety Conference on Thermal and Thermomechanical Phenomena in Electronic Systems (ITherm). IEEE*, Orlando, FL, 2017.

[37] R. Darveaux, "Thermal cycle fatigue life prediction for flip chip solder joints," *2014 IEEE 64th Electronic Components and Technology Conference (ECTC),* 2014.

[38] JEDEC STANDARD, Temperature Cycling. JESD22-A104D, JEDEC Solid State Technology Association, March 2009.

[39] D. R., "Solder joint fatigue life model.," in *In: Proceedings of the TMS annual meeting*, p. 213 - 8 , 1997 .

[40] S. A., "Predicting solder joint reliability for thermal, power, & bend cycle within 25% accuracy," *51st ECTC ,* pp. 255-63, 2001.

[41] J.-H. Zhao, V. Gupta, A. Lohia and D. Edwards, "Reliability Modeling of Lead-Free Solder Joints in Wafer-Level Chip Scale Packages," *Journal of Electronic Packaging,* vol. 132, no. 1, pp. 011005-1, 2010.

[42] H. S. Dhiman, X. Fan and T. Zhou, "JEDEC Board Drop Test Simulation for Wafer Level Packages (WLPs)," in *Electronic Components and Technology Conference* , San Diego, CA, May 26 2009.

[43] J.-e. Luan and T. Y. Tee, "Novel Board Level Drop Test Simulation using Implicit Transient Analysis with Input-G Method," in *Electronics Packaging Technology Conference*, Singapore, Singapore , 2004.

Chapter 5
Impact of Die Attach Sample Preparation on its Measured Mechanical Properties for MEMS Sensor Applications

5.1 Abstract

Computational modeling is often leveraged to design and optimize electronic packages for both performance and reliability purposes. One of the factors that affect the accuracy of computational models is the accuracy of the material properties. MEMS sensors, in particular, are usually extremely sensitive to slightest material property changes in the package [1] [2]. Therefore, even small measurement variations in material characterization due to different sample preparation methods or different testing techniques can impact accuracy of computational models that are leveraged for designing or analyzing sensor performance. The challenge in material characterization is even greater for materials that require curing. Die attach polymers, for example, have strict curing profile requirements that are used during the manufacturing process. Such curing conditions are usually hard to duplicate in laboratories, and the samples used for material characterization may not necessarily be representative of the actual component in the final product. In this paper, the effect of parameters such as temperature curing profile, application of pressure during curing, and sample preparation technique on temperature dependent thermo-mechanical properties of two types of die attach elastomers is investigated. The mechanical properties, including elastic modulus (E), coefficient of thermal expansion (CTE), and the glass transition temperature (Tg) of the die attach material, are measured using a suite of techniques such as dynamic mechanical analysis (DMA) and thermomechanical analysis (TMA). The analysis is performed for a wide temperature range corresponding to typical sensor applications. It is shown that sample preparation and characterization techniques have a considerable impact on the

measurements which results in different MEMS sensor performance predictions through computational modeling.

5.2 Introduction

Microelectromechanical systems (MEMS) are devices, ranging from microscale to centimeter scale, that are made of electrical and mechanical components and are used to simulate macroscopic devices on a microscopic scale [3]**.** The first MEMS device was invented by H.C. Nathanson less than a decade after the invention of integrated circuits [3]. Research in MEMS gained significant traction in the 1980s due to improvements in processing technologies and the start of MEMS workshops [4]. Since then, MEMS have been successfully used in wide range of applications including accelerometers, pressure sensors, gyroscopes, jet print heads, automotive (airbag) applications, and pressure sensors for engine management [5] [6]. MEMS devices have also been the focus of significant research for application in the space industry due to their low mass, volume, and power consumption [6]. MEMS are important components in developing cost-effective and ultra-miniaturized sensors and actuators for applications in the space industry [7].

Packaging of MEMS devices may be at the wafer level packaging (0^{th} level packaging) or discrete packaging (1^{st} level packaging) [8]. The major functions of MEMS packaging are to: distribute the signals to and from the MEMS device, remove heat, support and protect the MEMS device [9]. The techniques used for MEMS packaging share many similarities to those used in the microelectronics industry including hermeticity and chip level integration techniques including Multi-Chip-Modules [10]. However, unlike IC packaging, MEMS packaging is expensive and is custom built. The cost for MEMS packaging can be up to 60 - 80% of total product cost [9].

Figure 5-1 below shows major components of a MEMS package. There are three major components in a MEMS package: the MEMS device that is either a sensor or actuator, application

specific integrated circuit (ASIC) and a cap that provides protection. The mechanical parts in a MEMS package may include cantilever beams (single side clamped, double side clamped), membranes (either closed at the sides to another structural member, or as a free floating plate), springs (often doubling as cantilever beams), and hinges [11]. Due to the presence of these mechanical parts, there are failure modes that are unique to MEMS devices [10] [12] [13]. There are two levels of connections in a MEMS device: between the sensors/actuators and ASIC and between ASIC and substrate or printed circuit board (PCB). These connections could be made using wire bond, flip-chip solder bumps or ordinary solder balls. Die attach adhesive is used to attach the MEMS device and ASIC to the substrate as shown in Figure 5-1.

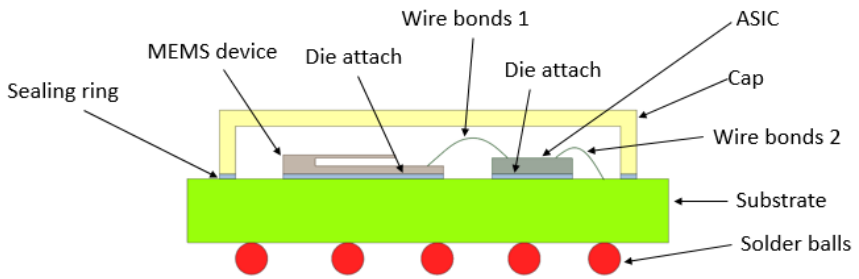

Figure 5-1: Schematic diagram showing components of a MEMS package.

Die attach materials play very important role in MEMS packaging. Functions of die attach adhesives include: mechanically attaching the die to substrate, providing efficient heat dissipation path, acting as intermediate material layer to partially offset the differences in thermal expansion coefficient (CTE) between die and substrate, and provide electrical reference to the back side of the die [14]. The die attach adhesives can be classified into two groups: soft and hard. Soft adhesives are made of polyimides, epoxies and organic based materials filled with thermally conductive fillers. On the other hand, hard adhesives may be gold-based eutectics or glass-based materials [14]. The process of curing the die attach adhesive materials require very high

temperatures and makes the MEMS devices susceptible to thermally induced stresses and strains [15]. Due to the large mismatch between the thermomechanical properties of silicon and commonly used adhesives, a drop-in temperature after curing induces strain in the package-die system and is relieved through deformations that impact the performance of the MEMS device [15]. Hence, accurate material characterization, modeling, and prediction of the effect of packaging on device is important in the design of MEMS devices [15].

Accurate material characterization, especially for thin film technology, is very challenging, and significant amount of time and resources are utilized to obtain accurate properties of materials at the microscale [11]. Macroscopic bulk behavior is often different from those measured at the microscale, and there have been databases such as the MEMS clearinghouse website [16] developed in order to consolidate the work done at the microscale. However, in most applications, macroscopic bulk properties of materials are often used in computational studies to assess designs and perform reliability assessments of electronic packages. Dynamic mechanical analysis (DMA), thermomechanical analysis (TMA), and tensile tester are some of the equipment commonly used to characterize the bulk properties of electronic packaging materials [17]. Nanoindentation has also been previously used to characterize material property of packaging materials [18].

Even at the macroscale, where multiple techniques are available to measure material properties, results reported by different researchers may not be consistent and prone to variations due to different factors. Testing conditions, techniques used for testing, and sample preparation methods are some of the main factors affecting the accuracy of material characterization. Sample preparation methods are even more critical for curable materials used in electronic packaging such as die attach adhesives and molding compounds among others. In this paper, the effect of several parameters such as temperature profile, applied pressure, sample thickness, and characterization

technique on temperature-dependent thermo-mechanical properties of die attach elastomers used for MEMS devices is thoroughly investigated. The materials and methods are presented in section 5.3, results are given in section 5.4, while discussion and conclusions are given in sections 5.5 and 5.6 respectively.

5.3 Materials and Methods

5.3.1 Sample Preparation

Often, sample preparation methods for material characterization differ from the conditions under which the materials will be cured and used in applications. In this study, focusing on die attach materials, different sample preparation methods are utilized and their impact on measurement results is analyzed. Two different kinds of commercially available die attach materials are used for this study. The following two sections show different sample preparation methods for curable die attach materials and die attach films (DAFs).

Curable Die Attach Materials

The curable die-attach materials investigated here are 'gel-like' materials that cure and harden after undergoing a certain temperature curing profile. The temperature profile used for the curing process is given in Figure 5-2. For mass productions, the die attach materials are cured for given thickness under certain pressure. It is not possible to duplicate during sample preparation the exact

conditions used when mass producing. For our study, four different approaches that give different levels of control for pressure and thickness that were proposed and used are discussed next.

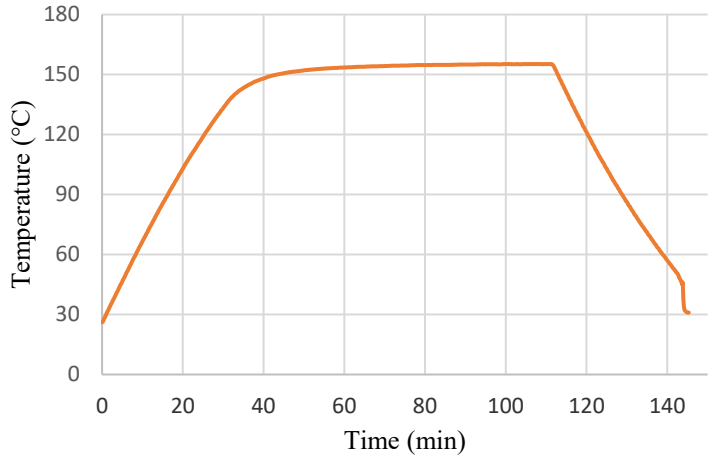

Figure 5-2: Temperature profile used for curing the samples.

Approach 1 - Curing without Pressure

The first approach involves curing the die attach samples without applying any pressure. In this technique, the sample was dispensed on a Teflon sheet placed on a steel plate. The sample was dispensed between brass spacers of 0.8 mm thickness and spread using a blade to ensure uniform thickness. The spacers were clamped on to the steel plates as shown in Figure 5-3 below. Using an oven, the samples were cured using the profile shown in Figure 5-2. This technique was the easiest for retrieving the samples after the curing as shown in Figure 5-3. However, no pressure was

applied during curing and this approach may not match the expected curing conditions used for mass production.

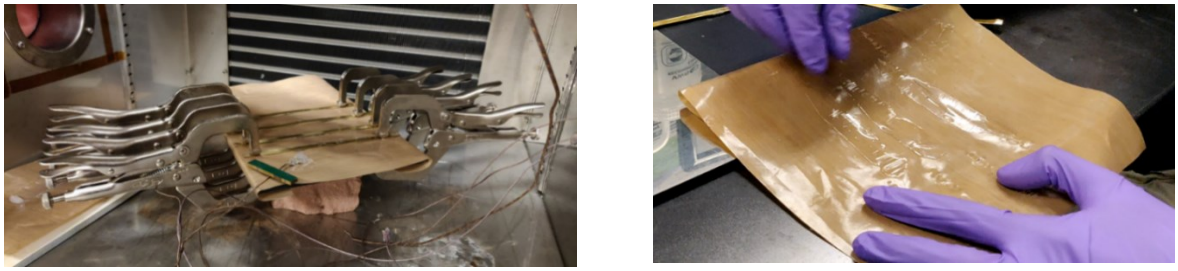

Figure 5-3: Sample preparation without the top plate (left) and cured sample (right).

Approach 2 - Curing with Pressure

Teflon sheets were cut to the dimensions of the steel plates (6" x 6") and attached to steel plates that were used to sandwich the die attach samples using a double-sided tape. The Teflon sheet was used in order to make the process of removing the cured samples easier. Spacers were used to prepare samples of 0.5 mm thickness. The other steel plate was placed with an offset and clamps were applied to increase the pressure. Using an oven, the sample was cured using the profile shown in Figure 5-2. The steps for preparing samples using this approach are given in Figure 5-4.

Figure 5-4: Sample dispensed on the Teflon sheet attached to the steel plate (left), assembly ready to cure on (right).

Approach 3 - Curing Using an Assembly with Controlled Torque

In the approach discussed in the previous section, multiple clamps were used to apply pressure during the curing process. However, the applied pressure was not measured. In this approach, 0.5 MPa of pressure was applied during curing by applying a measured torque on a set of nuts and

bolts. Spacers were used to obtain sample of 0.5 mm thickness. Like the previous two approaches, the sample was then placed in an oven to obtain the desired curing profile. An assembly that was used to prepare samples using this approach is shown in Figure 5-5.

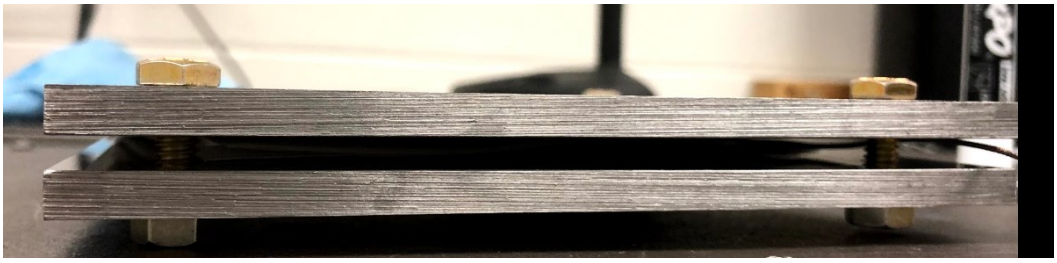

Figure 5-5: Sample preparation setup with torque control.

Approach 4 - Curing with Hot Press

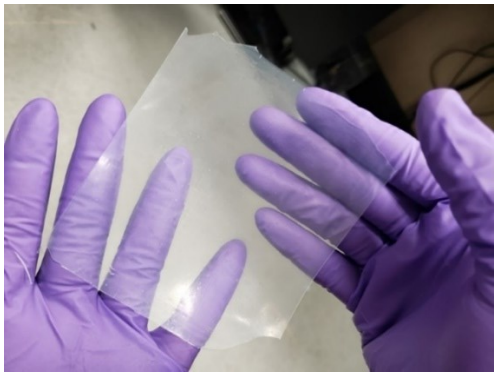

Figure 5-6: Sample prepared using a hot press machine.

A fourth approach was also implemented where a hot press was used to cure and prepare the samples. This approach gave a better control of the pressure applied on the samples. However, the specific hot press machine used for this test did not allow control of the ramp rate for the given profile. The plate temperature was set to the dwell temperature, and the temperature was ramped using the default setting of the machine. Teflon sheet were also used in this approach to prevent the samples sticking to the plates. Spacers were used to obtain 0.5 mm thick samples and the

samples were cured with ~ 0.5 MPa curing pressure. Figure 5-6 shows a sample prepared using the hot press.

DAF Materials

The DAF material used for this study was a 25 µm film that is cured during application. For our study, an oven was used to cure the DAF material. The DAF was cured by raising the temperature from room temperature to 160°C in 30 mins and keeping it at 160°C for 1 hour. For measurements on DMA, it was found that the 25 µm films were outside the measurement range for the equipment, and it was not possible to make measurements for the desired temperature ranges. Figure 5-7 shows that for sample thicknesses lower than 200 µm, the corresponding geometric factor and expected modulus at higher temperatures will be outside of the measurement envelop. To overcome this, eight 25 µm thick films were stacked on top of each other before curing to obtain 200 µm samples. The steps taken to obtain the 200 µm samples are shown in Figure 5-8.

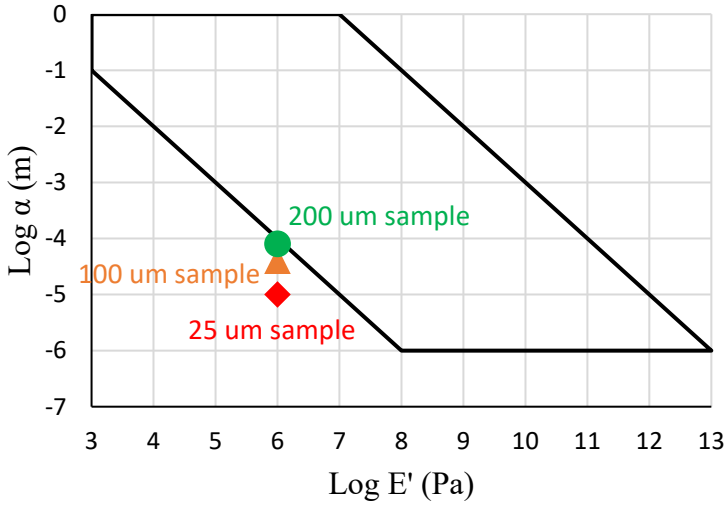

Figure 5-7: Log of geometric factor vs expected modulus for different sample sizes. The expected modulus shown here corresponds to temperatures above room temperature. The measurable ranges for DMA shown in black.

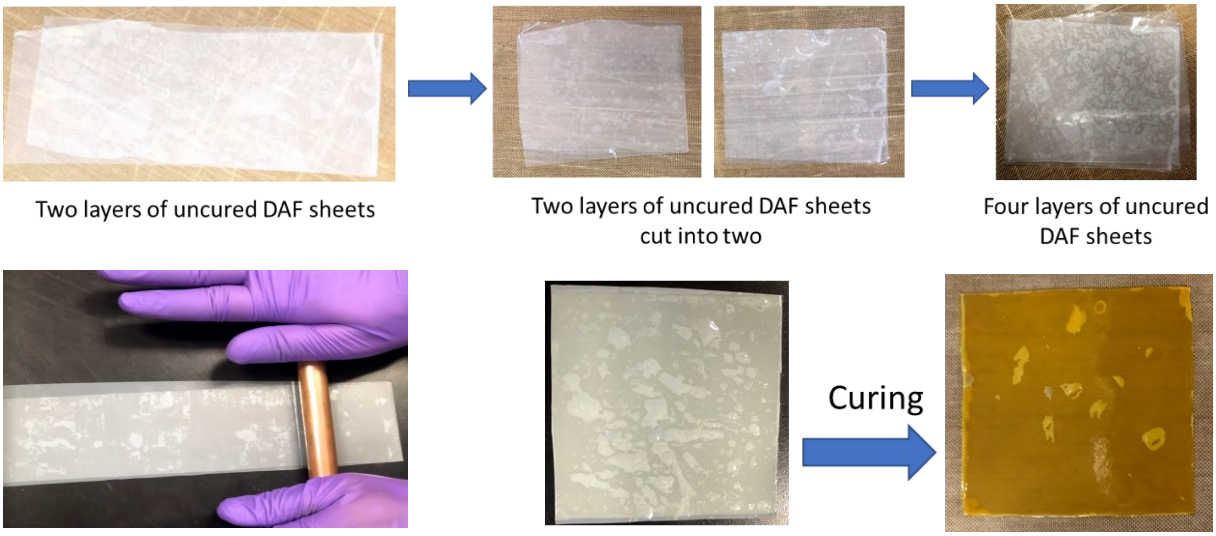

Figure 5-8: Sample preparation of DAF samples: thicker samples prepared without a roller (top), with a roller (bottom).

5.3.2 Experimental Procedure

After the samples were cured, they were cut to dimensions appropriate for testing on TMA and DMA. For both DMA and TMA, tensile attachments were used for testing as shown in Figure 5-9. A typical sample used for TMA testing has a length of 15 mm, width of 3 mm, and thickness of 0.1 – 0.5 mm. While a typical sample used for DMA testing has length of 20 mm, width of 10 mm, and thickness of 0.2 – 0.5 mm. Table 5-1 to Table 5-4 list the settings used for DMA and TMA measurements.

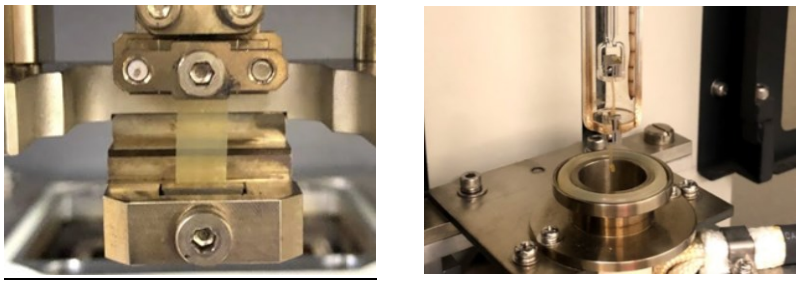

Figure 5-9: Die attach material mounted for DMA measurement (left) and TMA measurement (right).

Table 5-1: Settings used for testing die attach samples on TMA.

Parameter	Values
Temperature ramp rate	3 °C/min
Load during length measurement	20.33 mN
Load during testing	10 mN

Table 5-2: Settings used for testing die attach samples on DMA.

Parameter	Values
Minimum Tension Force	50 mN
Tension Force Gain	1.8
Force Amplitude Default Value	50 mN
L Amplitude	10 um
Temperature ramp rate	2 °C/min

Table 5-3: Settings used for testing DAF samples on TMA.

Parameter	Values
Temperature ramp rate	3 °C/min
Load during length measurement	20.33 mN
Load during testing	13 mN

Table 5-4: Settings used for testing DAF samples on DMA.

Parameter	Values
Minimum Tension Force	50 mN
Tension Force Gain	1.8
Force Amplitude Default Value	50 mN
L Amplitude	10 um
Temperature ramp rate	2 °C/min

5.4 Results

The results from tests done on TMA and DMA for the samples prepared using the techniques described in the previous section are shown below. Figure 5-10 and Figure 5-11 show the DMA results for die attach and DAF samples. Equation 1-2 was used to compute the complex modulus, and the results are shown below for different temperatures.

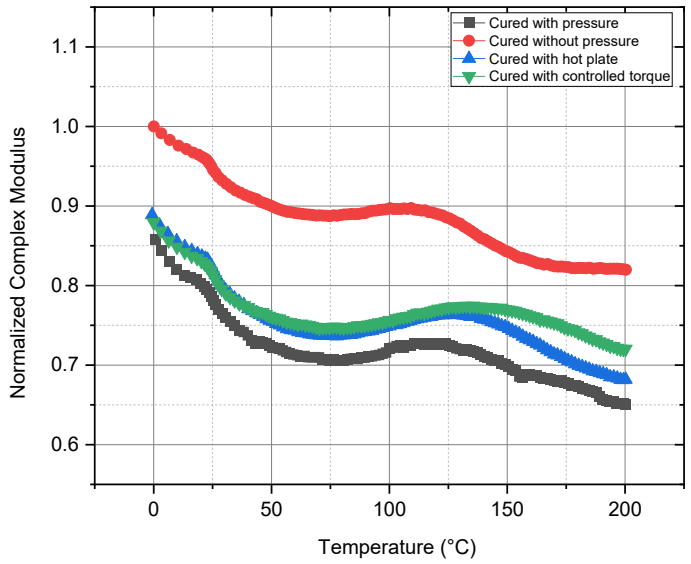

Figure 5-10: Normalized complex modulus as a function of temperature for different sample preparation methods for curable die attach samples.

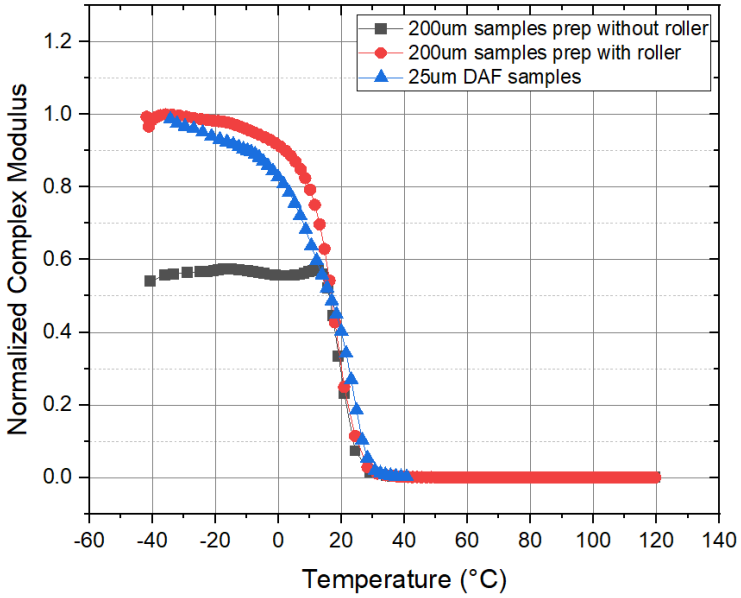

Figure 5-11: Comparison of DMA results for different sample preparation of DAF samples.

Figure 5-12 shows the comparison for TMA measurements performed on curable die attach samples prepared with different preparation methods. Figure 5-13 shows the complex modulus results for curable die attach samples after undergoing reflow profile commonly used for SnAgCu (SAC) alloys.

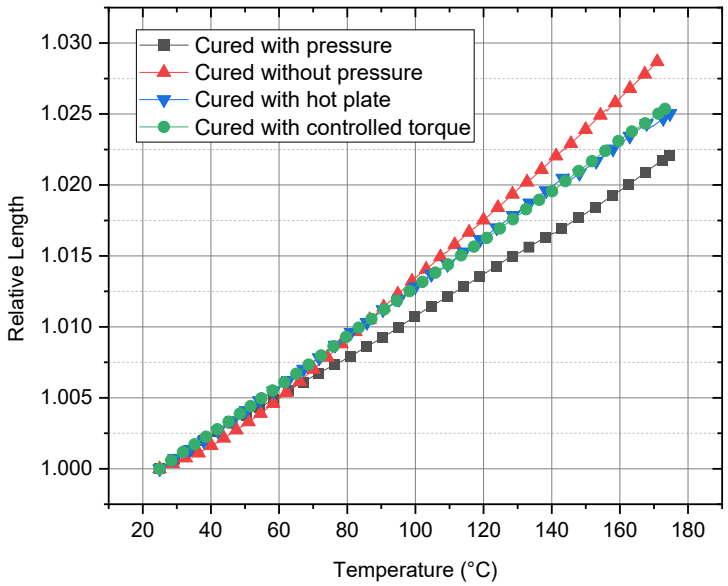

Figure 5-12: Change of relative length with temperature for different sample preparation methods for curable die attach samples.

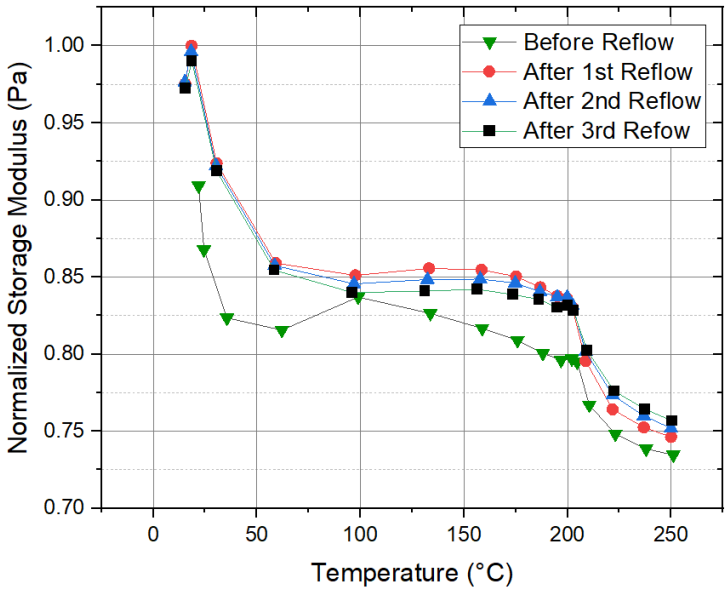

Figure 5-13: Normalized modulus of curable die attach materials after the samples were exposed to reflow temperature profile commonly used for SAC solder alloys.

5.5 Discussion

Two different kinds of die attach materials were studied. The curable die attach materials were prepared using the different techniques presented in section 5.3. Cured samples were cut to dimensions appropriate for DMA and TMA testing, and tested using the parameters given in Table 5-1 and Table 5-2. The sample preparation methods were selected in order to study the impact of pressure and curing profile used during sample preparation on the measurement results. Three sets of samples were prepared using an oven for curing but different amount of pressure applied during curing. Another set of samples were prepared using a hot plate. For each sample preparation method, three samples were tested on DMA and the average results are shown in Figure 5-10. The results were normalized to the highest modulus value at the initial temperature. With pressure applied during curing, the results show that the method used to obtain the curing profile has negligible impact on the measurement results. On the other hand, the application of pressure is shown to have a significant impact on the measurement results. Results for the case where pressure was applied during curing are shown to be lower than the cases where pressure was not applied during curing. This is in line to what has been previously reported in the literature as Nakamae et. al. have shown results where Young's modulus and tensile strength decreased with increasing curing pressure [19]. Similarly, three samples were tested on TMA and the results are shown in Figure 5-12. The results are shown as relative length using the sample thickness at the initial temperature. For the measured temperature ranges, the difference in CTE for the different sample preparation methods was found to not be significant.

Another set of measurements were also run on DMA to evaluate the impact of reflow on the measured properties of die attach materials. Figure 5-13 shows the normalized results for measurement after repeated exposure of the samples to curing profile used for SAC alloys. The

results after the initial reflow profile were consistent to each other. However, it can be seen that the initial results without the application of the reflow profile are lower for the measured temperature ranges except at 100 °C. The difference at 100 °C can be explained by the low sampling rate used for the measurement and potential noise during testing. This result shows that it is important to condition the samples properly before performing material characterization.

The second type of die attach materials tested are die attach films (DAFs). Unlike the gel like die attach materials which cure in place, the die attach films are solid at the initial temperature but cure after application. Depending on the required modulus value for application, acceptable tolerance of squeezed out material, and the desired bond line thickness of the material, one type of die attach material may be preferred over the other. For the second part of this work, a commercially available DAF material was studied. The authors faced unique challenges when preparing samples and testing DAF materials on DMA and TMA. The DAF material used for this study came at 25 um thickness. For DMA tests, it was observed that samples prepared for this thickness were outside of the measurement range as shown in Figure 5-7. In order to obtain samples with appropriate geometric factors, multiple DAF sheets were layered on top of each other before curing. The layered samples were prepared using two different ways: with and without using rollers to make the multi layered samples. For TMA tests, 100 um thick samples were prepared using four sheets of DAF films. For DMA tests, 200 um thick samples were prepared using 8 sheets of DAF films. The 200 um thickness was selected in order to satisfy the geometric factor requirement for measurements as shown in Figure 5-7. Another constraint for the measurements was the low glass transition temperature (Tg) of the DAF films. Using the onset of E' for the definition of Tg, the Tg was measured to be around 10 °C. For TMA measurements, the tests were run for temperature range of -40 °C to 160 °C. For some temperatures, negative

expansion coefficient values were observed. These inaccurate results were obtained because the same setting values were used for the whole temperature range. This implies that the mechanical properties significantly changed at the glass temperature, and the same setting values can not be used for the entire temperature ranges. One alternative work around for this would be to perform two measurements: -40 °C to Tg, and Tg to 160 °C. This would allow the use of suitable settings values for each temperature ranges and obtain reasonable values. Due to limitation of resources, this was not included as part of the current work and could be considered as future work. A second alternative would be the use of techniques such as laser and optical dilatometers for the measurement of thermal expansion coefficients. These techniques have been shown to have the capability to detect expansions in the nanometer range and would be able to measure the thermal expansion coefficient of the 25 um thick DAF films. For DMA measurement of DAF films, results were obtained only up to temperature slightly higher than Tg for the 25 um samples. This was because for higher temperature the expected modulus value and geometric factors were not within the measurement envelop for the equipment as shown in Figure 5-7. The thicker samples prepared were within the measurement envelop. However, the sample preparation techniques used has a major impact on the measurement results. As shown in Figure 5-11, for the lower temperature values, the results obtained for samples prepared with rollers were closer to results for 25 um DAF films. For samples prepared without a roller, the results were up to 40% lower for temperature ranges where comparison was possible. This is because for samples prepared without a roller, the films were not bonded properly and there were bubbles trapped between layers. These had impact and resulted in lower measured value for the modulus.

5.6 Conclusions

In conclusion, thermo-mechanical analysis and dynamic analysis were performed on die attach samples prepared with different sample preparation techniques. Results for commercially available curable die attaches and die attach films were used to study the impact of curing pressure, method used to create curing temperature profile, impact of reflow temperature, and sample preparation methods. It was shown that the method used to obtain the curing temperature profile (oven vs hot press) did not have an impact on the measurement results. On the other hand, curing pressure was shown to have a measurable impact, and samples prepared with no curing pressure were shown to have high modulus values. For DAF materials, it was shown that performing material characterization at the desired thickness values on DMA and TMA was not possible. Thicker samples had to be prepared in order to be in the measurable range for the respective equipment. The method used to prepare the thicker samples is shown to have significant impact and shows that special care must be taken when preparing such samples for measurement on DMA and TMA. Previous studies have shown that MEMS sensors are extremely sensitive to slight material property changes. The work presented here shows that extreme care must be taken in the sample preparation and characterization of packaging components, such as die attach materials, in order to develop accurate material models and perform accurate design analysis.

5.7 References

[1] X. Zhang, S. Park and M. Judy, "Accurate assessment of packaging stress effects on MEMS sensosrs by measurement and sensor-package interaction simulations," *Journal of microelectromechanical systems,* vol. 16, no. 3, pp. 639-649, 2007.

[2] R. Krondorfer, Y. Kim, C.-G. Gustafson and T. Lommasson, "Finite element simulation of package stress in transfer molded MEMS pressure sensors," *Microelectronics Reliability,* vol. 44, no. 22, pp. 1995-2002, 2004.

[3] B. Stark, "MEMS Reliability Assurance Guidelines For Space Applications," in *Jet Propulsion Laboratory Publication 99-1*, Pasadena, CA , January 1999.

[4] H. Fujita, "A decade of MEMS and its future," in *IEEE The Tenth Annual International Workshop on Micro Electro Mechanical Systems. An Investigation of Micro Structures, Sensors, Actuators, Machines, and Robots. (pp. 1 - 7)* , Nagoya, Japan, January 26 1997.

[5] I. De Wolf, "Reliability of MEMS," in *7th International Conference on Thermal, Mechanical and Multiphysics Simulation and Experiments in Micro-Electronics and Micro-Systems, EuroSimE.* , Como, Italy, 2006.

[6] H. R. Shea, "Reliability of MEMS for space application," in *Proc. SPIE 6111, Reliability, Packaging, Testing, and Characterization of MEMS/MOEMS V, 611110A. doi: 10.1117/12.651008*, 5 January 2006.

[7] S. Kayali, R. Lawton and B. Stark, *MEMS reliability assurance activities at JPL,* 1999.

[8] F. Santagata, J. J. M. Zaal, V. G. Huerta, L. Mele, F. Creemer and P. Sarro, "Mechanical Design and Characterization for MEMS Thin-Film Packaging," *Journal of Microelectromechanical Systems,* vol. 21, no. 1, pp. 100-109, February 2012.

[9] J. H. Lau, C. Lee, C. Premachandran and Y. Aibin, Advanced MEMS Packaging, New York: Mc Graw Hill, 2010.

[10] R. Krondorfer, Y. K. Kim, J. Kim, C.-G. Gustafson and T. C. Lommasson, "Finite element simulation of package stress in transfer molded MEMS pressure sensors," *Microelectronics Reliability,* vol. 44, no. 12, pp. 1995-2002, 2004.

[11] W. M. v. Spengen, "MEMS reliability from a failure mechanisms perspective," *Microelectronic Reliability,* vol. 43, no. 7, pp. 1049-1060, 2003.

[12] H. Tilmans, J. De Coster , P. Helin, V. Cherman, A. Jourdain, P. De Moor, B. Vandevelde, N. Pham, J. Zekry, A. Witvrouw and I. De Wolf, "MEMS packaging and reliability: An undividable couple," *Microelectronics Reliability,* vol. 52, no. 9-10, pp. 2228-2234, 2012.

[13] D. M. Tanner , J. A. Walraven, K. Helgesen, L. W. Irwin, F. Brown, N. F. Smith and N. Masters, "MEMS reliabiity in shock environments," in *38th Annual International Reliability Physics Symposium*, San Jose, California , 2000.

[14] R. K. Ulrich and W. D. Brown, Advanced Electronic packaging, Hoboken: John Wiley & Sons, 2006.

[15] M. Lishchynska, C. O'Mahony, O. Slattery, O. Wittler and H. Walter, "Evaluation of Packaging Effect on MEMS Performance: Simulation and Experimental Study," *IEEE Transactions on Advanced Packaging,* vol. 30, no. 4, pp. 629 - 635, 4 November 2007.

[16] "MEMSnet," [Online]. Available: http://www.memsnet.org/material/. [Accessed 11 November 2019].

[17] A. Misrak, T. Chauhan, P. Rajmane, R. Bhandari and D. Agonafer, "Impact of Aging On Mechanical Properties of Thermally Conductive GAP Fillers," *Journal of Electronic Packaging,* vol. 142, no. 1, 2020.

[18] A. Misrak, L. Nguyen, S. Kummerl and D. Agonafer, "Characterization of Mechanical Properties and Creep Behavior of Woven Glass/Epoxy Substrates by Nanoindentation," *Journal of Microelectronics and Electronic Packaging,* vol. 15, no. 2, pp. 95-100, 2018.

[19] K. Nakamae, T. Nishino, X. AiRu and K. Takatsuka, "Pressure Dependence of the Curing Behavior of Epoxy Resin," *Polymer Journal,* vol. 23, pp. 1157-1162, 1991.

Chapter 6
Summary and Conclusions

In chapters 2 – 5, important electronic packaging components such as PCBs, TIMs, and die attach materials are investigated. The nanoindentation techniques has been shown as a tool to characterize location dependent material properties of a given PCB substrate. From the work presented in chapter 2, it was shown that a maximum load of more than 4 mN is required to have indentation depth more than 3x the average surface roughness of the sample. The surface roughness, maximum load, hold time, and location on the substrate surface were shown to be the main factors affecting the measurement values. Using the standard linear solid model, it was also shown that the characteristic time is linearly dependent to the hold time. The work on PCBs further continued to chapter 4 where frequency domain master curve results from dynamic mechanical analysis were leveraged to characterize viscoelastic properties of PCBs. These results were used to investigate the impact of including viscoelastic properties in computational analysis. For computational studies with both Condition G and H of *JESD22-A014D* standard, it is shown that the inclusion of viscoelastic properties did not impact the computational results. However, for computational studies with drop testing boundary conditions, it is shown that for temperatures above the glass transition temperature, the inclusion of viscoelastic properties has significant impact on the board level analysis of deformation, strain, and acceleration.

Chapter 3 presents the work done on thermal interface materials. The thermomechanical properties of two thermally conductive gap fillers were studied using DMA, TMA, and FTIR. After the samples were prepared, half of them were tested for pre-aging measurement values, while the rest were placed in an environmental chamber for 720 hours at 125 °C and were tested afterwards. Multiple samples were tested to obtain average values and standard deviations. The complex

modulus of aged samples is shown to have increased when compared to measurements of pre aged samples. Among the two samples studied, the TIM with higher thermal performance (higher filler content) is shown to have higher modulus values. TMA results showed that the samples with lower filler content had higher CTE, and that high temperature aging reduced the CTE of both TIMs studied. The FTIR technique was used to identify the functional groups present in the sample and detect changes after high temperature aging. The sample preparation technique leveraged for this study can be used to prepare samples that match the thicknesses used in various applications. In this paper, it is shown that the changes in mechanical properties can be used to understand and assess reliability of thermal interface materials. There is a lack of work in the literature on the mechanical testing of TIMs, and this work may be used as a guide on the preparation and testing of samples for evaluation of mechanical properties. Moreover, the CTE and modulus values measured using the techniques discussed in this paper may be used to perform FEA and evaluate the reliability of TIMs under different loading conditions.

In chapter 5, results from thermo-mechanical analysis and dynamic analysis performed on die attach samples prepared with different sample preparation techniques were presented. It was shown that the method used to obtain the curing temperature profile (oven vs hot press) did not have an impact on the measurement results. On the other hand, curing pressure was shown to have a measurable impact, and samples prepared with no curing pressure were shown to have high modulus values. For DAF materials, it was shown that performing material characterization at the desired thickness values on DMA and TMA was not possible. Thicker samples had to be prepared in order to be in the measurable range for the respective equipment. The method used to prepare the thicker samples is shown to have significant impact and shows that special care must be taken when preparing such samples for measurement on DMA and TMA. Previous studies have shown

that MEMS sensors are extremely sensitive to slight changes in material property. The work presented here shows that extreme care must be taken in the sample preparation and characterization of packaging components, such as die attach materials, in order to develop accurate material models and perform accurate design analysis.

The work presented here can be used as a starting point for future work that aims at further investigating the material properties of electronic packaging materials. The characterization of location dependent material properties of PCBs can further be extended by performing tests at different temperatures. The technique can also be used to perform material characterization of other components such as substrate layers and dielectric layers, as well as understand the length scale dependency of material characterization. The viscoelastic characterization from frequency domain master curve results from dynamic mechanical analysis presented in chapter 4 can also be used to perform similar characterizations for other viscoelastic materials used for electronic packaging such as mold compounds, elastomers, etc… In chapter 5, it was shown that the mechanical properties significantly changed at the glass temperature, and the same setting values cannot be used for the entire temperature ranges. As a future work, measurements may be performed for two temperature ranges: -40 °C to Tg, and Tg to 160 °C in order to obtain data that can be used to develop more accurate material models. Another area that can be investigated as part of future work is the impact of different material characterization techniques on measurement results. Different techniques are available for measuring the same material properties. For example, DMA, TMA, and DSC can be used to measure the glass transition temperature. Each has their own advantages and limitations. It would be important to carry out studies that increase our understanding of the applicability of these techniques in characterization the mechanical properties of different electronic packaging materials.

Appendix I

Prony Series Terms for Different Temperatures

A. Prony series terms for 140 °C and 150 °C

i	140 °C		150 °C	
	α_i^G	τ_i^G	α_i^G	τ_i^G
Inf	2.86E-01	N/A	2.86E-01	N/A
1	0.05966	5.16E-03	5.97E-02	3.31E-06
2	0.06331	0.0349	6.33E-02	2.23E-05
3	7.68E-02	0.19885	7.68E-02	1.27E-04
4	0.09036	1.04E+00	9.04E-02	6.67E-04
5	9.70E-02	5.09646	9.70E-02	0.00326
6	9.15E-02	2.42E+01	9.16E-02	1.55E-02
7	7.70E-02	119.5669	7.70E-02	0.07653
8	0.06272	638.2983	6.27E-02	4.09E-01
9	5.15E-02	3.74E+03	5.15E-02	2.40E+00
10	0.04452	2.73E+04	4.45E-02	1.75E+01

B. Prony series terms for 180 °C and 190 °C

i	180 °C		190 °C	
	α_i^G	τ_i^G	α_i^G	τ_i^G
Inf	2.86E-01	N/A	2.86E-01	N/A
1	0.059633	3.76E-07	0.059634	4.84E-08
2	0.063275	2.54E-06	0.063276	3.27E-07
3	0.076769	1.45E-05	0.076771	1.86E-06
4	0.090333	7.59E-05	0.090335	9.76E-06
5	0.09696	3.71E-04	0.09696	4.77E-05
6	0.091582	0.00176	0.09158	2.26E-04
7	0.077027	0.00871	0.077026	0.00112
8	0.062746	0.04651	0.062745	0.00598
9	0.051513	0.27271	0.051512	0.03504
10	0.044534	1.99063	0.044533	0.25575

Appendix II

Comparison of Computed vs. Measured Modulus for Different Temperatures

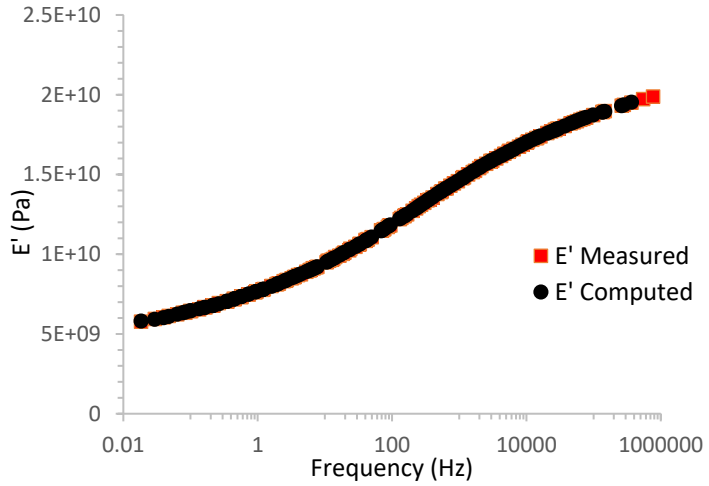

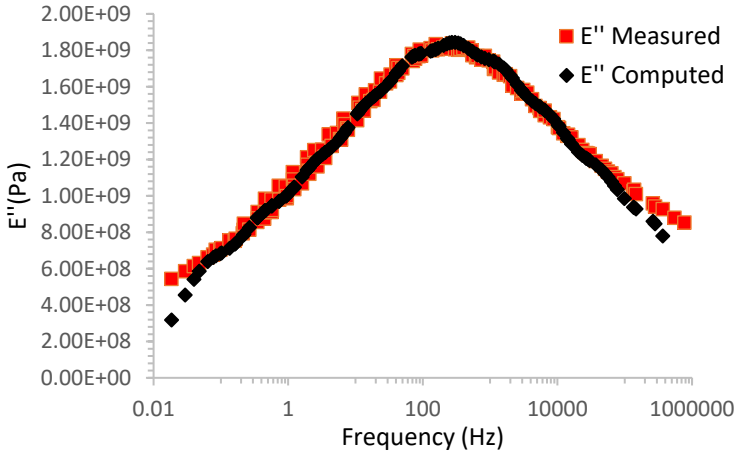

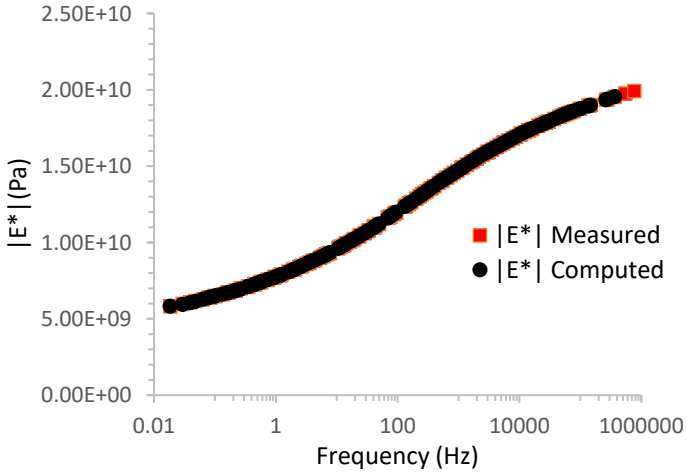

Computed vs measured storage, loss, and complex modulus for 170 °C.

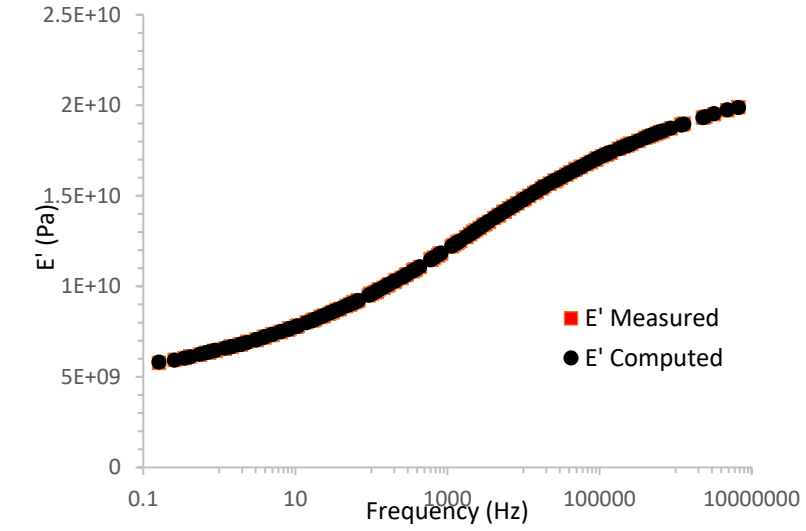

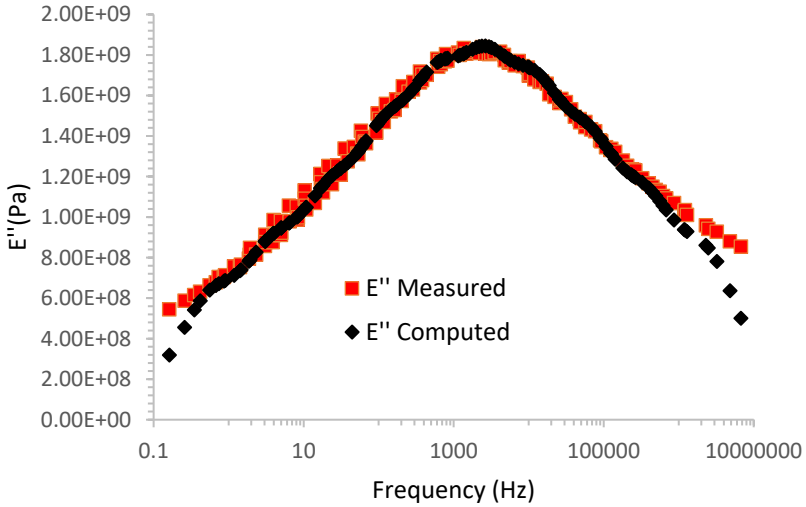

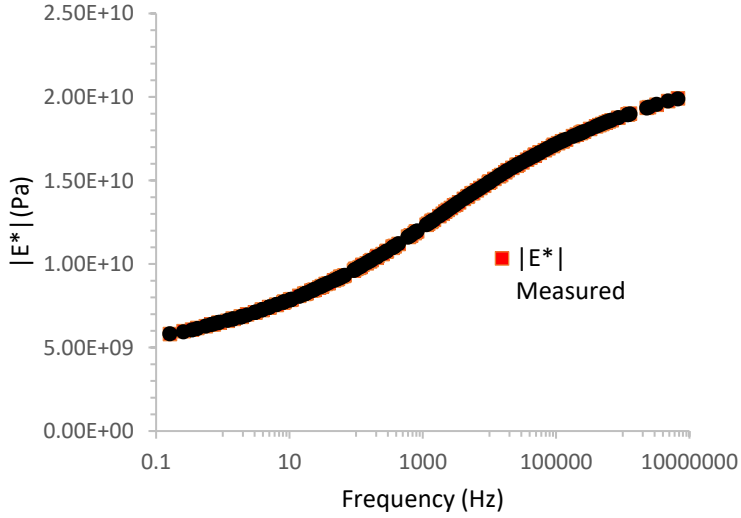

Computed vs measured storage, loss, and complex modulus for 180 °C.